CASCADE MODELING OF NONLINEAR SYSTEMS

A THESIS SUBMITTED TO
THE GRADUATE SCHOOL OF NATURAL AND APPLIED SCIENCES
OF
MIDDLE EAST TECHNICAL UNIVERSITY

BY

ERDEM TÜRKER ŞENALP

IN PARTIAL FULFILLMENT OF THE REQUIREMENTS
FOR
THE DEGREE OF DOCTOR OF PHILOSOPHY
IN
ELECTRICAL AND ELECTRONICS ENGINEERING

AUGUST 2007

Approval of the Thesis

"CASCADE MODELING OF NONLINEAR SYSTEMS"

Submitted by **ERDEM TÜRKER ŞENALP** in partial fulfillment of the requirements for the degree of **Doctor of Philosophy in Electrical and Electronics Engineering** by,

Prof. Dr. Canan Özgen
Dean, Graduate School of **Natural and Applied Sciences**   _____

Prof. Dr. İsmet Erkmen
Head of Department, **Electrical and Electronics Engineering** _____

Prof. Dr. Ersin Tulunay
Supervisor, **Electrical and Electronics Engineering, METU** _____

Examining Committee Members

Prof. Dr. Önder Yüksel (*)
Electrical and Electronics Engineering, METU   _____

Prof. Dr. Ersin Tulunay (**)
Electrical and Electronics Engineering, METU   _____

Prof. Dr. Yurdanur Tulunay
Aerospace Engineering, METU   _____

Assoc. Prof. Dr. Tolga Çiloğlu
Electrical and Electronics Engineering, METU   _____

Prof. Dr. Alper Uraz
Electrical and Electronics Engineering, Başkent University _____

                                              Date: _____

(*)   Head of Examining Committee
(**)   Supervisor

I hereby declare that all information in this document has been obtained and presented in accordance with academic rules and ethical conduct. I also declare that, as required by these rules and conduct, I have fully cited and referenced all material and results that are not original to this work.

Erdem Türker Şenalp

ABSTRACT

CASCADE MODELING OF NONLINEAR SYSTEMS

Şenalp, Erdem Türker

PhD., Department of Electrical and Electronics Engineering

Supervisor   : Prof. Dr. Ersin Tulunay

August 2007, 188 pages

Modeling of nonlinear systems based on special Hammerstein forms has been considered. In Hammerstein system modeling a static nonlinearity is connected to a dynamic linearity in cascade form.

Fundamental contributions of this work are: 1) Introduction of Bezier curve nonlinearity representations; 2) Introduction of B-Spline curve nonlinearity representations instead of polynomials in cascade modeling. As a result, local control in nonlinear system modeling is achieved. Thus, unexpected variations of the output can be modeled more closely.

As an important demonstration case, a model is developed and named as Middle East Technical University Neural Networks and Cascade Model (METU-NN-C).

Application examples are chosen by considering the Near-Earth space processes, which are important for navigation, telecommunication and many other technical applications. It is demonstrated that the models developed based on the contributions of this work are especially more accurate under disturbed conditions, which are quantified by considering Space Weather parameters.

Examples include forecasting of Total Electron Content (TEC), and mapping; estimation of joint angle of simple forced pendulum; estimation of joint angles of spring loaded inverted double pendulum with forced table; identification of Van der Pol oscillator; and identification of speakers.

The operation performance results of the International Reference Ionosphere (IRI-2001), METU Neural Networks (METU-NN) and METU-NN-C models are compared qualitatively and quantitatively. As a numerical example, in forecasting the TEC by using the METU-NN-C having Bezier curves in nonlinearity representation, the average absolute error is 1.11 TECu.

The new cascade models are shown to be promising for system designers and operators.

Keywords: Cascade modeling, Hammerstein system modeling, Neural Networks, Near-Earth space processes, telecommunication.

ÖZ

DOĞRUSAL OLMAYAN DİZGELERİN ARDIŞIK MODELLENMESİ

Şenalp, Erdem Türker

Doktora, Elektrik ve Elektronik Mühendisliği Bölümü

Tez Yöneticisi   : Prof. Dr. Ersin Tulunay

Ağustos 2007, 188 sayfa

Doğrusal olmayan dizgelerin özel Hammerstein biçimlerine dayanan modellenmesi dikkate alınmıştır. Hammerstein dizge modellemesinde bir dural doğrusalsızlık bir devingen doğrusallığa ardışık şekilde bağlanır.

Bu çalışmanın temel katkıları: 1) Ardışık modellemede polinomlar yerine Bezier eğri doğrusalsızlık gösterimlerinin tanıtımı; 2) B-Spline eğri doğrusalsızlık gösterimlerinin tanıtımıdır. Sonuç olarak, doğrusal olmayan dizge modellemesinde yerel denetim elde edilir. Böylece, çıktıdaki beklenmeyen değişmeler daha yakın olarak modellenebilir.

Önemli bir gösterme durumu olarak bir model geliştirilir ve Orta Doğu Teknik Üniversitesi Sinirsel Ağlar ve Ardışık Modeli (METU-NN-C) olarak adlandırılır.

Uygulama örnekleri sefer, iletişim ve diğer birçok teknik uygulamalar için önemli olan Yer'e yakın uzay süreçleri dikkate alınarak seçilir. Bu çalışmanın katkılarına dayanarak geliştirilen modellerin Uzay Havası değiştirgenleri dikkate alınarak nicelenen bozuculu koşullar altında özellikle daha doğru olduğu gösterilir.

Örnekler Toplam Elektron Miktarı (TEC) öngörümünü ve haritalamasını; basit kuvvet etkili sarkacın eklem açısının kestirimini; üzerine kuvvet uygulanan masa üzerinde yaylı ters çift sarkacın eklem açılarının kestirimini; Van der Pol salınım yapıcısının tanınmasını ve konuşmacıların tanınmasını içerir.

Uluslararası Referans İyonosfer (IRI-2001), ODTÜ Sinirsel Ağlar (METU-NN) ve METU-NN-C modellerinin uygulama başarım sonuçları niteliksel ve niceliksel karşılaştırılır. Sayısal bir örnek olarak, doğrusalsızlığı göstermede Bezier eğrilerine sahip METU-NN-C kullanılarak TEC öngörülerinde bulunmada ortalama mutlak yanılgı 1.11 TECu'dur.

Yeni ardışık modellerin dizge tasarımcıları ve uygulayıcıları için umut verici olduğu gösterilir.

Anahtar Sözcükler: Ardışık modelleme, Hammerstein dizge modellemesi, Sinirsel Ağlar, Yer'e yakın uzay süreçleri, haberleşme.

To My Parents and Brother

ACKNOWLEDGMENTS

TABLE OF CONTENTS

xiii

LIST OF TABLES

LIST OF FIGURES

xviii

xix

LIST OF ABREVIATIONS

AI   : Artificial Intelligence

ARX   : Auto-Regressive with eXogenous input

B-Spline   : Basis Spline

CDF   : Empirical Cumulative Distribution Function

CME   : Coronal Mass Ejection

COSPAR   : Committee on Space Research

COST   : European Cooperation in the field of Scientific and Technical
              Research

COST 238   : PRIME (Prediction and Retrospective Ionospheric Modelling
              over Europe)

COST 251   : Improved Quality of Service in Ionospheric
              Telecommunication Systems Planning and Operation

COST 271   : Effects of the Upper Atmosphere on Terrestrial and Earth-
              Space Communications

COST 296   : MIERS (Mitigation of Ionospheric Effects on Radio Systems)

COST 724   : Developing the scientific basis for monitoring, modeling and
              predicting Space Weather

EU   : European Union

FIR   : Finite Impulse Response

foF2   : Ionospheric Critical Frequency

HF   : High Frequency

LT   : Local Time

IRI   : International Reference Ionosphere

METU   : Middle East Technical University

METU-C   : Middle East Technical University Cascade Model

METU-NN : Middle East Technical University Neural Networks Model

METU-NN-C : Middle East Technical University Neural Networks and
       Cascade Model

MFCC   : Mel Frequency Cepstrum Coefficients

MIMO   : Multi Input Multi Output

MISO   : Multi Input Single Output

MPEG   : Moving Picture Expert Group

RAL   : Rutherford Applied Laboratory

TEC   : Total Electron Content

TECu   : Total Electron Content Unit

SW   : Space Weather

UMLCAR : Center for Atmospheric Research in the University of
       Massachusetts Lowell

URSI   : International Union of Radio Science

UT   : Universal Time

CHAPTER 1

INTRODUCTION

1.1 Objective

The forecasting of the Earth and near-Earth space processes by using the structural methodologies of the Neural Networks techniques have been developed and implemented since 1990's in Middle East Technical University (METU), Ankara [Tulunay E., 1991] [Altinay, 1996] [Altinay et al., 1997] [Kumluca, 1997] [Ozkaptan, 1999] [Senalp, 2001] [Tulunay Y. et al., 2001a] [Tulunay Y. et al., 2001b] [Senalp et al., 2002b] [Senalp et al., 2002c] [Tulunay E. et al., 2002b] [Tulunay Y. et al., 2002a] [Tulunay Y. et al., 2002b] [Tulunay E. et al., 2003] [Tulunay Y. et al., 2003a] [Tulunay Y. et al., 2003b] [Senalp et al., 2004] [Tulunay E. et al., 2004a] [Tulunay E. et al., 2004b] [Tulunay E. et al., 2004c] [Tulunay Y. et al., 2004a] [Tulunay Y. et al., 2004b] [Tulunay Y. et al., 2004c] [Tulunay Y. et al., 2004d] [Tulunay Y. et al., 2005a] [Tulunay Y. et al., 2005b] [Altuntas et al., 2006] [Tulunay E. et al., 2006a] [Tulunay E. et al., 2006b] [Tulunay E. et al., 2006f] [Altuntas et al., 2007] [Tulunay Y. et al., 2007a] [Tulunay Y. et al., 2007b] [Tulunay Y. et al., 2007c]. Experimental and measurement works on Near-Earth space processes were performed as well [Ertac et al., 1979] [Tulunay E. et al., 2002a] [Tulunay E. et al., 2006c] [Tulunay E. et al., 2006d] [Tulunay E. et al., 2006e]. The works have also been presented in European Union (EU), European Cooperation in the field of Scientific and Technical Research (COST) Actions: COST 238,

COST 251, COST 271, COST 296 and COST 724 [COST 238, 1999] [COST 251, 1999] [COST 271, 2004] [COST 296, 2007] [COST 724, 2007].

With such a background, in this current work, some design techniques of parametric identification by cascade modeling of the nonlinear processes are developed. The models designed and their performances in case studies are presented in national and international scientific conferences, meetings and international scientific journals [Senalp et al., 2005] [Senalp et al., 2006a] [Senalp et al., 2006b] [Senalp et al., 2006c] [Senalp et al., 2006d] [Senalp et al., 2006e] [Tulunay et al., 2006a] [Senalp et al., 2007b] [Senalp et al., 2007d]. EU COST 296 and EU COST 724 Actions provided scientific international platform in presenting the case studies [COST 296, 2007] [COST 724, 2007].

Modeling dynamic linear systems is relatively well developed [Ikonen and Najim, 1999]. Linear modeling techniques approximate only the behavior of the system around a fixed operating point. However, in reality, most of the dynamical systems are nonlinear. Nonlinear system modeling is more complicated due to the lack of general mathematical tools and also lack of information on properties of those systems. However, most of the dynamical systems can be represented by nonlinear modeling techniques. Nonlinear modeling is capable of describing the global system behavior for the overall operating range [Ikonen and Najim, 1999].

As the real processes present nonlinear characteristics, it is inevitable to have some degree of approximation in linear modeling. This approach can be satisfactory for few real applications [Ikonen and Najim, 1999]. Applying nonlinear model identification is inevitable for most of the real complex nonlinear processes including the near-Earth space processes.

In modeling of complex nonlinear processes, cascade modeling provides better understanding of the monitoring of the system of interest. For example, the system can be an industrial plant and in this case cascade modeling can be employed in plant optimization. Interaction of the user with the model and transparency are to be taken into account for real world modeling of complex processes [Ikonen and Najim, 1999]. In such cases there are some other methods. For example, techniques based on Artificial Intelligence (AI) are popular. In most of those techniques, black box modeling of the overall process is the characteristics of the method, whereas in the cascade models the static and dynamic components of the process are considered individually. Thus, cascade modeling provides transparency to the internal variables [Ikonen and Najim, 1999].

For many nonlinear dynamic processes it is required to express nonlinearities in the gain of the processes and provide dynamics in a linear block [Narendra and Gallman, 1966]. This can be achieved by cascade modeling. For many nonlinear dynamic processes, cascade models based on Hammerstein system modeling provide sufficient approximation [Ikonen and Najim, 1999]. In Hammerstein system modeling, a nonlinear static block is cascaded to a linear dynamic block as shown in Figure 1.1 [Narendra and Gallman, 1966].
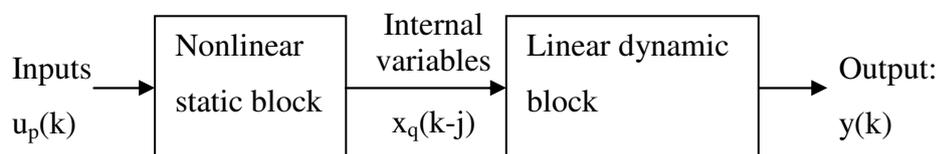
Figure 1.1. Cascade modeling based on Hammerstein system modeling

3

In Wiener systems, the order of the blocks is reversed, i.e. for Wiener systems the nonlinear static part follows the linear dynamic part [Zhu, 2002].

These types of dynamic nonlinear process modeling provide some important features. Since the process identification task is simplified by modeling the dynamic part in the linear block, data collection, computation of parameters and dynamic system analysis are simplified [Ikonen and Najim, 1999]. Also, to present nonlinearity in only the static gain decreases the degrees of freedom in the nonlinear system identification and the cascade models based on Hammerstein system modeling have got accurate and robust approximations for a large class of real complex processes [Ikonen and Najim, 1999].

The objective of this work is to develop some special forms of nonlinearities for cascade models based on Hammerstein system modeling and then to calculate the parameters of the static nonlinear block and dynamic linear block in cascade modeling by using some intelligent techniques so that high accuracy and high sensitivity in process identification is to be attained.

Near-Earth space processes such as Total Electron Content (TEC) variations are complex and nonlinear real processes to identify for various navigation and telecommunication applications. TEC is the number of electrons in a column of one meter-squared cross-section along a path through the ionosphere [Chilbolton Weather Web, 2004]. The unit of TEC is TECu (1 TECu = 10^{16} el / m^2). In the case studies, real processes are used to test the performance of the models developed herewith. For example, TEC values and TEC maps are forecast by using the models developed.

The International Reference Ionosphere (IRI) is an international project sponsored by the Committee on Space Research (COSPAR) and the International Union of Radio Science (URSI) [Bilitza, 2001] [IRI, 2007]. The aim of this project is to develop and improve the international IRI standards for the specification of ionospheric densities and temperatures [Bilitza, 2001]. In one of the case studies within the Thesis, the TEC forecasting results of the models developed herewith are compared with the TEC outputs of the IRI-2001 Model during the Space Weather events of April 2002.

In order to further show the generalization capability of the modelling technique, cascade models are also developed herewith for other nonlinear dynamic processes including simple forced pendulum, spring loaded inverted double pendulum with forced table, Van der Pol oscillator, and identification of speakers.

Some advantages of the cascade modeling techniques employed in this work can be summarized as follows:

i. The static nonlinearity in cascade modeling can also present hysteresis or discontinuities [Alonge et al., 2003]. There is no restriction in the cascade models developed herewith.

ii. In practice, the process identification tasks are problems of parameter estimation under constraints [Ikonen and Najim, 1999]. A cascade modeling technique, which has got intelligent optimization algorithms for the appropriate cost functions and constraints of complex nonlinear processes, is geared to be successful.

iii. Instead of having to deal with a single black box unit, cascade modeling technique based on Hammerstein system modeling has got the advantage of separability into a nonlinear static block and a

5

linear dynamic block in design of control systems [Ikonen and Najim, 1999].

iv. In contrast to the black box modeling of the nonlinear dynamic systems, cascade models based on Hammerstein system modeling have operational advantage of transparency of the internal stage parameters for operators [Ikonen and Najim, 1999].

v. Some of the iterative optimization methods were constructed based on the values of the cross-correlation coefficients. However, it is difficult to have convergence in such methods [Westwick and Kearney, 2000]. Cascade modeling with gradient-based parametric optimization methods, as employed in this work, has got advantages over the cross-correlation based ones. They serve both for sensitivity and accuracy of optimization.

The main disadvantage of Hammerstein system modeling is that the mathematical model obtained is still an approximation, as in all nonlinear system identification approaches, and in some cases strictly accurate steady state models can be difficult to obtain [Ikonen and Najim, 1999]. However, in general, this is of minor importance when the advantages are considered.

1.2 Review of Previous Applications

In modeling the nonlinear part of the Hammerstein systems, polynomials, sigmoid neural networks, fuzzy models and semi-physical models have been used [Duwaish et al., 1997].

Finite Impulse Response (FIR) and Auto-Regressive with eXogenous input (ARX) type of models have been considered for the linear dynamic part in most of the previous studies [Ikonen and Najim, 1999]. In many cases, simple

linear dynamics are sufficient for control design or fault diagnosis purposes and they provide simple and powerful techniques [Ikonen and Najim, 1999]. However, it is anticipated that modeling the nonlinear block is complicated. Most of the Hammerstein system models reported in literature have got a no-memory nonlinear gain of a polynomial form followed by a linear dynamic system [Narendra and Gallman, 1966] [Fruzzetti et al., 1997] [Marchi et al., 1999] [Bai and Fu, 2002] [Westwick and Kearney, 2000]. If the input is u(t) for the nonlinear block of these models, the output of the nonlinear element is then given by a series of (m+1) terms as given as,

$$x(t) = f[u(t)] = \sum_{i=0}^{m} \gamma_i . u^i(t) = \gamma_0 + \gamma_1 . u^1(t) + \gamma_2 . u^2(t) + ... + \gamma_m . u^m(t) \quad (1.1)$$

where γ_i are coefficients to be determined.

Thus, for this case, the internal variable x(t) is represented as a power series of the input variable u(t) as given in Equation 1.1. This representation is a special case of a general form, which is given as,

$$f(u(t),...,u(t-l),\gamma) = \sum_{i=0}^{m} \gamma_i . f_i(u(t),...,u(t-l)) \quad (1.2)$$

The dynamical behavior of the system is represented by a linear dynamic element as given as,

$$y(k) = \sum_{j=0}^{n} h(j) . x(k-j), \qquad \text{where } x(k) = f(u(k)) \quad (1.3)$$

The number n in Equation 1.3 represents the past history of the stored internal variables in memory. For the linear dynamic block, the impulse response h(j), j=0,…,n, and for the polynomial representation of the nonlinear static block, the parameters γ_i , i=1,…,m, should be determined.

7

For many industrial processes, the input/output models prove to be crucial in process control applications [Fruzzetti et al., 1997]. Structured nonlinear models can deal with stability, robustness and algorithmic efficiency problems. Cascade modeling techniques, i.e. Wiener and Hammerstein system models, have special architecture, which facilitates the nonlinear process analysis. They also have potential for control design [Fruzzetti et al., 1997].

Most of the nonlinear industrial and chemical processes, i.e. distillation columns, reactors, furnaces, heat exchangers, pH neutralization, and electromechanical systems can be modeled by a static nonlinearity cascaded to a dynamic linearity [Fruzzetti et al., 1997] [Kapoor et al., 1986] [Eskinat et al., 1991].

Cascade modeling on signal processing and communications was reported long time ago [Stapleton and Bass, 1985].

Biology is another science of real life. It possesses many nonlinear processes. Modeling the stretch reflex EMG using Hammerstein system modeling is also applicable in this area [Westwick and Kearney, 2000]. In identification of muscular response Hammerstein system model was used to find a suitable approach for Functional Electric Stimulation [Schultheiss and Re, 1998]. The nature of the process is strongly nonlinear, time varying and has many parameters. The combination of nonlinearities and time varying parameters makes the use of standard and / or adaptive methods extremely dangerous, because it is rarely possible to have convergence under poor excitation that is allowable within the tests with patients [Schultheiss and Re, 1998].

Most of the previous Hammerstein system models have employed power series representation in the nonlinear block [Narendra and Gallman, 1966] [Fruzzetti et al., 1997] [Marchi et al., 1999] [Bai and Fu, 2002] [Westwick and Kearney, 2000]. Very few of them mentioned about the applicability of cubic splines in representing the nonlinearities, e.g. [Dempsey and Westwick, 2004] [Guarnieri et al., 1999] [Zhu, 2002].

Generally, cubic splines are well suited for representing sharp and smooth curves [Rogers and Adams, 1990]. But the order is limited and it is three. Thus, it has got both advantages and disadvantages compared to polynomial representations. In polynomial representations, curves with sharp turnings are difficult to be modeled. However, higher order polynomials are applicable.

On the other hand, the Voltera series employed in modeling the nonlinearity limits cascade modeling to relatively low order systems, i.e. second order nonlinearities [Westwick and Kearney, 2000].

Near-Earth space processes are important for navigation, telecommunication and many other technical application system planners, developers and operators. The forecasting of the Earth and near-Earth space processes by using Neural Network models have been taking place since 1990's in METU. [Tulunay E., 1991] [Altinay, 1996] [Altinay et al., 1997] [Kumluca, 1997] [Ozkaptan, 1999] [Senalp, 2001] [Tulunay Y. et al., 2001a] [Tulunay Y. et al., 2001b] [Senalp et al., 2002b] [Senalp et al., 2002c] [Tulunay E. et al., 2002b] [Tulunay Y. et al., 2002a] [Tulunay Y. et al., 2002b] [Tulunay E. et al., 2003] [Tulunay Y. et al., 2003a] [Tulunay Y. et al., 2003b] [Senalp et al., 2004] [Tulunay E. et al., 2004a] [Tulunay E. et al., 2004b] [Tulunay E. et al., 2004c] [Tulunay Y. et al., 2004a] [Tulunay Y. et al., 2004b] [Tulunay Y. et al., 2004c]

[Tulunay Y. et al., 2004d] [Tulunay Y. et al., 2005a] [Tulunay Y. et al., 2005b] [Altuntas et al., 2006] [Tulunay E. et al., 2006a] [Tulunay E. et al., 2006b] [Tulunay E. et al., 2006f] [Altuntas et al., 2007] [Tulunay Y. et al., 2007a] [Tulunay Y. et al., 2007b] [Tulunay Y. et al., 2007c].

In order to increase the performance of the Neural Network models, new techniques in Cascade Models based on Hammerstein system modeling have been achieved herewith. These have also enabled the author to check the performance of the Hammerstein system modeling which is an interesting approach.

1.3 Models

Referring to the cascade modeling based on Hammerstein system modeling of the static nonlinearity and the dynamic linearity as illustrated in Figure 1.1, first of all, the internal variables, x(k), which are the outputs of the static nonlinear block and the inputs of the dynamic linear block, are obtained by an estimator. Then, using the information of the inputs, u(k), and the internal variables, x(k), the static nonlinearity is estimated. And then, using the internal variables at present time and history of the internal variables, *x(k),…,x(k-n)*, as inputs to the dynamic linear block and using the outputs, y(k), the dynamic linearity is estimated. It is to be noted that the memory takes place at the second block, which is in the linear dynamic block only.

Let a general continuous dynamic linear block be represented by a state-space equation as,

$$\dot{q}(t) = A.q(t) + b.x(t) \qquad (1.4)$$

10

$$y(t) = c.q(t) \qquad\qquad (1.5)$$

where q(t) is the state vector of size q_s; x(t) is a single input; y(t) is a single output; A is a square matrix of size q_s by q_s; b and c^T are vectors of size q_s. The general equivalent discrete time equation with a given sampling time, T, is depicted as,

$$q[(k+1)T] = K.q[kT] + L.x[kT] \qquad\qquad (1.6)$$

$$y[kT] = c.q[kT] \qquad\qquad (1.7)$$

A general discrete transfer function, G(z), from x(k) to y(k) can be expressed as,

$$G(z) = c(zI - K)^{-1} L = \frac{b_1 z^{-1} + b_2 z^{-2} + ... + b_n z^{-n}}{1 - a_1 z^{-1} - a_2 z^{-2} - ... - a_n z^{-n}} \qquad\qquad (1.8)$$

$$Y(z) = G(z).X(z) \qquad\qquad (1.9)$$

It is to be noted that different processes with the same inputs could produce similar outputs at the sampling instants, kT, in discrete time system identification. To avoid such a problem, fast sampling at the output can be performed and blind identification with the output measurements can be done [Bai and Fu, 2002].

When the internal variables are obtained by an estimator with the given inputs and output of the overall system, the static nonlinearity and the dynamic linearity can be obtained. Also the inverse transfer function of the general

dynamic linearity block can be obtained as follows from the point of system analysis [Bai and Fu, 2002],

$$X(z) = G^{-1}(z).Y(z) \tag{1.10}$$

$$x[kT] = \frac{1}{b_1}\left(-b_2 x[(k-1)T] - \ldots - b_n x[(k-n+1)T]\right)$$
$$+ \frac{1}{b_1}\left(y[(k+1)T] - a_1 y[kT] - \ldots - a_n y[(k-n+1)T]\right) \tag{1.11}$$

In order to identify the results of the cascade form in static and steady state models, the static nonlinear block is used. The linear dynamic block behaves as a filter. A steady state model can be achieved from the overall dynamical considerations of the system. In practice, a far better understanding and experience of the steady state performance do exist as in all nonlinear system identification approaches. This is evident if we consider the validation and initialization of nonlinear dynamic systems [Ikonen and Najim, 1999]. The important goal, however, is to satisfy the requirement of determining the model coefficients and the order of the model without a priori information on the process. Also for Multi Input Single Output (MISO) or Multi Input Multi Output (MIMO) systems it should be noted that the inputs are commonly parameterized. Each output may be a function of all the inputs and the past values of the internal variables [Fruzzetti et al., 1997]. This general form requires smart and complex techniques in determination of the input parameters. The order of the model can be determined by some expert systems or trial and error methods with the advantage of high-speed computer capabilities.

Even though the time required in optimizations for process identification with cascade modeling seems long from the practical point of view, it can be shortened by employing some parallel architectures inside the blocks.

Ad hoc experiments need to be performed for system identification [Alonge et al., 2003]. The experimental input/output data should represent the overall process in such cases. If this is not possible, more than one model can be developed for different operating regions of the process.

For optimization of the parameters of the cascade models some cost functions and constraints are used in optimization algorithms. It is to be noted that some approximation errors occurred can prevent convergence of the parameters. In such cases, the problems arisen can be controlled by using random initialization and smart optimization technique. For example, the Levenberg-Marquardt optimization algorithm for optimizing the mean square error of the cost function of the parameters in the cascaded blocks is one such method.

In an Artificial Intelligent optimization algorithm such as the Backpropagation Algorithm, it may be possible to converge to several local optima instead of global optimum. Backpropagation Algorithm has two major drawbacks. It may lead suboptimal approximations because of the probable existing local optimums as mentioned. In addition to this, the convergence of the Backpropagation Algorithm is slow and it is inadequate for online operations. The drawbacks can be removed by using Levenberg-Marquardt optimization method and by introducing validation stops [Senalp, 2001] [Tulunay Y. et al., 2001a] [Tulunay Y. et al., 2004a] [Tulunay Y. et al., 2004b] [Tulunay Y. et al., 2005a]. It is possible to use this optimization method in near real time applications by the support of the high-speed computers of today, provided that

an efficient implementation of the algorithm and representative determination of the inputs to the nonlinear block of the possible cascade model are available.

Cascade modeling based on Hammerstein system modeling is used for the forecast of the ionospheric-plasmaspheric processes in the selected case studies of this work. As a case study, the most common nonlinearity representation in Hammerstein system model literature, the polynomial representation, is employed in cascade modeling.

In this work, two new techniques are presented for building the nonlinear block of the cascade modeling. In the first new technique the static nonlinearity is modeled by using Bezier curves in the input representations. In the second new technique, B-Spline curves in the input representations are used to model the nonlinearity.

Both of these techniques have local control in contrast to the previous works. Neither polynomials nor cubic splines have local control. However for Bezier curves and B-Spline curves the more defining polygon vertices you introduce, the more local control you obtain.

In addition to this, B-Splines have more elasticity. Multiple points may be put for the common vertices of the defining polygons in B-Splines.

Those advantages of Bezier curves and B-Splines are introduced into the nonlinear static block of the cascade modeling with the intelligent parameter optimization methods.

The background and the theory of the models developed are given herewith in Chapter 1.

Forecasting the TEC values and maps are vital near-Earth space processes for various navigation and telecommunication applications via ionosphere. In Chapters 2 to 7, the case studies on forecasting TEC values and TEC maps by using the models developed herewith are given.

Models are also developed for other nonlinear dynamic processes including simple forced pendulum, spring loaded inverted double pendulum with forced table, Van der Pol oscillator, and identification of speakers. Those case studies are given in Chapter 8.

In the performance results of the case studies, Absolute Errors (AE), Normalized Errors (NE), Root Mean Square Errors (RMSE), and Cross Correlation Coefficients (r_{fo}) of the observed and forecast values of process parameters of interest are calculated by using the well-known definitions as,

$$AE = \frac{\sum_{i=1}^{N}(f_i - o_i)}{N} \tag{1.12}$$

$$NE = \frac{\sum_{i=1}^{N}\frac{(f_i - o_i)}{o_i}}{N} \tag{1.13}$$

$$RMSE = \sqrt{\frac{\sum_{i=1}^{N}[f_i - o_i]^2}{N}} \tag{1.14}$$

$$r_{fo} = \frac{C(f,o)}{\sqrt{C(f,f).C(o,o)}} \tag{1.15}$$

where i is the forecast time order, f_i is the forecast value at time i, o_i is the observed value at time i, N is the total number of forecast or observed instants, and C is the covariance function.

A general conclusion and some comments on the thesis are given in Chapter 9.

1.3.1 Middle East Technical University Neural Networks and Cascade Models (METU-NN-C)

Middle East Technical University Neural Networks and Cascade Models (METU-NN-C) are developed herewith. First of all, the METU-NN model is used to estimate the internal variables of the METU-C models. Then, the block parameters of the METU-C models are obtained [Senalp et al., 2005] [Senalp et al., 2006b] [Senalp et al., 2006c] [Senalp et al., 2006d] [Senalp et al., 2006e] [Senalp, 2007a] [Senalp et al., 2007b] [Senalp et al., 2007d]. Figure 1.2 illustrates the development modes of the METU-NN-C model blocks, which will be discussed in this and in the next sections, i.e. Sections 1.3.1 to 1.3.4. Later, in the operation mode, the METU-C models are ready to be used in operation.
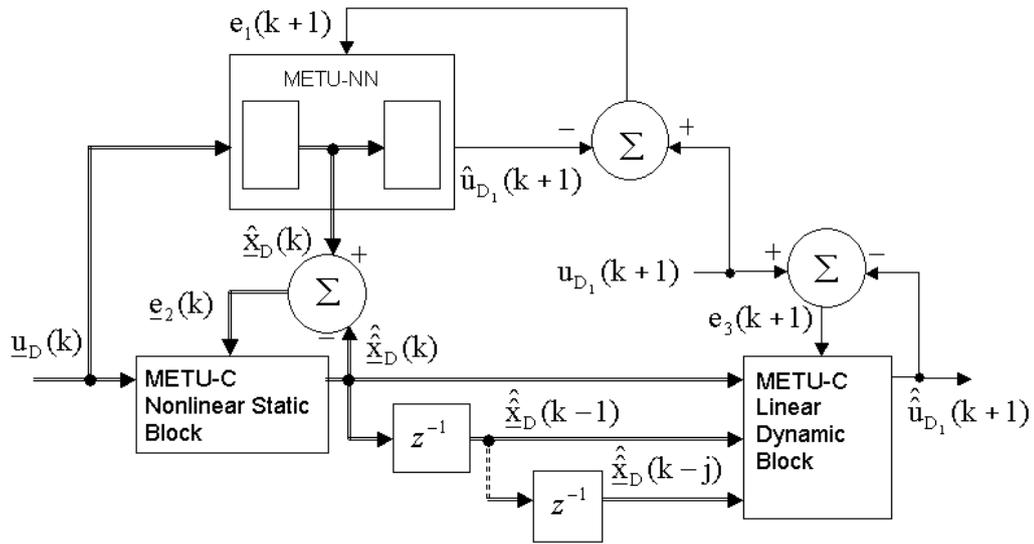
Figure 1.2. Development of the METU-NN-C Models

In the METU-NN model, Feedforward Neural Network architecture with neurons in one hidden layer is used. The basic architecture of the METU-NN model is demonstrated in Figure 1.3.
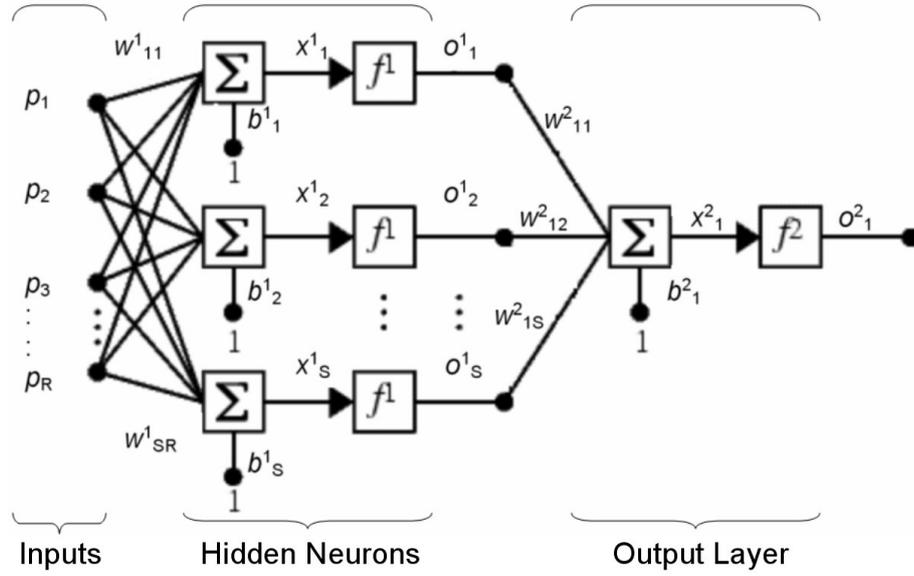
Figure 1.3. Architecture of the Neural Network Model

The activation functions in the hidden layer are hyperbolic tangent sigmoid functions and the activation function in the output layer is a linear function, so that the hidden layer outputs, x(k), can represent the static part of the state-like internal variables in cascade modeling. Hyperbolic tangent sigmoid functions, 'Tansig', and linear transfer functions, 'Purelin', are as follows,

$$Tansig(n) = \frac{2}{1+e^{-2.n}} - 1 \qquad (1.16)$$

$$Purelin(n) = a.n \qquad (1.17)$$

Levenberg-Marquardt Backpropagation algorithm is used during training [Hagan and Menhaj, 1994] [Haykin, 1999]. Levenberg-Marquardt algorithm is an approximation to Newton's method [Hagan and Menhaj, 1994] [Haykin,

18

1999]. Instead of the basic backpropagation algorithm the Levenberg-Marquardt Backpropagation algorithm using the approximation to Newton's method is faster in terms of computation time and more accurate near an error minimum. The Newton's method modification to the steepest descent algorithm, and random initialisations of the model parameters provide the model parameters to reach near global optimum values in the training.

The METU-NN is used to estimate the internal variables. The outputs of the hidden layer in METU-NN are the internal variables for the METU-C.

1.3.2 Representing Nonlinearity by Polynomials

Representing the nonlinearity by polynomials is the most common nonlinearity representation in Hammerstein system modeling [Narendra and Gallman, 1966] [Fruzzetti et al., 1997] [Marchi et al., 1999] [Bai and Fu, 2002] [Westwick and Kearney, 2000]. Figure 1.1 illustrates the architecture of the special Hammerstein form, the Middle East Technical University Cascade Model (METU-C).

The polynomial representations of the inputs are considered to model the static nonlinearity [Senalp et al., 2005] [Senalp et al., 2006c]. Let the inputs be denoted as $u_p(k)$, then the outputs of the nonlinear element, i.e. the internal variables $x_q(k)$, may be expressed as,

$$x_q(k) = \sum_{p=1}^{R} f\left[u_p(k)\right] = \sum_{p=1}^{R} \sum_{i=0}^{m} \gamma_{pi} . u_p^i(k) =$$

$$= \sum_{p=1}^{R} \left[\gamma_{p0} + \gamma_{p1} . u_p^1(k) + \gamma_{p2} . u_p^2(k) + ... + \gamma_{pm} . u_p^m(k)\right]$$

(1.18)

where R is the number of inputs, m+1 is the length of the series, and γ_{pi} are coefficients to be determined.

The output y(k) is represented by using a dynamic linearity which is obtained by optimizing a linear relationship for the internal variables $x_q(k)$ and their past values $x_q(k-j)$, as,

$$y(k) = \sum_{q=1}^{S}\sum_{j=0}^{n} h_q(j).x_q(k-j) \qquad (1.19)$$

where S is the number of the static internal variables and n is the number representing the history of the stored internal variables in memory. Thus, the product S(n+1) gives the number of dynamic internal variables. The coefficients of the linearity in Equation 1.19, i.e. $h_q(j)$, are also determined in the development mode.

1.3.3 Representing Nonlinearity by Bezier Curves

Cubic splines, Bezier curves, and B-splines are space curves used in computer graphics applications, i.e. skin of vehicles, platforms, fuselage of aircrafts, wings, hull of ships, engine manifolds, mechanical and structural parts etc [Rogers and Adams, 1990]. In cubic spline technique the curves pass through the existing data points. Practical usage of cubic spline curves suffers the necessity of specifying precise, non-intuitive mathematical information such as position, tangent and twist vectors [Rogers and Adams, 1990]. These difficulties are overcome by using Bezier curves. In contrast to the cubic spline representation of nonlinearities, Bezier curves satisfy functional requirements. The mathematical basis of this alternate method of shape description for design of free form curves and surfaces was derived from geometrical considerations by Pierre Bézier [Rogers and Adams, 1990] [Bézier, P.E., 1972]. Bézier also named them as Unisurf curves.

Bezier curves are determined by defining polygons. Defining polygon points may also be called local control points. In practice, it is possible to have more

local control on the results by introducing more defining polygon points. Thus, representing nonlinearities by using Bezier curves is promising and provides some advantages [Rogers and Adams, 1990]. By local control we mean to be able to include variations in a small segment of interest around a local control point without interfering other localities in the whole curve, which are spatially distant to the local segment of interest [Tulunay E. et al., 2006a]. Bezier curves provide more local control in contrast to the polynomial representations.

The Bezier basis is also the Bernstein basis. The basis functions of Bezier curves are real. The curves generally follow the shape of the defining polygons. Their start and end points are coincident with the start and end points of the defining polygons. The tangent vectors at the ends have the same direction as the spans of the first and the last polygons. The curves take place in the convex hulls of the defining polygons, and they are invariant under affine transformations [Rogers and Adams, 1990]. Formulation of the Bezier curves is as follows,

$$P(u) = \sum_{i=0}^{m} B_i . J_{m,i}\{u\} \qquad (1.20)$$

where

(m+1) is the number of defining polygon points,

u is the normalized variable,

B_i are the defining polygon points,

$J_{m,i}\{u\}$ are the Bernstein Basis Functions as,

$$J_{m,i}\{u\} = \binom{m}{i} u^i [1-u]^{m-i} = \frac{m!}{i!(m-i)!} u^i [1-u]^{m-i} \qquad (1.21)$$

The number (m-1) represents the degree of the defining polygon. The first three defining polygon points define the curvature at the beginning, and the last

three define the curvature at the end of the Bezier curve. If high flexibility is required, the degree of the defining polygon can be increased by increasing the number of defining polygon points [Rogers and Adams, 1990]. Thus, more defining polygon points mean more local control on the shape of the Bezier curve.

Additional flexibility can also be achieved by dividing a Bezier curve into two Bezier curves. When those two curves are combined the resultant curve is identical with the original curve [Rogers and Adams, 1990].

It is evident that since $J_{m,0}\{0\} = 1$ only the first defining polygon point, i.e. B_0, is defining the start point on Bezier curve, i.e. $P(0)$. Similarly, since $J_{m,m}\{1\} = 1$ only the last defining polygon point, i.e. B_m, is defining the end point on Bezier curve, i.e. $P(1)$.

To visualize Bezier curves and their defining polygons on Cartesian space, Figure 1.4 shows graphical output examples obtained by Computer Graphics software developed by the author within a graduate course in his department, i.e. METU – EE642 Computer Graphics.
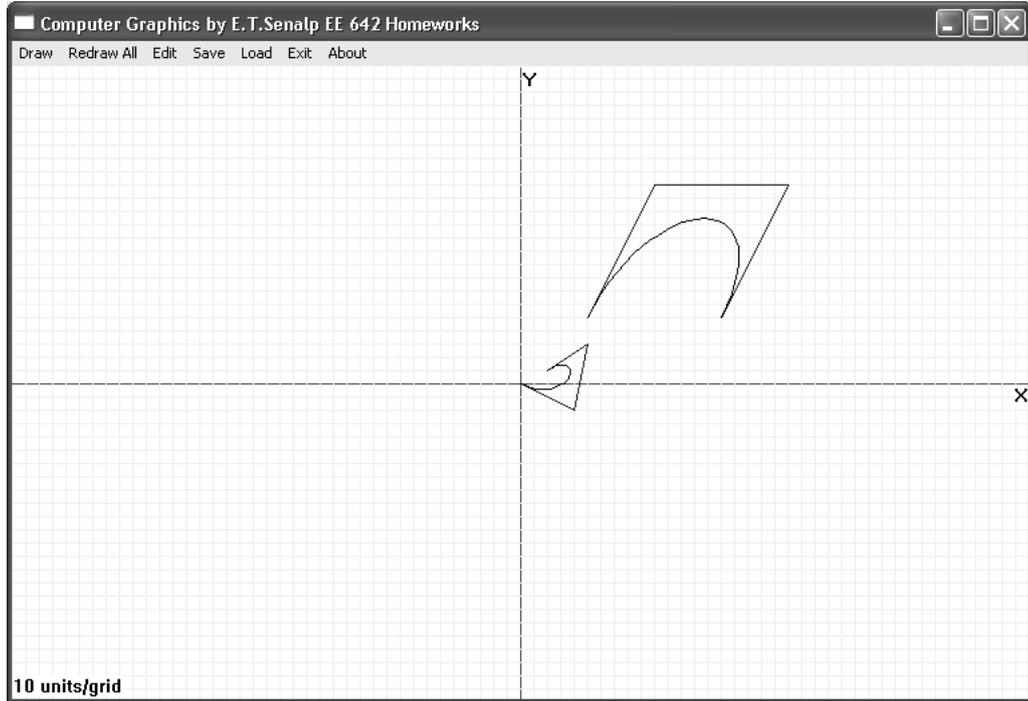
Figure 1.4. Examples of Bezier curves and their defining polygons on Cartesian space

To the best knowledge of the author, in this work, static nonlinear block of a cascade model, METU-C, based on Hammerstein system modeling is represented by Bezier curves for the first time [Senalp et al., 2006b]. The internal variables of the METU-C model, i.e. $x_q(k)$, may be formulated as follows,

$$x_q(k) = \sum_{p=1}^{R} f[u_p(k)] = \sum_{p=1}^{R} \sum_{i=0}^{m} B_{pi}.J_{m,i}\{u_p(k)\} \qquad (1.22)$$

where

R is the number of inputs,

$(m+1)$ is the number of defining polygon points,

$u_p(k)$ are the normalized input variables.

B_{pi} are the coefficients to be determined,

$$J_{m,i}\{u_p(k)\} = \binom{m}{i} u_p^i(k)[1 - u_p(k)]^{m-i} = \frac{m!}{i!(m-i)!} u_p^i(k)[1 - u_p(k)]^{m-i} \quad (1.23)$$

Thus, the product $R(m+1)$ gives the number of static block coefficients, i.e. B_{pi}, to be determined.

The output $y(k)$ is represented as

$$y(k) = \sum_{q=1}^{S} \sum_{j=0}^{n} h_q(j).x_q(k-j) \quad (1.24)$$

where S is the number of the static internal variables, n is the number representing the history of the stored internal variables in memory.

In Equation 1.24, the output $y(k)$ is represented by using a dynamic linearity and by optimizing a linear relationship for the internal variables $x_q(k)$ and their past values $x_q(k-j)$ which constitute their history. Thus, the product $S(n+1)$ gives the number of dynamic internal variables. The coefficients of the linearity in Equation 1.24, i.e. $h_q(j)$, are also to be determined in the development stage.

1.3.4 Representing Nonlinearity by B-Splines
A curve generated by defining polygon vertices is dependent on the approximation to form a relationship between the curve and the polygon by choosing the basis function. For Bezier curves the basis function is the Bernstein function [Rogers and Adams, 1990].

In Bezier curves, the number of defining polygon vertices determines the order of the curve representation. Also in Bezier curves, the Bernstein basis function is nonzero and representing local changes on the curve is limited [Rogers and Adams, 1990].

Schoenberg suggested the B-Spline curves [Schoenberg, 1946] [Rogers and Adams, 1990]. In B-Spline curves, B-Spline bases (Basis splines) are used. B-Spline basis is nonglobal, because each vertex has its correspondent unique basis function and affects the curve where the correspondent basis function is nonzero. The degree of the B-Spline curve or the order of the basis function is not dependent on the number of the defining polygon vertices, which is not the case in Bezier curves [Rogers and Adams, 1990]. However, formation of a B-Spline curve has more computations than formation of a Bezier curve, which can be a drawback for complex systems.

To visualize B-Spline curves and their defining polygons on Cartesian space, Figure 1.5 shows graphical output examples obtained by the Computer Graphics software mentioned in the Section 1.3.3.
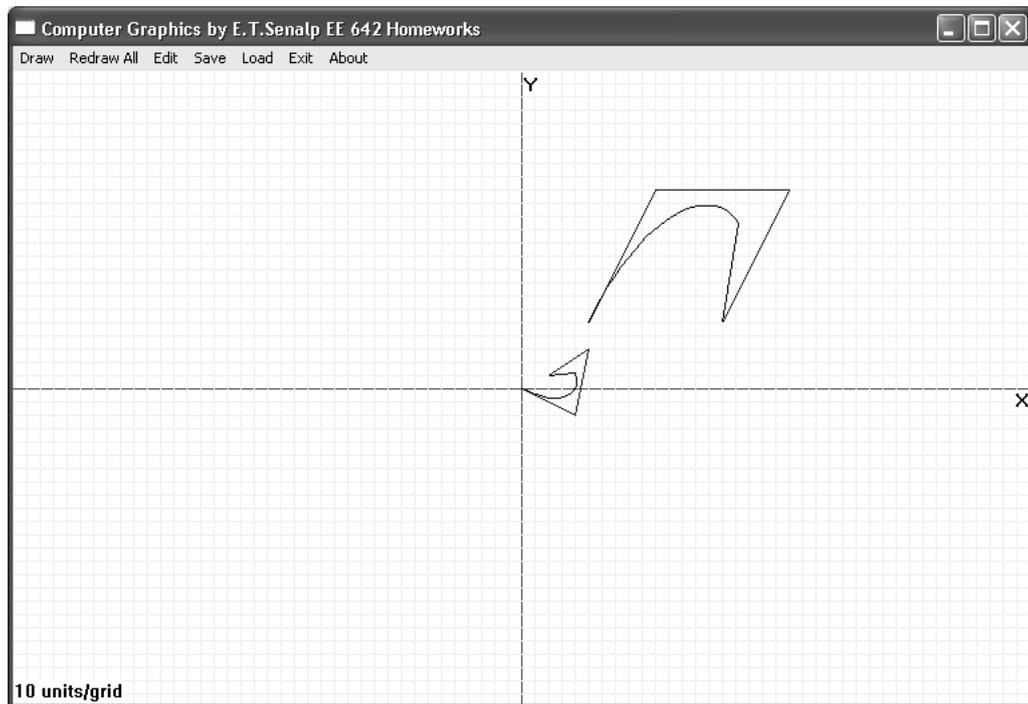
Figure 1.5. Examples of B-Spline curves and their defining polygons on Cartesian space

Formulation of the B-Spline curves is as follows,

$$P(u) = \sum_{i=0}^{m} B_i . N_{i,s}\{u\} \qquad (1.25)$$

where

(m+1) is the number of defining polygon points,

u is the normalized variable between 0 and u_{max},

u_{max} is the maximum value of u, i.e.

$$u_{max} = m - s + 2 \qquad (1.26)$$

s is the order of the correspondent basis function; s-1 is the degree,

i is vertex number of the defining polygon,

B_i are the defining polygon points,

$N_{i,s}\{u\}$ are the normalized B-Spline basis functions,

$$N_{i,s}\{u\} = \frac{(u - z_i)N_{i,s-1}\{u\}}{z_{i+s-1} - z_i} + \frac{(z_{i+s} - u)N_{i+1,s-1}\{u\}}{z_{i+s} - z_{i+1}} \qquad (1.27)$$

$$N_{i,1}\{u\} = \begin{cases} 1, & if \quad z_i \le u \le z_{i+1} \\ 0, & otherwise \end{cases} \qquad (1.28)$$

z is the knot vector,

$$z_i = \begin{cases} 0, & if \quad i < s \\ i - s + 1, & if \quad s \le i \le m \\ m - s + 2, & if \quad i > m \end{cases} \qquad (1.29)$$

Similar to the Bezier curves, B-Spine curves lie within the convex hull of their defining polygons. All points of a B-Spline curve lie in convex hull defined by taking defining polygon vertices following each other [Rogers and Adams, 1990].

To the best knowledge of the author, in this work, static nonlinear block of a cascade model is represented by B-Spline curves for the first time [Senalp et al., 2006d]. The internal variables of the METU-C model, i.e. $x_q(k)$, may be formulated as follows,

$$x_q(k) = \sum_{p=1}^{R} f[u_p(k)] = \sum_{p=1}^{R} \sum_{i=0}^{m} B_{pi}.N_{i,s}\{u_p(k)\} \qquad (1.30)$$

where

R is the number of inputs,

(m+1) is the number of defining polygon points,

$u_p(k)$ are the normalized input variables between 0 and u_{max},

u_{max} is the maximum value of u as in Equation 1.26,

s is the order of the correspondent basis function; s-1 is the degree,

i is vertex number of the defining polygon,

B_{pi} are the coefficients to be determined,

$N_{i,s}\{u_p(k)\}$ are the normalized B-Spline basis functions,

$$N_{i,s}\{u_p(k)\} = \frac{(u_p(k) - z_i)N_{i,s-1}\{u_p(k)\}}{z_{i+s-1} - z_i} + \frac{(z_{i+s} - u_p(k))N_{i+1,s-1}\{u_p(k)\}}{z_{i+s} - z_{i+1}} \quad (1.31)$$

$$N_{i,1}\{u_p(k)\} = \begin{cases} 1, & if \quad z_i \leq u_p(k) \leq z_{i+1} \\ 0, & otherwise \end{cases} \quad (1.32)$$

z is the knot vector as in Equation 1.29.

Thus, the product $R(m+1)$ gives the number of static block coefficients, i.e. B_{pi}, to be determined.

The output $y(k)$ is represented as,

$$y(k) = \sum_{q=1}^{S} \sum_{j=0}^{n} h_q(j).x_q(k-j) \quad (1.33)$$

where S is the number of the static internal variables, n is the number representing the history of the stored internal variables in memory. The output $y(k)$ is represented by using a dynamic linearity and by optimizing a linear relationship for the internal variables $x_q(k)$ and their past values $x_q(k-j)$ which constitute their history. Thus, the product $S(n+1)$ gives the number of dynamic internal variables. The coefficients of the linearity in Equation 1.33, i.e. $h_q(j)$, are also to be determined in the development stage.

CHAPTER 2

FORECASTING THE GPS TOTAL ELECTRON CONTENT VALUES BY A CASCADE MODELING TECHNIQUE WITH POLYNOMIAL NONLINEARITY REPRESENTATION

2.1 Introduction

Unpredictable variability of the ionospheric parameters due to disturbances limits the efficiency of communications, radar and navigation systems, which employ especially HF radio waves propagating via ionosphere. It also limits other frequency bands, i.e. the communication bands with the satellites. The Total Electron Content (TEC) is the number of electrons in a column of one meter-squared cross-section along a path through the ionosphere [Chilbolton Weather Web, 2004]. Forecasting TEC is crucial for satellite based navigation systems especially in the stormy space weather conditions.

The use of the Middle East Technical University Neural Network and Cascade Modeling (METU-NN-C) technique to forecast the 10 minutes values of the TEC, one hour ahead, during high solar activity in the solar cycle have been examined [Senalp et al., 2005] [Senalp et al., 2006c]. The model is designed to forecast TEC data evaluated from GPS measurements. The performance results of the cascade modeling of the near-Earth space processes are discussed in terms of system identification.

Applying nonlinear model identification is inevitable for most of the real complex nonlinear processes including the near-Earth space processes. The author has studies on structural methodologies, i.e. Neural Network based approaches, in modeling of the ionospheric processes [Senalp, 2001], [Tulunay E. et al., 2000], [Tulunay Y. et al., 2000], [Tulunay E. et al., 2001], [Tulunay Y. et al., 2001a], [Senalp et al., 2002a], [Tulunay Y. et al., 2004b], [Tulunay E. et al., 2004a] [Tulunay Y. et al., 2005a] [Tulunay E. et al., 2006a]. Those studies have provided insight on the system identification of the near-Earth space processes. In these previous studies, the processes were modeled in black box forms.

In this work, to the best knowledge of the author, it is the first time special models based on Hammerstein system modeling have been developed for near-Earth space processes [Senalp et al., 2005] [Senalp et al., 2006c].

The internal variables of the METU-C model have memory. They store the internal values of the present, one hour past, and two hours past. In the development mode, first of all, the internal variables of the METU-C model are estimated by using the METU-NN model [Tulunay Y. et al., 2004a] [Tulunay Y. et al., 2004b]. Then the estimated internal variables, and inputs and outputs of the METU-C model in development mode are used to optimize the parameters of the METU-C.

The METU-C model based on Hammerstein system modeling is designed and trained with significant inputs. In our approach, the basic inputs for the METU-C are temporal inputs and the polynomial representation of the present TEC value. In addition, the model also contains intrinsic information about the solar activity.

30

The development of the METU-NN-C models is demonstrated in Figure 1.2 in Chapter 1. The METU-C architecture has one static nonlinear block and one dynamic linear block cascaded as shown in Figure 1.1 in Chapter 1. Levenberg-Marquardt optimization algorithm is used in optimizing the nonlinear and linear block parameters. Then such trained model is used to forecast the TEC values 1 hour in advance.

This chapter outlines the TEC forecasting problem and preparation of data, explains the METU-C models based on Hammerstein system modeling as a system identification approach for forecasting ionospheric processes, gives the results with error tables, cross correlation coefficients and scatter diagrams, and discusses the generalized and fast learning and operation of the METU-C Models.

2.2 Preparation of Data

GPS TEC data for Chilbolton (51.8° N; 1.26° W) and Hailsham (50.9° N; 0.3° E) are used [COST271 WG 4 STSM, 2002]. For the training, test and validation within the development modes of the METU Neural Network and Cascade Models, TEC data evaluated from GPS measurements from 2000 to 2001 at Chilbolton receiving station are used. Operation has been performed on another validation data set by producing the forecast TEC values at Hailsham GPS receiving station for selected months in 2002. Table 2.1 summarizes selected training, validation within development and validation within operation time intervals.

Table 2.1. The time periods for the input data

	Year	Month
Train	2000	April and May
Test and validation in the development procedure	2001	April and May
Validation in the operational use	2002	April and May

The chosen years correspond to the similar solar activity. This is the basic criterion in the selection of the train, test and validation years. The current high solar activity time periods, i.e. years with high sunspot number values, are selected in the time intervals.

2.3 Construction of the Neural Network Model

The basic architecture of the METU-NN model is demonstrated in Figure 1.3 in Chapter 1. In METU-NN, for the current process, Feedforward Neural Network architecture with six neurons in one hidden layer is used.

The activation functions in the hidden layer are hyperbolic tangent sigmoid functions and the activation function in the output layer is a linear function, so that the hidden layer outputs represent the static part of the state-like internal variables in cascade modeling. Levenberg-Marquardt Backpropagation algorithm is used during training [Hagan and Menhaj, 1994] [Haykin, 1999]. The METU-NN is used to estimate the internal variables. The 5 inputs used for the METU-NN are as follows,

1. The present value of the TEC:

$$u_1(k) = f(k) \qquad (2.1)$$

2. Cosine component of the minute, m, of the day:

$$u_2(k) = C_m = -Cos(2.\pi.m / 1440) \qquad (2.2)$$

3. Sine component of the minute of the day:

$$u_3(k) = S_m = Sin(2.\pi.m / 1440) \qquad (2.3)$$

4. Cosine component of the day, d, of the year:

$$u_4(k) = C_d = -Cos(2.\pi.d / 366) \qquad (2.4)$$

5. Sine component of the day of the year:

$$u_5(k) = S_d = Sin(2.\pi.d / 366) \qquad (2.5)$$

The output layer of the METU-NN hosts the value of the TEC being observed 60 minutes later than the present time. The outputs of the hidden layer in METU-NN are six of the internal variables for the METU-C.

2.4 Construction of the Cascade Model

In the development mode, the construction work of the METU-C model is carried out. It is composed of "training phase" and "test phase" as in the Neural Network approach [Tulunay Y. et al., 2004a]. In the training phase the parameters of the cascaded static nonlinear block and dynamic linear block are optimized. For training and validation within development procedure, data sets of same month but different year are used as shown on Table 2.1 to take the seasonal dependency into account.

The "Levenberg-Marquardt" optimization algorithm is used within training for fast learning of the process with input data of very large size. If training data were used alone during training then the training error would go to zero

corresponding to the memorization. Memorization means the loss of the generalization capability in system identification. For preventing the memorization, independent validation data are used. The decrease in the validation error is noted during the development. When the gradient of the error in the validation within development becomes near zero, a "stop training" signal is produced, and thus the training is terminated. The optimized parameters of the cascade model are saved. The model is then ready for its use in the operation mode for forecasting of the TEC values. In the operation mode another validation data set is used for calculating the errors, point by point, to measure the performance of the model.

For considering the first, second and third order terms in the polynomial representation, i.e. the Equation 1.18, m is selected to be 3 for the TEC input. Thus, m=3 for p=1 in the model. For the temporal inputs m is selected to be 1, i.e. m=1 for p>1 in the model. The value of the TEC at the time instant k is designated by f(k). The 7 inputs used for the METU Cascade Model are as follows,

1. i. The present value of the TEC: $u_1(k) = $ f(k),

1. ii. Second Power: $u_1^2(k) = $ f ^{2}(k),

1.iii. Third Power: $u_1^3(k) = $ f ^{3}(k),

2. Cosine component of minute, m, of the day: $u_2(k) = C_m = -Cos(2\pi.m / 1440)$ is

3. Sine component of the minute of the day: $u_3(k) = S_m = Sin(2\pi.m / 1440)$,

4. Cosine component of day, d, of the year: $u_4(k) = C_d = -Cos(2\pi.d / 366)$,

5. Sine component of the day of the year: $u_5(k) = S_d = Sin(2\pi.d / 366)$,

The outputs of the first stage, i.e. 6 outputs for the static nonlinear block designated by $x_1(k),\ldots, x_6(k)$, and their one hour past and two hours past values are stored as internal variables so that S=6 and n=2 in Equation 1.19. These internal variables are the inputs to the second stage of the cascade model, i.e. 18 inputs for the dynamic linear block of the METU-C model, which are designated by $x_1(k),\ldots, x_6(k)$, $x_1(k-1),\ldots, x_6(k-1)$, $x_1(k-2),\ldots, x_6(k-2)$ in Equation 1.19. However, since the unit of the time instant k is minutes instead of hours, the internal variables are designated by $x_1(k),\ldots, x_6(k)$, $x_1(k-60),\ldots, x_6(k-60)$, $x_1(k-120),\ldots, x_6(k-120)$.

The output of the cascade model is designated by $y(k) = f(k+60)$ which is the value of the TEC to be observed 60 minutes later than the present time.

2.5 Results

The operation mode performance analyses and results of the TEC forecast cover the time interval between April and May 2002 for the Hailsham receiving station. Forecast of the TEC values one hour in advance is performed for the validation data set in 10 minutes interval. Then the cross correlation coefficients between the observed GPS TEC and forecast TEC are calculated. The root mean square, normalized and absolute error values are also calculated. Table 2.2 is the error table displaying the results. Figure 2.1 is the scatter diagram of the forecast and observed TEC values for Hailsham GPS receiving station for April and May 2002. Forecast and observed TEC values versus the order of data points in April and May 2002 for Hailsham GPS receiving station are plotted in Figure 2.2 where 1 hour in advance forecast values of the TEC are plotted with the solid line.

35

Table 2.2. Error Table

Absolute Error (TECu)	1.17
Normalized Error (%)	6.39
Root Mean Square Error (TECu)	1.79
Cross Correlation Coefficient (x10^{-2})	98.63
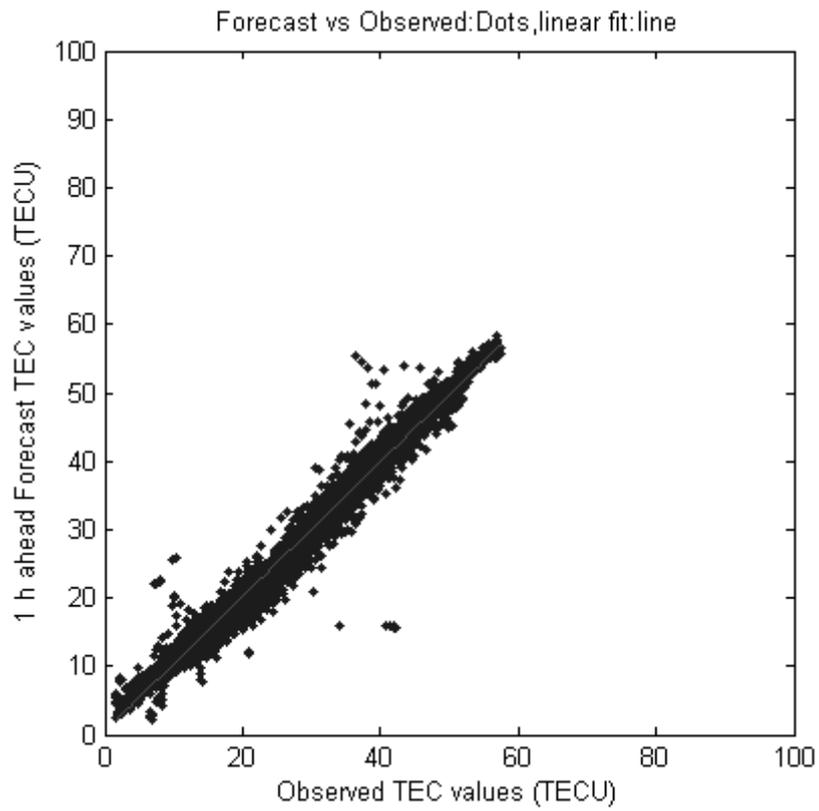
Figure 2.1. One hour ahead Forecast TEC versus Observed GPS TEC values
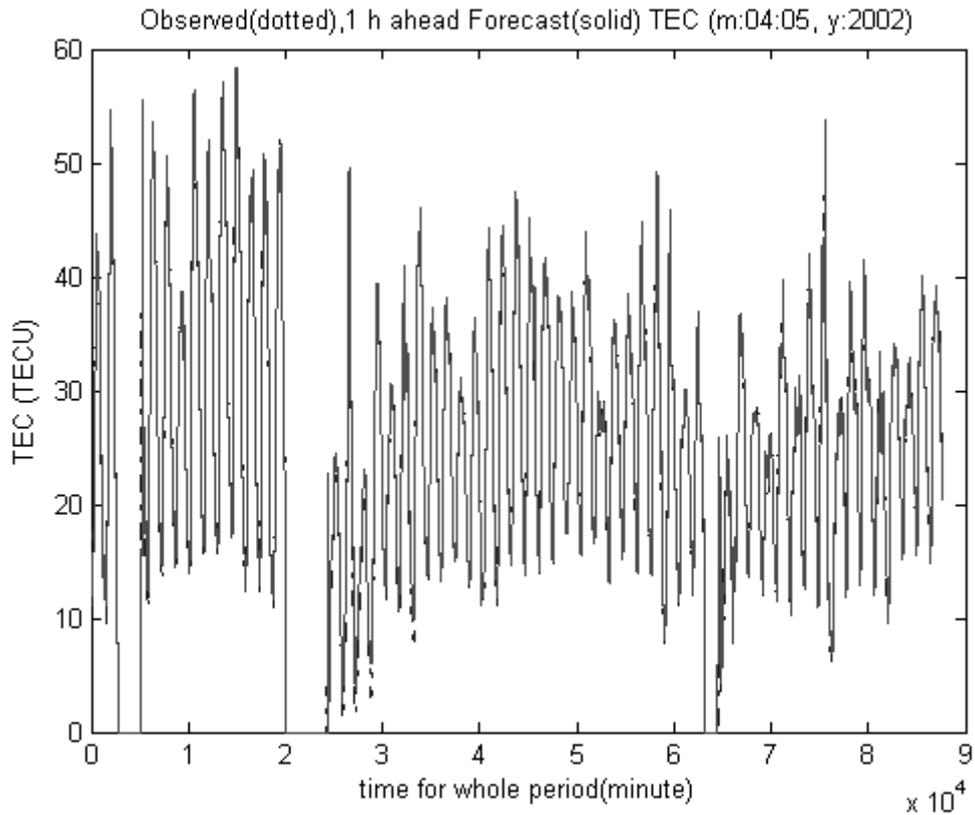
Figure 2.2. Observed GPS TEC (dotted) and 1 hour ahead Forecast (solid) TEC values for the whole time of validation period: April-May 2002 for Halisham.

In the scatter diagram in Figure 2.1, the fitted line has a slope close to one, i.e. it has ~ 45° of angle with respect to the observed TEC axis, and it passes through the origin. Therefore the forecasting errors are small. This fact is the indication of the system reaching the correct operating point within the system identification. In other terminology, the system is prevented to reach local minima and it is succeeded to reach the global minimum of the error cost function. The correlation coefficients are very close to unity, which means that

the METU-C model learned the shape of the inherent nonlinearities. Therefore, the deviations from straight line are small in the scatter diagram.

The daily solar-terrestrial indices for the geomagnetically quiet, 5-7 April 2002, and disturbed, 18-21 April 2002, periods of interest are summarized on Table 2.3 [Tulunay E. et al., 2004a].

Table 2.3 Solar-terrestrial indices for the considered validation periods

Date	RC	10CM	Ak	BKG	M	X
05 Apr 2002	213	217	004	C1.3	0	0
06 Apr 2002	249	206	004	C1.1	0	0
07 Apr 2002	211	208	010	C1.5	0	0
18 Apr 2002	155	188	043	C1.3	0	0
19 Apr 2002	147	180	045	B8.6	0	0
20 Apr 2002	224	177	056	C1.0	0	0
21 Apr 2002	142	173	006	C1.3	0	1

The Solar-terrestrial indices in Table 2.3 are as follows:

RC: Sunspot index from Catania Observatory (Italy),

10cm: 10.7 cm radioflux (DRAO, Canada)

Ak: Ak Index Wingst (Germany)

BKG: Background GOES X-ray level (NOAA, USA)

M,X: Number of X-ray flares in M and X class, (NOAA, USA)

Figure 2.3 and 2.4 are the enlarged portions of some data points of Figure 2.2, i.e. the diurnal variations of the observed, and forecast TEC values during 18-22 April 2002 and 5-7 April 2002, respectively. That is, the horizontal axes are expanded.
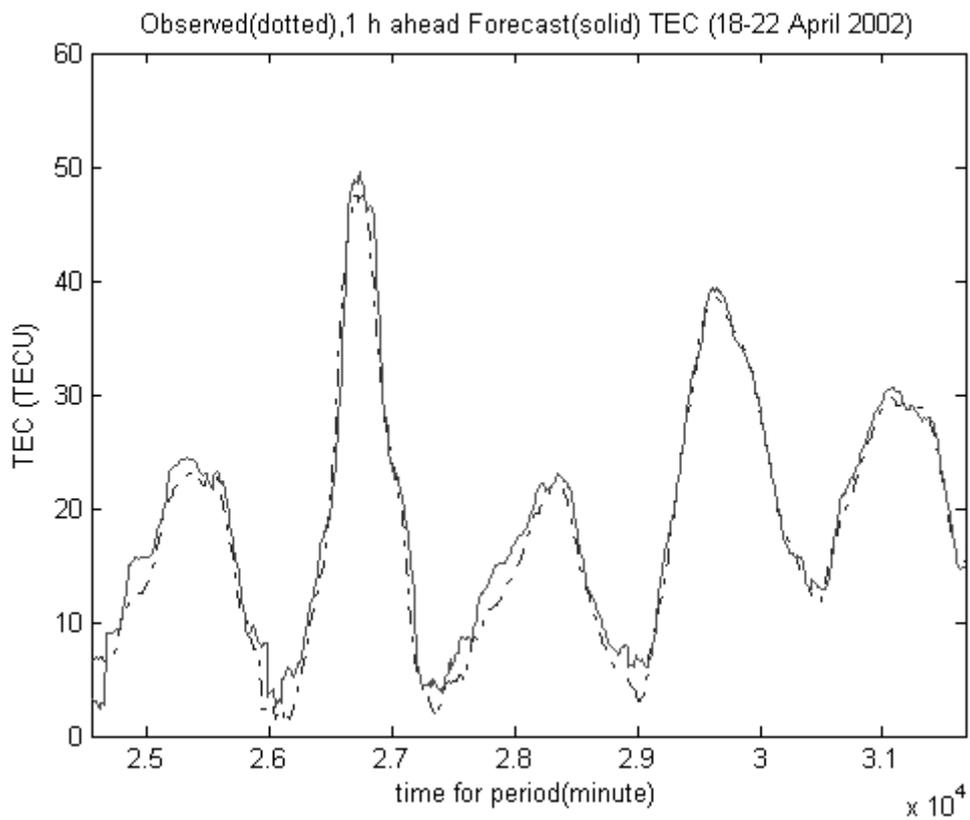
Figure 2.3. Observed GPS TEC values for disturbed solar-terrestrial conditions (dotted), and 1 hour ahead Forecast TEC values (solid) for the enlarged portion of the time of validation period: 18-22 April 2002.
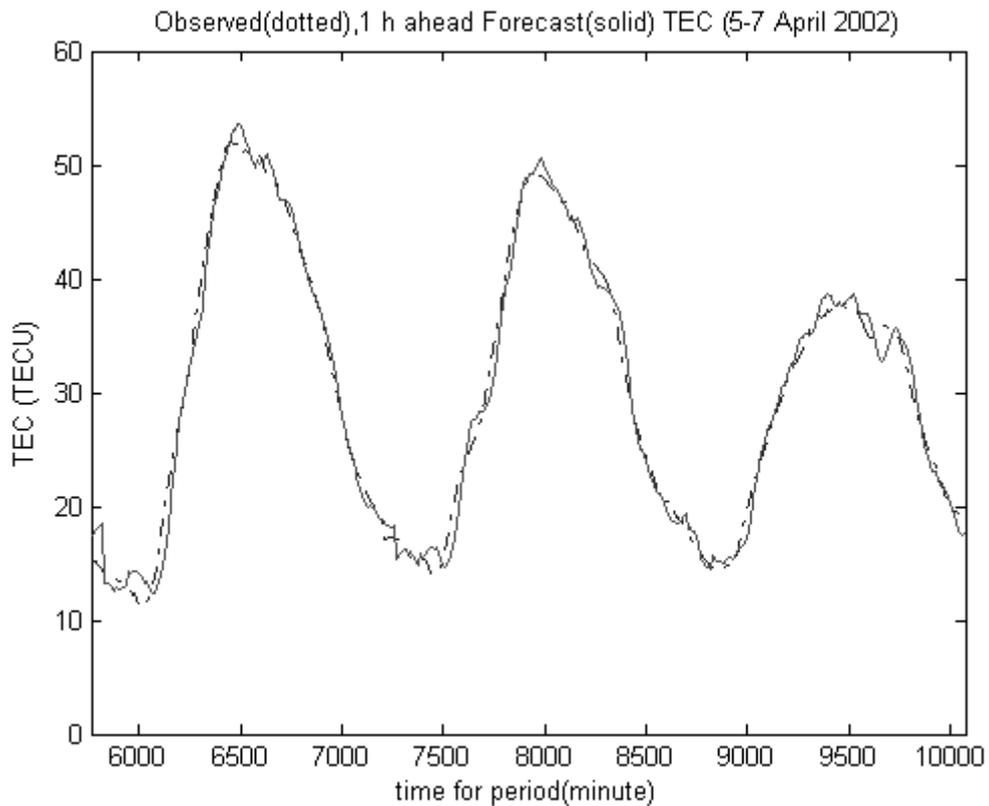
Figure 2.4. Observed GPS TEC values for quiet solar-terrestrial conditions (dotted), and 1 hour ahead Forecast TEC values (solid) for the enlarged portion of the time of validation period: 5-7 April 2002.

It can be concluded that the model gives accurate forecasts before, during and after the disturbed solar-terrestrial conditions.

2.6 Conclusions

Forecasting of the TEC values, especially in the stormy space weather conditions, is crucial for communication, radar and navigation systems

40

employing HF radio waves to cope with the effects of unpredictable variability of the ionospheric parameters.

In this work, to the best knowledge of the author, cascade modeling based on Hammerstein system modeling has been used first time for the forecast of an ionospheric-plasmaspheric process, namely the TEC variation 1 hour in advance [Senalp et al., 2005] [Senalp et al., 2006c]. The model learned the shape of the inherent nonlinearities and the system reached the correct operating point. The cascade modeling of the process is also capable of forecasting the TEC values for disturbed solar-terrestrial conditions.

It is demonstrated that the identification of the complex nonlinear processes, such as the TEC variation, can be achieved by cascading a static nonlinear block and a linear dynamic block as in the Hammerstein system modeling.

Summary of the main contributions of this work may be given as follows:

1) Organization of representable data for learning complex processes,
2) Cascade modeling of a highly complex nonlinear process such as the TEC variation, and
3) General demonstration of learning capability by calculating cross correlations and general demonstration of reaching a proper operating point by calculating errors.

CHAPTER 3

FORECASTING THE GPS TOTAL ELECTRON CONTENT VALUES BY A CASCADE MODELING TECHNIQUE WITH BEZIER CURVE NONLINEARITY REPRESENTATION

3.1 Introduction

The use of the Middle East Technical University Neural Networks and Cascade Modeling (METU-NN-C) technique to forecast the 10 minutes values of the total electron content (TEC), one hour ahead, during high solar activity in the solar cycle have been examined with the emphasis on Bezier curves in repsesenting the nonlinearities. To the best knowledge of the author, static nonlinear block of a cascade model, METU-C, based on Hammerstein system modeling is represented by Bezier curves for the first time [Senalp et al., 2006b] [Senalp et al., 2006d].

In this approach, the basic inputs for the model are the Bezier curve representation of the temporal inputs and the Bezier curve representation of the present TEC value. The internal variables store the internal values of the present, one hour past, and two hours past. They are estimated by METU-NN. Using the inputs, outputs, and estimated internal variables, Levenberg-Marquardt optimization algorithm is employed in optimizing the nonlinear and linear block parameters of the METU-C model in development mode. The

development of the METU-NN-C models is demonstrated in Figure 1.2 in Chapter 1. Then such trained model is used in operation mode to forecast the TEC values 1 hour in advance.

This chapter explains the METU-C model based on Hammerstein system modeling with Bezier curves as a system identification approach for forecasting ionospheric processes, gives the results with error tables, cross correlation coefficients and scatter diagrams, and discusses the generalized and fast learning and operation of the METU-C Models.

3.2 Preparation of Data

As in Chapter 2, for the training, test and validation within the development mode of the METU-NN-C, TEC data evaluated from GPS measurements in 1 April – 31 May 2000 and 2001 at Chilbolton (51.8º N; 1.26º W) receiving station are used. Operation has been performed on another data set by producing the forecast TEC values at Hailsham (50.9º N; 0.3º E) GPS receiving station for selected months in 2002.

In the model, again intrinsic information about the solar activity is achieved by choosing the time periods for input data with the similar solar activity. Also the seasonal dependency is again taken into account. Table 2.1 in Chapter 2 summarizes selected training, validation within development and validation within operation time intervals.

3.3 Construction of the Neural Network Based Model

The METU-NN model explained in Chapter 2 is used to estimate the internal variables of the METU-C model herewith. For more details refer Chapter 2.

3.4 Construction of the Cascade Model

The 5 inputs used for the METU-C are as follows,

1. The present value of the TEC: see Equation 2.1 in Chapter 2

2. Cosine component of minute, m, of the day: see Equation 2.2 in Chapter 2

3. Sine component of the minute of the day: see Equation 2.3 in Chapter 2

4. Cosine component of day, d, of the year: see Equation 2.4 in Chapter 2

5. Sine component of the day of the year: see Equation 2.5 in Chapter 2

The inputs are normalized so that they can be used in Bezier curve representation of the static nonlinearity in the METU-C model as in Equations 1.22 and 1.23 in Chapter 1. The output of the METU-C hosts the value of the TEC being observed 60 minutes later than the present time.

In this work, the internal variables of the METU-C model, i.e. $x_q(k)$, are formulated as in Equation 1.22, in Chapter 1. In Equation 1.22, $R = 5$ is the number of inputs, $m + 1 = 3 + 1 = 4$ is the number of defining polygon points. Thus, the product $R(m + 1) = 5(3 + 1) = 20$ gives the number of static block coefficients, i.e. B_{pi}, to be determined.

The output $y(k)$ is represented as shown in Equation 1.24 in Chapter 1. It is represented by using a dynamic linearity obtained by optimizing a linear relationship for the internal variables, $x_q(k)$, and their past values, $x_q(k - j)$. In the Equation 1.24, $S = 6$ is the number of the static internal variables, $n = 2$ is the number representing the history of the stored internal variables in memory. Thus, the product $S(n + 1) = 6(2 + 1) = 18$ gives the number of dynamic internal variables. The coefficients of the linearity in Equation 1.24, i.e. $h_q(j)$, are also determined in the development mode.

In the development mode, the parameters of the METU-C are determined using the internal variable estimates of the METU-C obtained by the METU-NN, and the inputs and outputs of the METU-C. Levenberg-Marquardt optimization method is used in training.

3.5 Results

As in Chapter 2, the operation mode performance analyses and results of the TEC forecast cover the time interval between April and May 2002 for the Hailsham receiving station. Forecast of the TEC values one hour in advance is performed for the validation data set in 10 minutes interval. Then the cross correlation coefficients between the observed GPS TEC and forecast TEC are calculated. The root mean square, normalized and absolute error values are also calculated. Table 3.1 is the error table displaying the results.

Table 3.1. Error Table

Absolute Error (TECu)	1.11
Normalized Error (%)	5.51
Root Mean Square Error (TECu)	1.75
Cross Correlation Coefficient $(x10^{-2})$	98.69

It is to be noted that the error values in this work are smaller than the ones in Chapter 2. Also the cross-correlation coefficient is larger than the one in Chapter 2. Thus, modeling the nonlinearity by using Bezier curves provide remarkable increase in the operation performance with higher accuracy and

higher sensitivity when compared with the operation results of the METU-C model with polynomial nonlinearity representation discussed in Chapter 2.

Figure 3.1 is the scatter diagram of the forecast and observed TEC values for Hailsham GPS receiving station for April and May 2002. Forecast and observed TEC values versus the order of data points in April and May 2002 for Hailsham GPS receiving station are plotted in Figure 3.2 where 1 hour in advance forecast values of the TEC are plotted with the solid line.
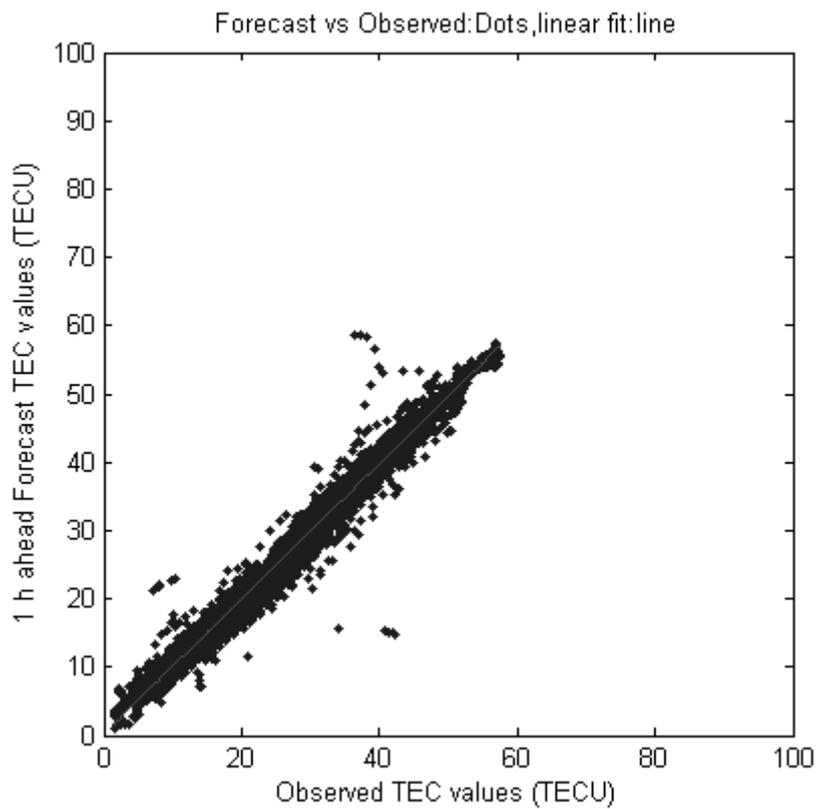
Figure 3.1. One hour ahead Forecast TEC versus Observed GPS TEC values
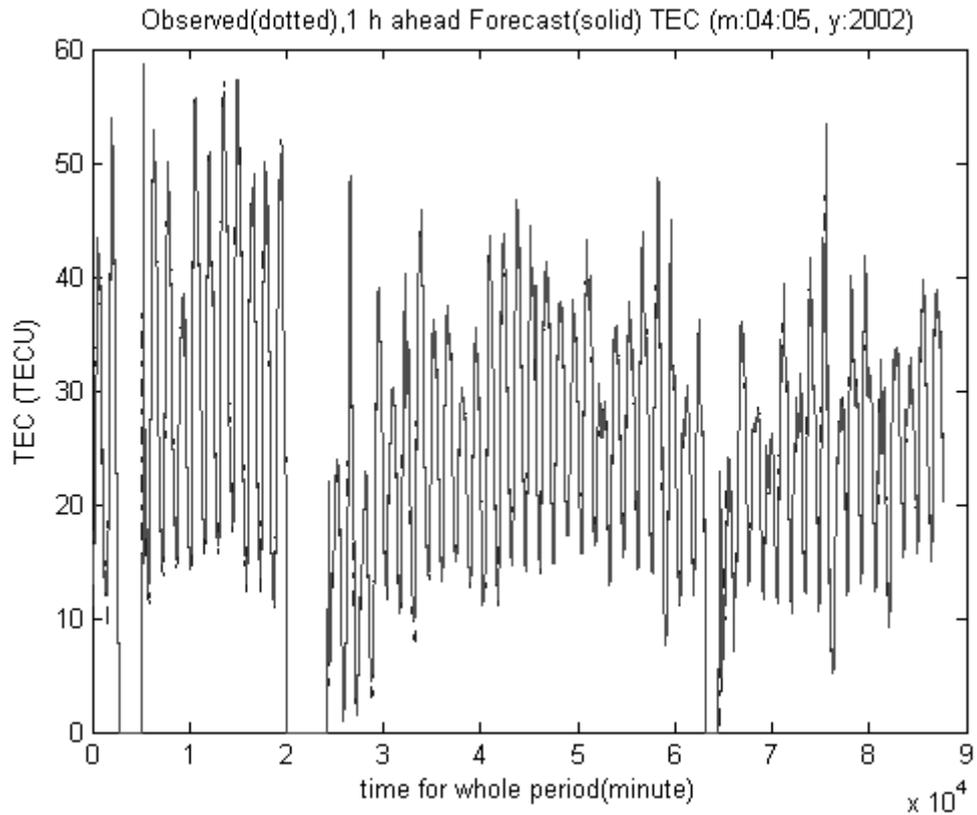
Figure 3.2. Observed GPS TEC (dotted) and 1 hour ahead Forecast (solid) TEC values for the whole time of validation period: April-May 2002 for Halisham.

The system reached the correct operating point within the system identification. Thus the fitted line in the scatter diagram in Figure 3.1 has a slope close to one, passes through the origin, and the forecasting errors are small. Also the METU-C model learned the shape of the inherent nonlinearities. Thus the deviations from straight line are small in the scatter diagram, and the correlation coefficients are very close to unity.

47

The daily solar-terrestrial indices for the geomagnetically quiet, 5-7 April 2002, and disturbed, 18-21 April 2002, periods of interest are summarized on Table 2.3 in Chapter 2. Figures 3.3 and 3.4 are the enlarged portions of some data points of Figure 3.2, i.e. the diurnal variations of the observed, and forecast TEC values during 18-22 April 2002 and 5-7 April 2002, respectively.
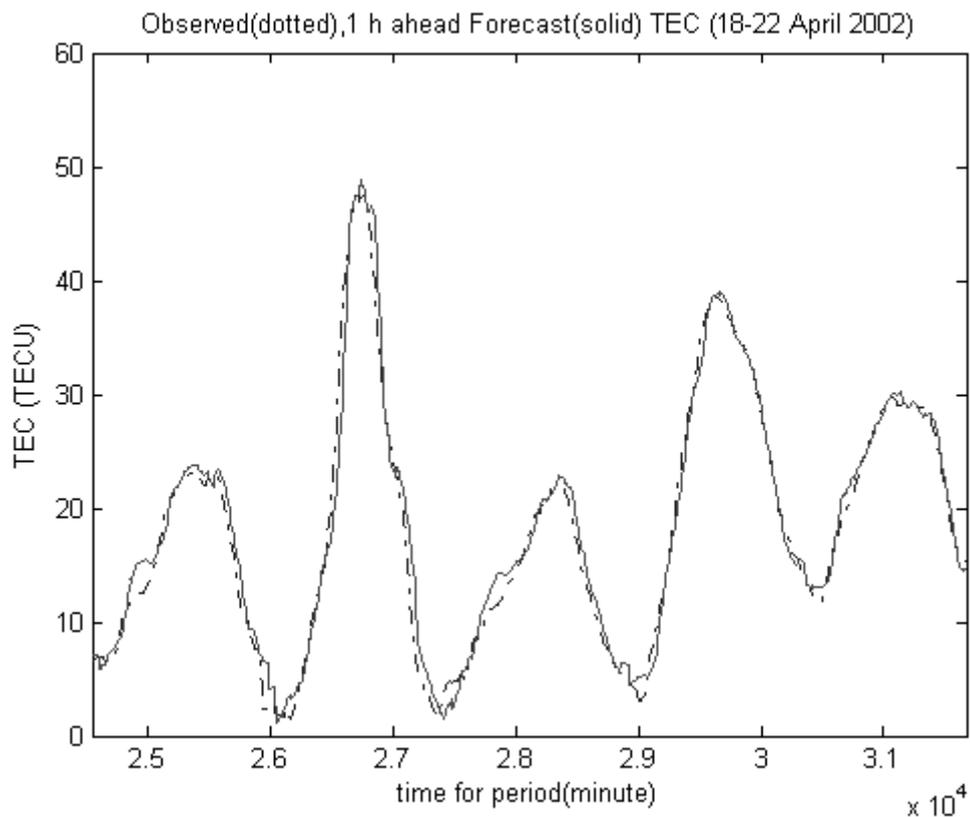
Figure 3.3. Observed GPS TEC values for disturbed solar-terrestrial conditions (dotted), and 1 hour ahead Forecast TEC values (solid) for the enlarged portion of the time of validation period: 18-22 April 2002.
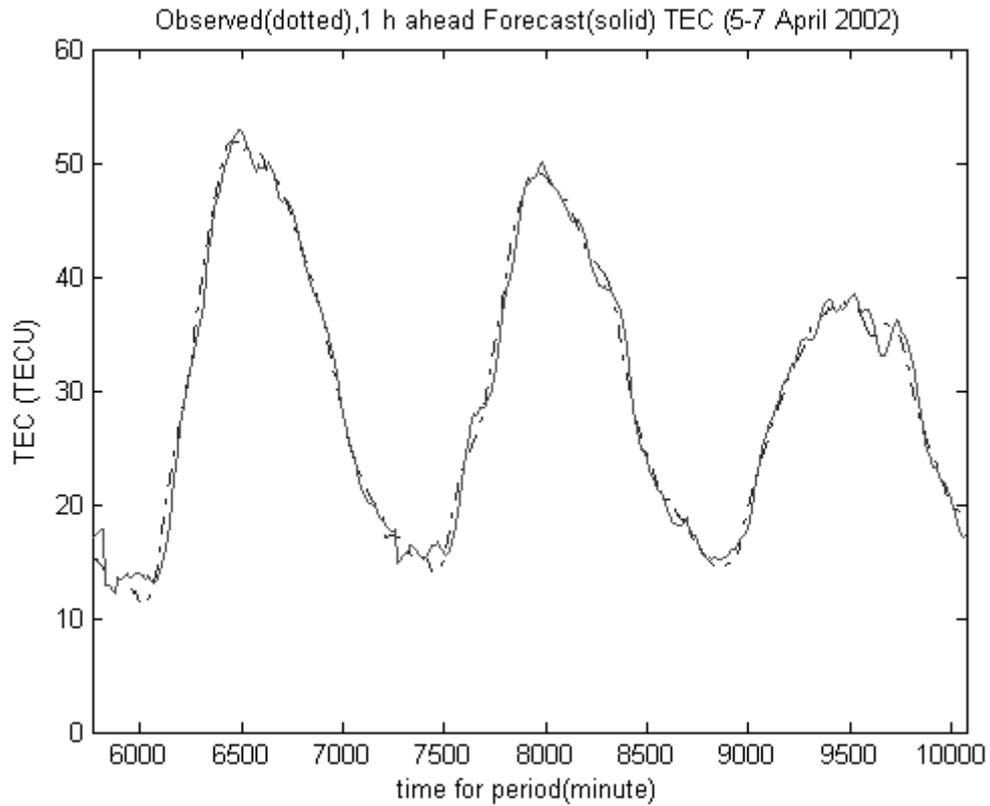
Figure 3.4. Observed GPS TEC values for quiet solar-terrestrial conditions (dotted), and 1 hour ahead Forecast TEC values (solid) for the enlarged portion of the time of validation period: 5-7 April 2002.

The model gives accurate forecasts before, during and after the disturbed solar-terrestrial conditions.

3.6 Conclusions

In this work, to the best knowledge of the author, static nonlinear block of a cascade model, METU-C, based on Hammerstein system modeling is

49

represented by Bezier curves for the first time [Senalp et al., 2006b] [Senalp et al., 2006d]. The forecast of the ionospheric-plasmaspheric process, namely the TEC variation 1 hour in advance is performed. The model learned the shape of the inherent nonlinearities and the system reached the correct operating point. The cascade modeling of the process is also capable of forecasting the TEC values for disturbed solar-terrestrial conditions.

It is demonstrated that the identification of the complex nonlinear processes, such as the TEC variation, can be achieved by cascading a static nonlinear block of Bezier curve representations and a linear dynamic block.

CHAPTER 4

FORECASTING THE GPS TOTAL ELECTRON CONTENT VALUES BY A CASCADE MODELING TECHNIQUE WITH B-SPLINE CURVE NONLINEARITY REPRESENTATION

4.1 Introduction

The use of the Middle East Technical University Neural Networks and Cascade Modeling (METU-NN-C) technique to forecast the 10 minutes values of the total electron content (TEC), one hour ahead, during high solar activity in the solar cycle have been examined with the emphasis on B-Spline curves in repsesenting the nonlinearities. To the best knowledge of the author, static nonlinear block of a cascade model, METU-C, based on Hammerstein system modeling is represented by B-Spline curves for the first time [Senalp et al., 2006d].

In this approach, the basic inputs for the model are the B-Spline curve representation of the temporal inputs and the B-Spline curve representation of the present TEC value. The internal variables store the internal values of the present, one hour past, and two hours past. They are estimated by METU-NN. Using the inputs, outputs, and estimated internal variables, Levenberg-Marquardt optimization algorithm is employed in optimizing the nonlinear and linear block parameters of the METU-C model in development mode. The

development of the METU-NN-C models is demonstrated in Figure 1.2 in Chapter 1. Then such trained model is used in operation mode to forecast the TEC values 1 hour in advance. This chapter explains the METU-C model based on Hammerstein system modeling with B-Spline curves as a system identification approach for forecasting ionospheric processes, gives the results with error tables, cross correlation coefficients and scatter diagrams, and discusses the generalized and fast learning and operation of the METU-C Models.

4.2 Preparation of Data

As in Chapter 2, for the training and validation within development mode of the METU-NN-C, TEC data evaluated from GPS measurements at Chilbolton (51.8º N; 1.26º W) receiving station in 1 April – 31 May 2000 and 2001 are used, respectively. Operation has been performed on another data set by producing the forecast TEC values at Hailsham (50.9º N; 0.3º E) GPS receiving station for selected months in 2002.

In the model, again intrinsic information about the solar activity is achieved by choosing the time periods for input data with the similar solar activity. Also the seasonal dependency is again taken into account. Table 2.1 in Chapter 2 summarizes selected training, validation within development and validation within operation time intervals.

4.3 Construction of the Neural Network Based Model

The METU-NN model explained in Chapter 2 is used to estimate the internal variables of the METU-C model. For more details refer Chapter 2.

4.4 Construction of the Cascade Model

The 5 inputs used for the METU-C are as follows,

1. The present value of the TEC: see Equation 2.1 in Chapter 2

2. Cosine component of minute, *m*, of the day: see Equation 2.2 in Chapter 2

3. Sine component of the minute of the day: see Equation 2.3 in Chapter 2

4. Cosine component of day, *d*, of the year: see Equation 2.4 in Chapter 2

5. Sine component of the day of the year: see Equation 2.5 in Chapter 2

The inputs are normalized so that they can be used in B-Spline curve representation of the static nonlinearity in the METU-C model as in Equations 1.30, 1.31 and 1.32 in Chapter 1. The output of the METU-C hosts the value of the TEC being observed 60 minutes later than the present time.

In this work, the internal variables of the METU-C model, i.e. $x_q(k)$, are formulated as in Equation 1.30, in Chapter 1. In Equation 1.30, s = 4 is the order of the correspondent basis function, s-1 = 3 is the degree, $R = 5$ is the number of inputs, $m+1 = 3+1 = 4$ is the number of defining polygon points. Thus, the product $R(m+1) = 5(3+1) = 20$ gives the number of static block coefficients, i.e. B_{pi}, to be determined.

The output $y(k)$ is represented as shown in Equation 1.33 in Chapter 1. It is represented using a dynamic linearity which is obtained by optimizing a linear relationship for the internal variables, $x_q(k)$, and their past values, $x_q(k-j)$. In the Equation 1.33, $S = 6$ is the number of the static internal variables, $n = 2$ is the number representing the history of the stored internal variables in memory. Thus, the product $S(n+1) = 6(2+1) = 18$ gives the number of

dynamic internal variables. The coefficients of the linearity in Equation 1.33, i.e. $h_q(j)$, are also determined in the development mode.

In the development mode, the parameters of the METU-C are determined using the internal variable estimates of the METU-C obtained by the METU-NN, and the inputs and outputs of the METU-C model. Levenberg-Marquardt optimization method is used in training.

4.5 Results

As in Chapter 2, the operation mode performance analyses and results of the TEC forecast cover the time interval between April and May 2002 for the Hailsham receiving station. Forecast of the TEC values one hour in advance is performed for the validation data set in 10 minutes interval. Then the cross correlation coefficients between the observed GPS TEC and forecast TEC are calculated. The root mean square, normalized and absolute error values are also calculated. Table 4.1 is the error table displaying the results.

Table 4.1. Error Table

Absolute Error (TECu)	1.10
Normalized Error (%)	5.5
Root Mean Square Error (TECu)	1.75
Cross Correlation Coefficient ($x10^{-2}$)	99

It is to be noted that the error values in this work are smaller than the ones in Chapter 2. Also the cross-correlation coefficient is larger than the one in Chapter 2. Thus, modeling the nonlinearity by using B-Spline curves provide remarkable increase in the operation performance with higher accuracy and higher sensitivity when compared with the operation results of the METU-C model with polynomial nonlinearity representation discussed in Chapter 2. When the results of the model using B-Spline curves are compared with the results of the model using Bezier curves in Chapter 3, it is noted that two models have similar performance. However, the METU-C model with B-Spline curve nonlinearity representations has higher number of calculations than the model using Bezier curves because of the high complexity in the formulations of the B-Spline curves and their basis functions. It can be a drawback for very complex processes.

Figure 4.1 is the scatter diagram of the forecast and observed TEC values for Hailsham GPS receiving station for April and May 2002.
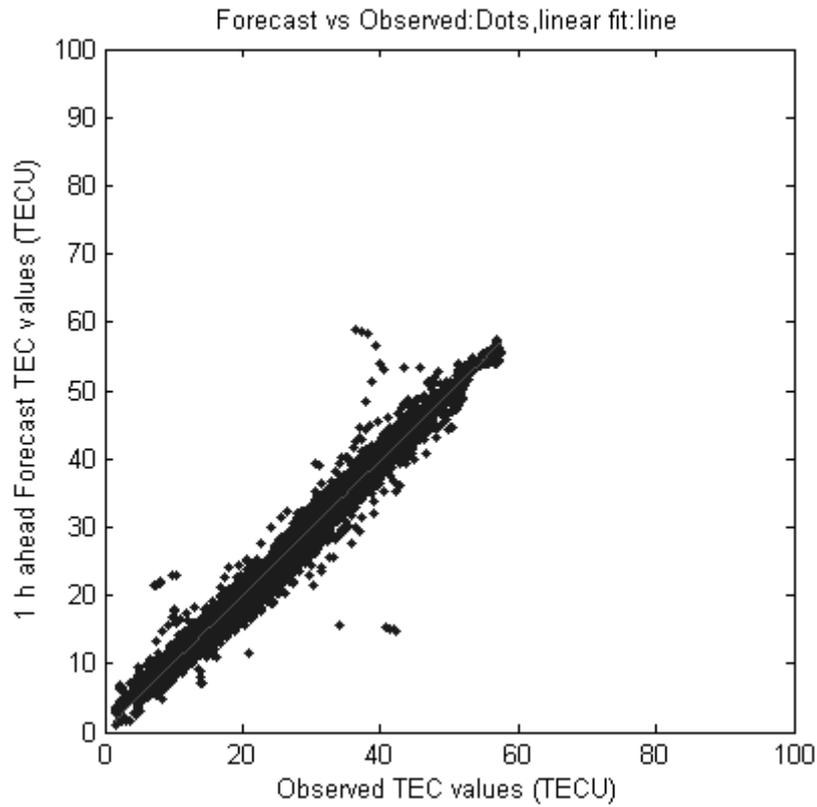
Figure 4.1. One hour ahead Forecast TEC versus Observed GPS TEC values

Forecast and observed TEC values versus the order of data points in April and May 2002 for Hailsham GPS receiving station are plotted in Figure 4.2 where 1 hour in advance forecast values of the TEC are plotted with the solid line.

In METU-C modeling with B-Spline curve nonlinearity representations, the system reached the correct operating point within the system identification and the METU-C model learned the shape of the inherent nonlinearities, as well.
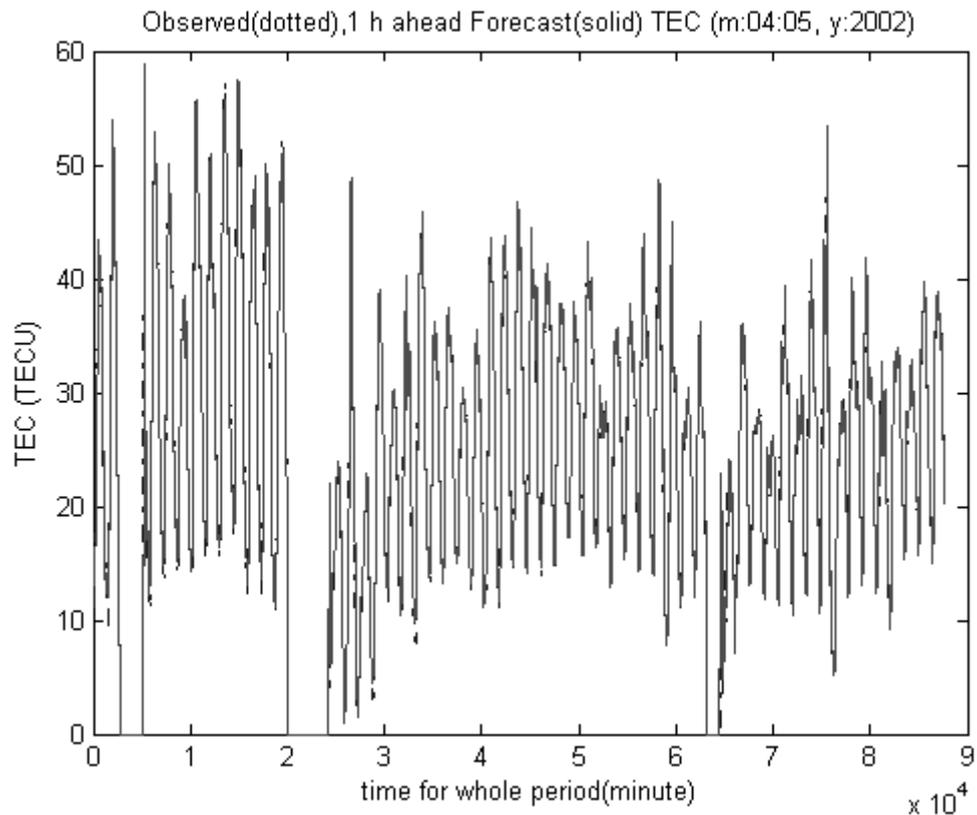
Figure 4.2. Observed GPS TEC (dotted) and 1 hour ahead Forecast (solid) TEC values for the whole time of validation period: April-May 2002 for Halisham.

The daily solar-terrestrial indices for the geomagnetically quiet, 5-7 April 2002, and disturbed, 18-21 April 2002, periods of interest are summarized on Table 2.3 in Chapter 2.

Figures 4.3 and 4.4 are the enlarged portions of some data points of Figure 4.2, i.e. the diurnal variations of the observed, and forecast TEC values during 18-22 April 2002 and 5-7 April 2002, respectively. It can again be concluded that

the model gives accurate forecasts before, during and after the disturbed solar-terrestrial conditions.
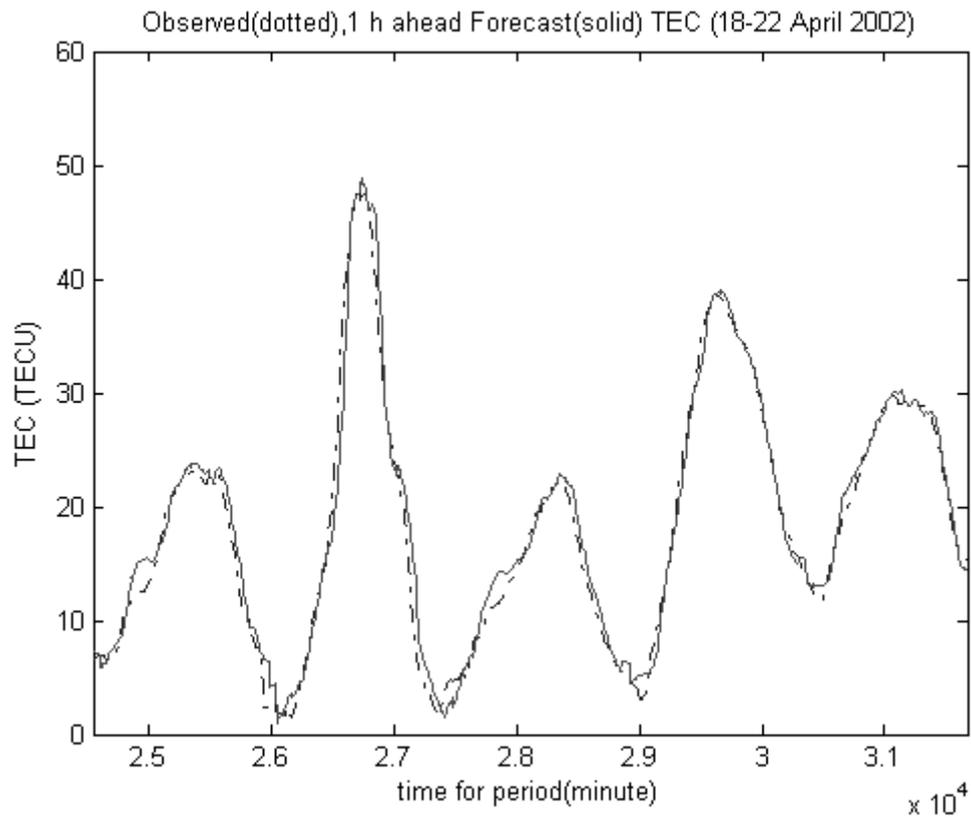
Figure 4.3. Observed GPS TEC values for disturbed solar-terrestrial conditions (dotted), and 1 hour ahead Forecast TEC values (solid) for the enlarged portion of the time of validation period: 18-22 April 2002.
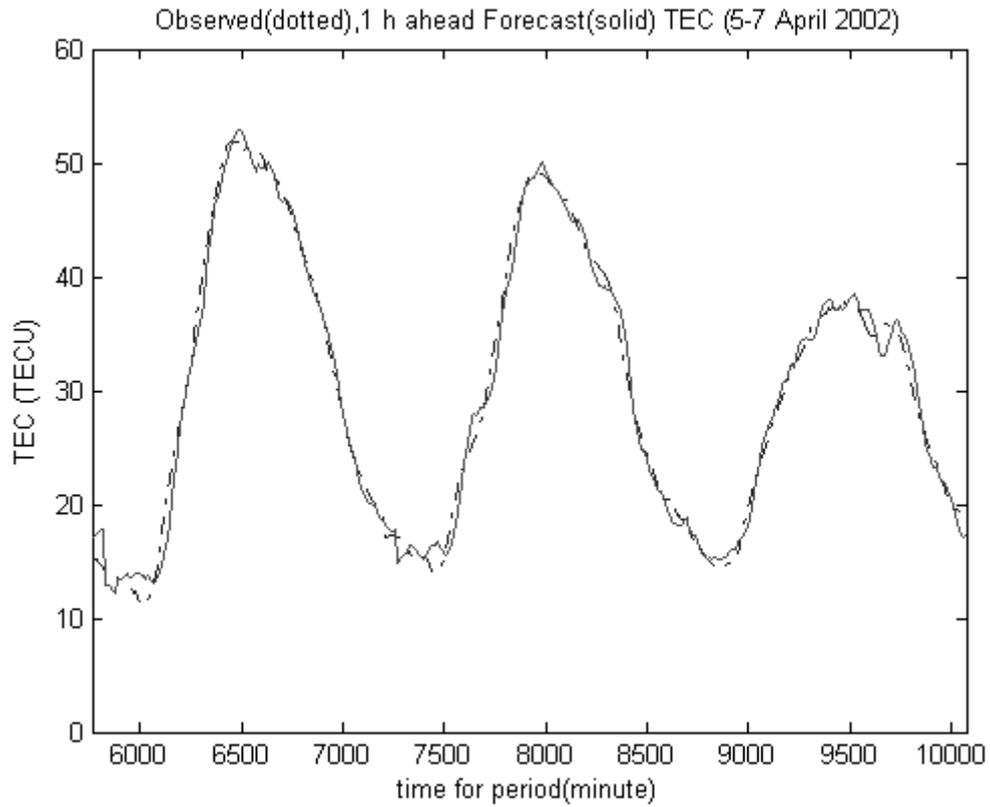
Figure 4.4. Observed GPS TEC values for quiet solar-terrestrial conditions (dotted), and 1 hour ahead Forecast TEC values (solid) for the enlarged portion of the time of validation period: 5-7 April 2002.

4.6 Conclusions

In this work, to the best knowledge of the author, static nonlinear block of a cascade model, METU-C, based on Hammerstein system modeling is represented by B-Spline curves for the first time [Senalp et al., 2006d]. The forecast of the ionospheric-plasmaspheric process, namely the TEC variation 1 hour in advance is performed. The model learned the shape of the inherent

59

nonlinearities and the system reached the correct operating point. The cascade modeling of the process is capable of forecasting the TEC values for disturbed conditions, as well.

It is demonstrated that the identification of the complex nonlinear processes, such as the TEC variation, can be achieved by cascading a static nonlinear block of B-Spline curve representations and a linear dynamic block.

CHAPTER 5

ERROR COMPARISON AND ANALYSIS FOR THE MODELS: METU-NN, METU-C WITH POLYNOMIAL, BEZIER AND B-SPLINE CURVE NONLINEARITY REPRESENTATIONS

5.1 Introduction

The use of the Middle East Technical University Neural Networks (METU-NN) technique and Middle East Technical University Neural Networks and Cascade Modeling (METU-NN-C) techniques to forecast the 10 minutes values of the total electron content (TEC), one hour ahead, during high solar activity in the solar cycle have been examined with the emphasis on Polynomials, Bezier curves and B-Spline curves in repsesenting the nonlinearities.

International Reference Ionosphere (IRI) is an important international project sponsored by the Committee on Space Research (COSPAR) and the International Union of Radio Science (URSI) [Bilitza, 2001] [IRI, 2007]. The aim of the project is to develop and improve the international IRI standards for the specification of ionospheric densities and temperatures [Bilitza, 2001]. The Center for Atmospheric Research in the University of Massachusetts Lowell (UMLCAR) adapted the IRI-2001 model to be used in MS-Windows platform

[UMLCAR, 2007]. In order to show the capabilities of the models, the results of the METU-C models have been compared with the UMLCAR edition of the IRI-2001 model results for the time period of interest during well-known Space Weather events of April 2002 [Senalp et al., 2007d]. The results have also been compared with the results of the METU-NN model.

The case study of METU-NN-C Model with Polynomial representation in nonlinearity was presented in Chapter 2. The case studies of METU-NN-C Models with Bezier Curve representation and B-Spline Curve representation in nonlinearity were presented in Chapter 3 and 4, respectively.

The construction work of the METU-NN and METU-NN-C models are carried out in the development mode. It is composed of "training phase or learning phase" and "test phase" [Tulunay Y. et al., 2004a]. METU-NN model for forecasting TEC and a case study using the model were presented [Tulunay E. et al., 2004a].

As in Chapter 2, 3 and 4, for the training and validation within the development mode of the METU-NN model, TEC data evaluated from GPS measurements in 1 April – 31 May 2000 and 2001 at Chilbolton (51.8º N; 1.26º W) receiving station have been used. Operation has been performed on another data set by producing the forecast TEC values at Hailsham (50.9º N; 0.3º E) GPS receiving station for selected months in 2002. The intrinsic information about the solar activity is again achieved by choosing the time periods for input data with the similar solar activity. Also the seasonal dependency is again taken into account. Table 2.1 in Chapter 2 summarizes selected training, validation within development and validation within operation time intervals.

The value of the TEC at the time instant k is designated by f(k). The output is f(k+60). It is the value of the TEC to be observed 60 minutes later than the present time. There are eight inputs fed into the METU-NN model. The eight input parameters are explained as follows,

1. The present value of the TEC, f(k): see Equation 2.1 in Chapter 2
2. First Difference,

$$\Delta_1(k) = f(k) - f(k\text{-}60) \tag{5.1}$$

3. Second Difference,

$$\Delta_2(k) = \Delta_1(k) - \Delta_1(k\text{-}60) \tag{5.2}$$

4. Relative Difference,

$$R\Delta(k) = \Delta_1(k) / f(k) \tag{5.3}$$

5. Cosine component of minute, *m*, of the day: see Equation 2.2 in Chapter 2
6. Sine component of the minute of the day: see Equation 2.3 in Chapter 2
7. Cosine component of day, d, of the year: see Equation 2.4 in Chapter 2
8. Sine component of the day of the year: see Equation 2.5 in Chapter 2

Among the various Neural Network structures the best configuration is found to be the one with one hidden layer. In the previous study [Tulunay E. et al., 2004a] 8 neurons were used in the hidden layer. In this study 6 hidden neurons were tried. No significant increases in the errors were observed. Therefore, in this work, the structure with 6 hidden neurons is preferred for the METU-NN instead of 8 for the sake of similar architecture as in the METU-NN-C models. There are eight inputs, six hidden neurons and 1 output in the feed-forward structure. Figure 1.3 in Chapter 1 shows the architecture of the Neural Network model. Here, the activation functions in the hidden layer are hyperbolic tangent sigmoid transfer functions and the activation function in the output layer is

pure linear transfer function. Levenberg-Marquardt Backpropagation algorithm is used in training.

In this chapter, the results of the models have been compared.

5.2 Test of Hypothesis

It is useful to make assumptions about the populations involved in order to reach statistical decisions on error values [Spiegel et al., 2000]. Such assumptions are called "statistical hypotheses". A "null hypothesis" denoted by H_0 occures when there is no difference between two decisions, i.e. any observed difference is due to fluctuations in sampling from the same population. Any hypothesis different from H_0 is called an "alternative hypothesis" and denoted by H_1. For example, if the null hypothesis is H_0: population mean: $\mu = 0.01$, then one possible alternative hypothesis may be H_1: $\mu \neq 0.01$ [Spiegel et al., 2000].

Procedures that help us to decide whether to accept or reject null hypothesis are called "tests of hypotheses" [Spiegel et al., 2000]. In testing a null hypothesis, the maximum probability with which we can risk an error is named as "level of significance" of the test. For example, $\alpha = 0.05$ level of significance means 95% confidence. [Spiegel et al., 2000].

One of the "tests of hypotheses" is "t-test" [MATLAB, 2002]. One tailed or two tailed t-tests can be used. Depending on the number of tails and the level of significance, critical values or z scores on the distribution plots can be found in lookup tables. As an example, Table 5.1 gives some of the critical values of z [Spiegel et al., 2000].

Table 5.1. Critical Values of z [Spiegel et al., 2000]

Level of Significance, α	0.10	0.05	0.01	0.005	0.002
Critical values of z for one-tailed tests	-1.28 or 1.28	-1.645 and 1.645	-2.33 or 2.33	-2.58 or 2.58	-2.88 or 2.88
Critical values of z for two-tailed tests	-1.645 and 1.645	-1.96 and 1.96	-2.58 and 2.58	-2.81 and 2.81	-3.08 and 3.08

To determine whether a sample from a normal distribution (x: i.e. errors) could have mean μ, t-test can be used [MATLAB, 2002]. In t-test, the test statistic is chosen to be as follows [Spiegel et al., 2000],

$$z = \frac{\bar{x} - \mu}{\sigma} \sqrt{n} \qquad (5.4)$$

where μ is the population mean, $\bar{x}$ is the sample mean, σ is the sample standard deviation, i.e. square root of varience, and n is the sample size.

As an example, if the level of significance, α, is 0.05, and two-tailed test is to be performed, then by using the Table 5.1 and the Equation 5.4, the interval of z can be obtained as,

$$-1.96 \le \frac{\bar{x} - \mu}{\sigma} \sqrt{n} \le 1.96 \qquad (5.5)$$

If z is not in the interval, then the result, h, is 1 and you can reject the null hypothesis that a sample from a normal distribution (x: errors) could have mean μ, at the significance level α. If h is 0, then you can not reject the null hypothesis at the α level of significance [MATLAB, 2002].

5.3 Error Distributions for METU-NN and METU-C Models

The error values, i.e. the difference of observed and forecast TEC values, are used in observing the distributions for the results of the four of the models. The models are METU-NN, METU-C with Polynomial nonlinearity, METU-C with Bezier nonlinearity, and METU-C with B-Spline nonlinearity.

The error histograms for four of the model results are plotted. In addition to those, the histograms of random samples from normal distributions with the same means and same standard deviations are plotted for four of the cases. Figures 5.1, 5.3, 5.5 and 5.7 are the error histograms for METU-NN, METU-C with polynomial nonlinearity, METU-C with Bezier curve nonlinearity, and METU-C with B-Spline curve nonlinearity model results, respectively. Figures 5.2, 5.4, 5.6 and 5.8 are the histograms of random samples from normal distributions with the same means and same standard deviations for four of the cases in Figures 5.1, 5.3, 5.5 and 5.7, respectively.
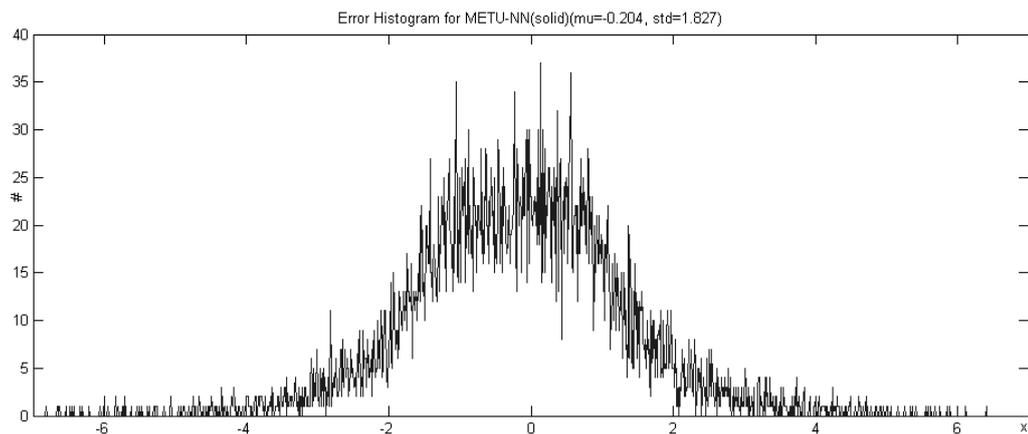
Figure 5.1. The error histogram for METU-NN model results.
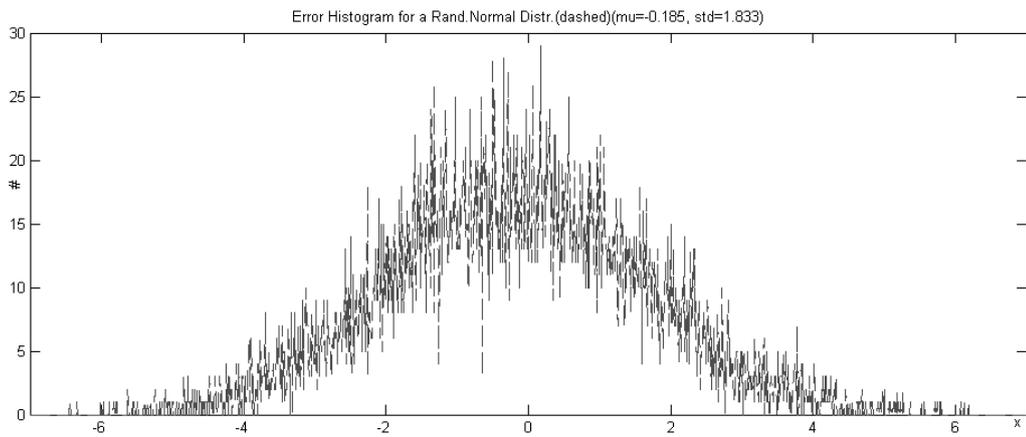
Figure 5.2. The histogram of a random sample from a normal distribution with the same mean and same standard deviation for the case in Figure 5.1.
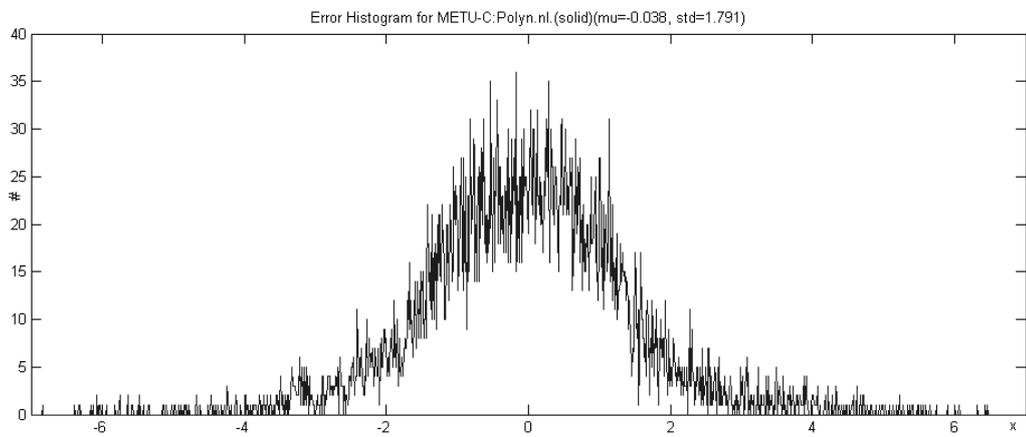
Figure 5.3. The error histogram for METU-C with Polynomial nonlinearity representation model results.
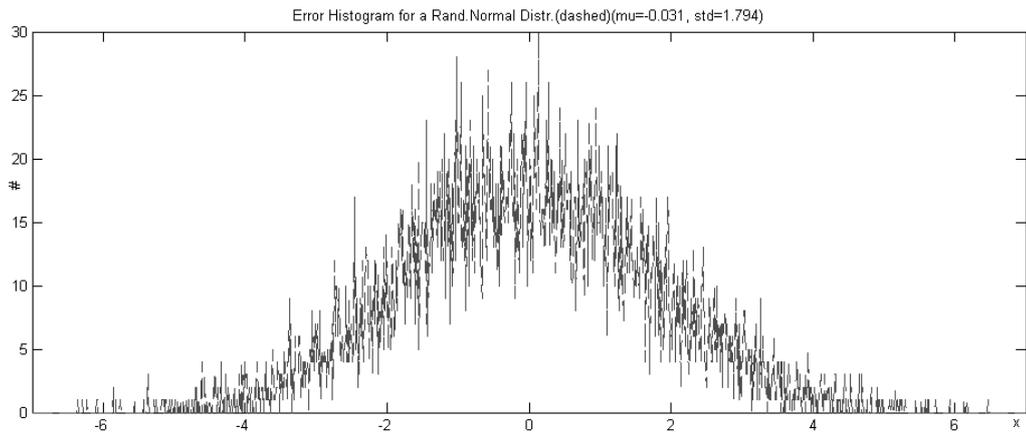
Figure 5.4. The histogram of a random sample from a normal distribution with the same mean and same standard deviation for the case in Figure 5.3.
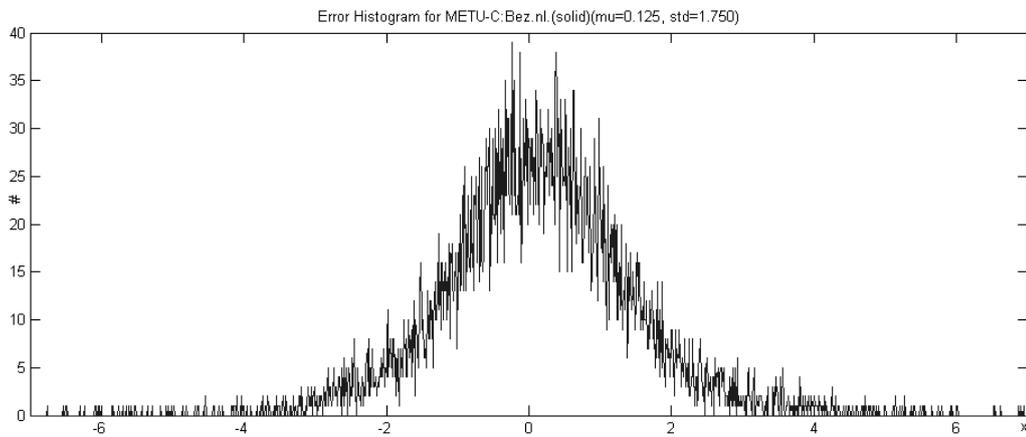
Figure 5.5. The error histogram for METU-C with Bezier curve nonlinearity representation model results.

68
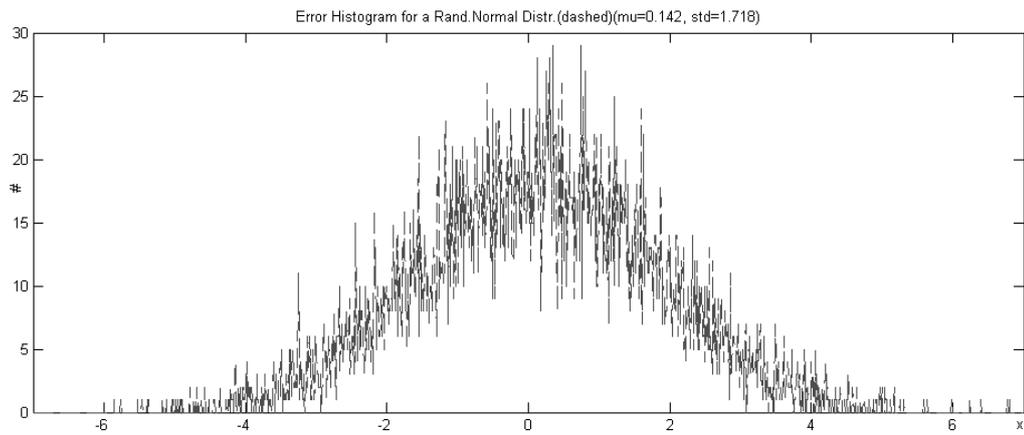
Figure 5.6. The histogram of a random sample from a normal distribution with the same mean and same standard deviation for the case in Figure 5.5.
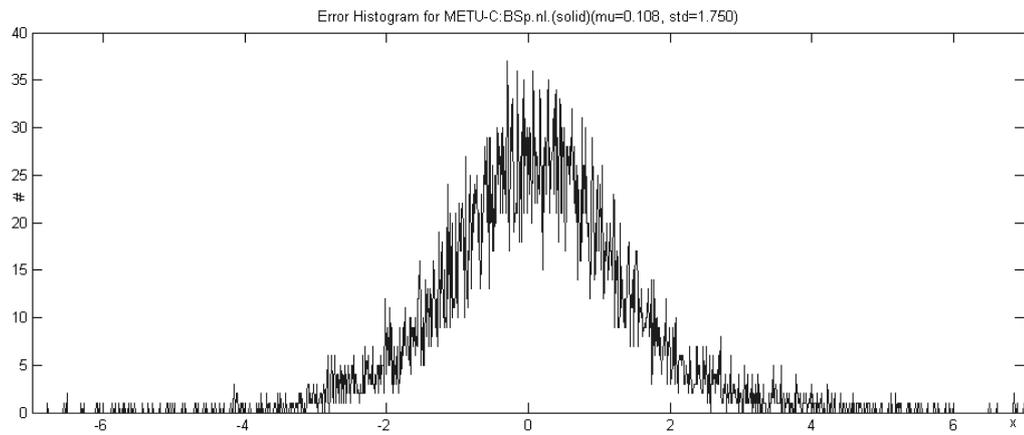
Figure 5.7. The error histogram for METU-C with B-Spline curve nonlinearity representation model results.
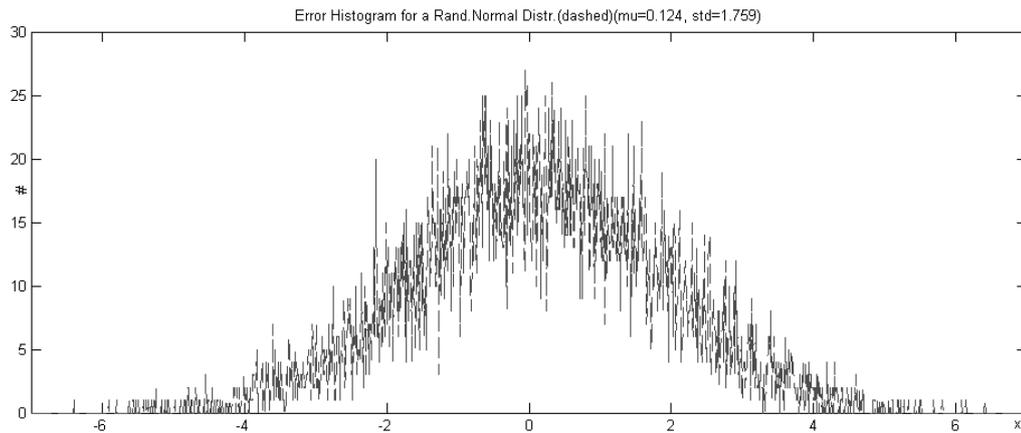
Figure 5.8. The histogram of a random sample from a normal distribution with the same mean and same standard deviation for the case in Figure 5.7.

The empirical cumulative distribution function (CDF) plots have qualitative visual values. In addition to those, they are useful for general-purpose goodness-of-fit hypothesis testing, such as the Kolmogorov-Smirnov tests. In those tests the test statistic is the largest deviation of the empirical CDF from a hypothesized theoretical CDF [MATLAB, 2002]. For each of the model, empirical cumulative distribution function (CDF) of the error values in the data sample is plotted. Superimposeed to this, the CDF of a random sample from a normal distribution with the same mean and same standard deviation is plotted for each case. Figures 5.9, 5.10, 5.11, and 5.12 have the empirical CDF plots (in solid) for METU-NN, METU-C with polynomial nonlinearity, METU-C with Bezier curve nonlinearity, and METU-C with B-Spline curve nonlinearity model results, respectively. Superimposed to those, the empirical CDF plots (in dashed) for random samples from normal distributions with the same means and same standard deviations for four of the cases.

70

F(x)of Err.Hist.for METU-NN(solid)(mu=-0.204, std=1.827) and Rand.Nor.Distr.(dashed)
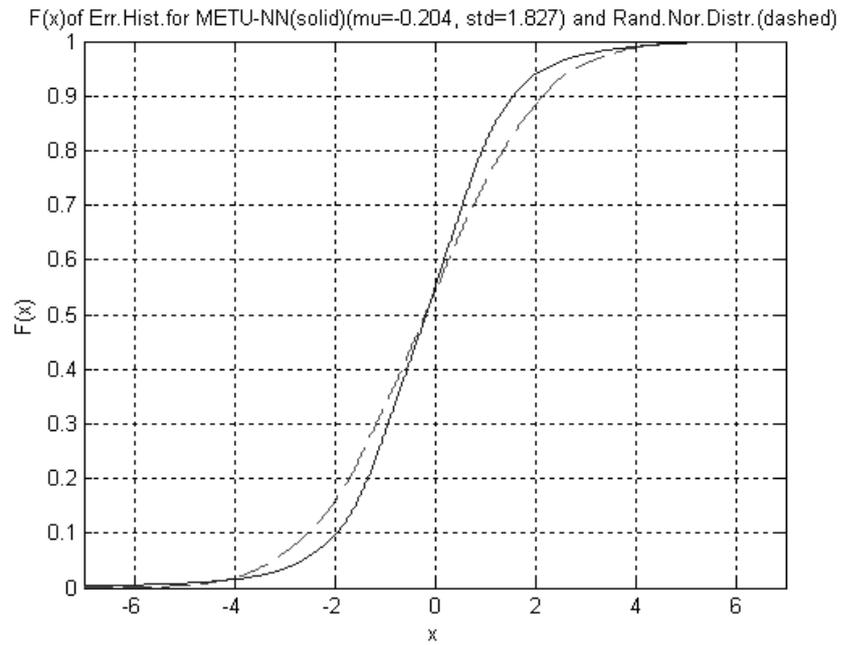
Figure 5.9. The empirical CDF plots for METU-NN model results (solid), and for random sample from a normal distr. with the same μ and same σ (dashed).

F(x)of Err.Hist.for METU-C:Polyn.nl.(solid)(mu=-0.038, std=1.791) and Rand.Nor.Distr.(dashed)
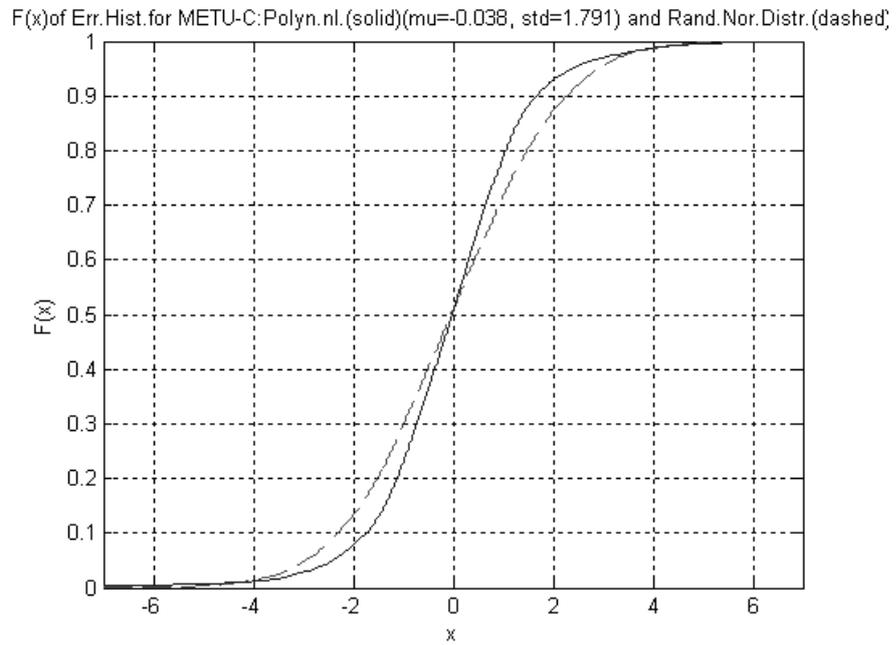
Figure 5.10. The empirical CDF plots for METU-C with Polynomial
nonlinearity representation model results (solid), and for random sample from a
normal distr. with the same μ and same σ (dashed) for the case.

F(x)of Err.Hist.for METU-C:Bez.nl.(solid)(mu=0.125, std=1.750) and Rand.Nor.Distr.(dashed)
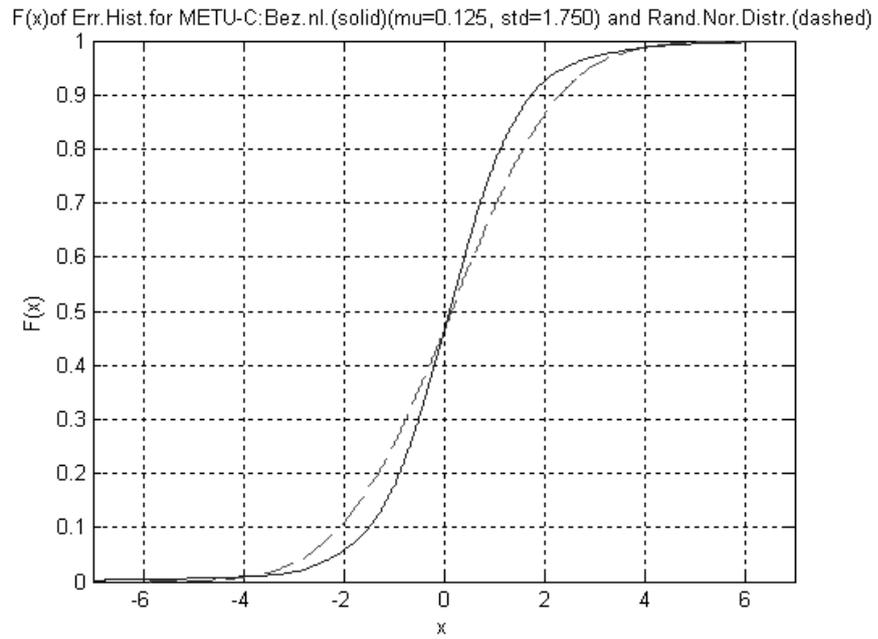
Figure 5.11. The empirical CDF plots for METU-C with Bezier curve nonlinearity representation model results (solid), and for random sample from a normal distr. with the same μ and same σ (dashed) for the case.

F(x)of Err.Hist.for METU-C:BSp.nl.(solid)(mu=0.108, std=1.750) and Rand.Nor.Distr.(dashed)
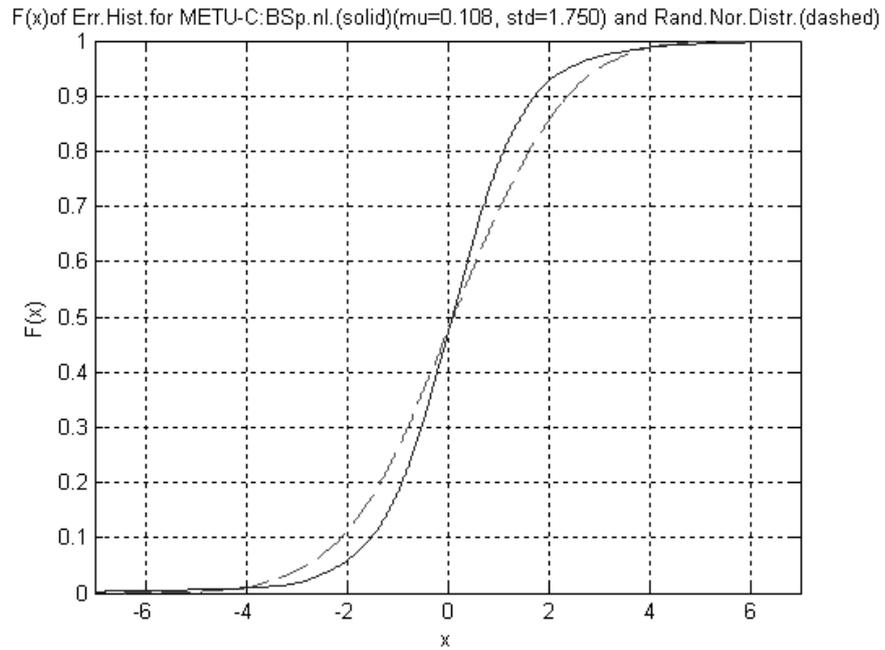
Figure 5.12. The empirical CDF plots for METU-C with B-Spline curve nonlinearity representation model results (solid), and for random sample from a normal distr. with the same μ and same σ (dashed) for the case.

When the empirical CDF are plotted, it is observed that the error distributions for the model results do not exactly fit to corresponding normal distributions, but a rough assumption that they fit to the normal distributions can be made.

In order to observe the deviations, each cumulative distribution can be plotted on the same x axis but this time on specially scaled y axis so that the normal distributions will fit to a line. Thus, when the plot is linear, it indicates that the sample can be modeled by a normal distribution. The plot is named as normal probability plot [MATLAB, 2002]. Each plot has the error statistic of the

corresponding model displayed with the symbol '+'. Superimposed is a robust linear fit of the sample order statistics [MATLAB, 2002]. To sum up, the purpose of a normal probability plot is to graphically decide whether the data in x could come from a normal distribution. If the data are normal the plot will be linear, otherwise there will be curvatures in the plot [MATLAB, 2002].

Figures 5.13, 5.14, 5.15, and 5.16 have the normal probability plots (in +) for METU-NN, METU-C with polynomial nonlinearity, METU-C with Bezier curve nonlinearity, and METU-C with B-Spline curve nonlinearity model results, respectively. Superimposed to those, linear fits (in dashed) are plotted.
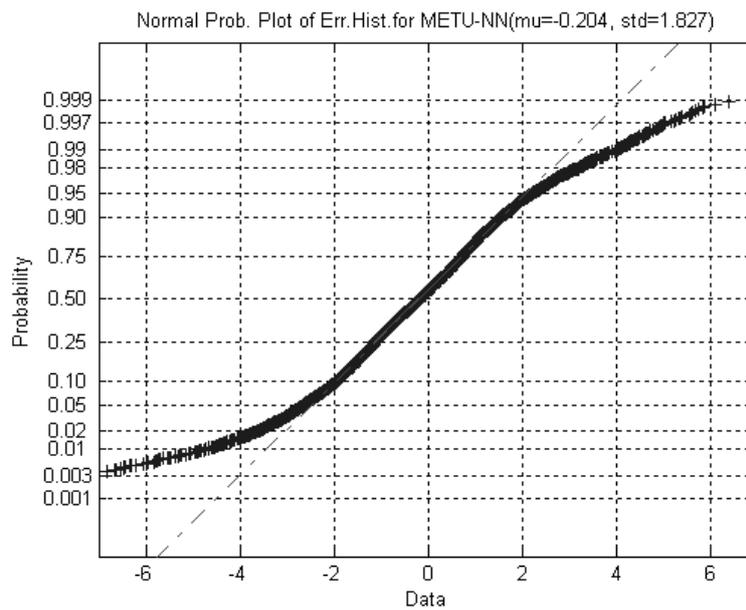
Figure 5.13. The normal probability plot (in +) for METU-NN model results, and the linear fit (in dashed)
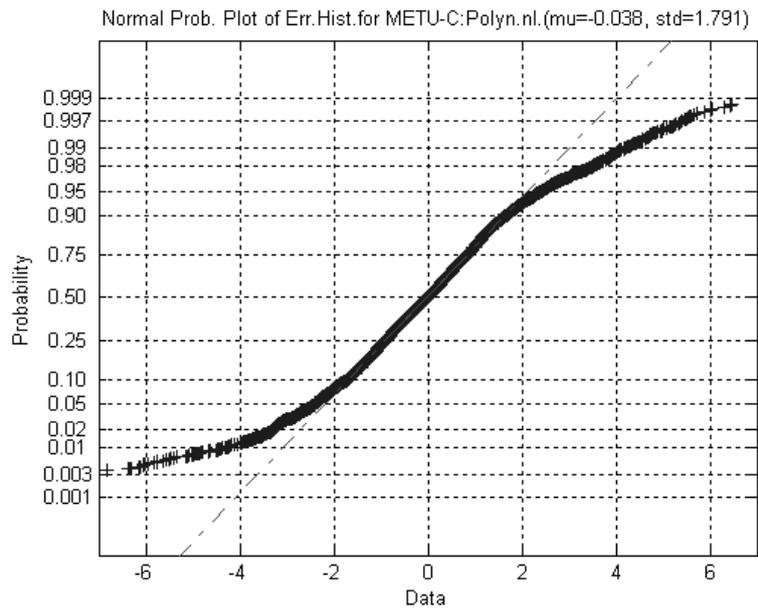
Figure 5.14. The normal probability plot (in +) for METU-C with polynomial
nonlinearity model results, and the linear fit (in dashed)
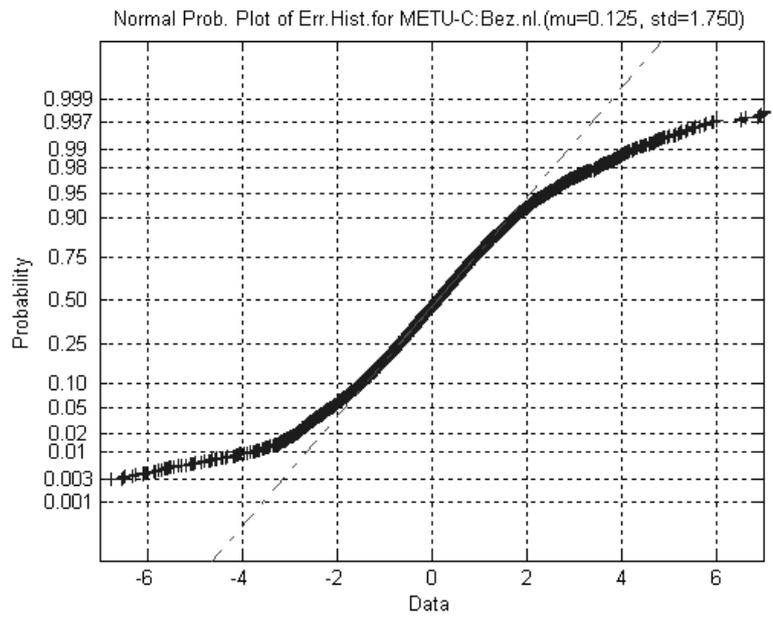
Figure 5.15. The normal probability plot (in +) for METU-C with Bezier curve nonlinearity model results, and the linear fit (in dashed)
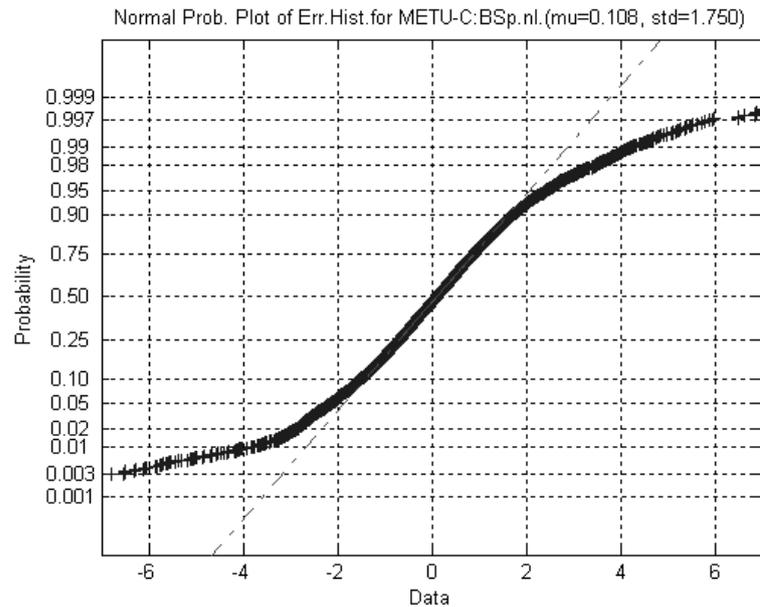
Figure 5.16. The normal probability plot (in +) for METU-C with B-Spline curve nonlinearity model results, and the linear fit (in dashed)

When the normal probability plots are plotted, it is observed that the error distributions for the model results have curvatures and do not exactly fit to the superimposed lines. Thus, they do not exactly fit to corresponding normal distributions, but a rough assumption that they fit to the normal distributions can be made, as it has been made in observing the empirical CDF plots.

In Figures 5.15 and 5.16, for the METU-C models with Bezier and B-Spline nonlinearity representations, the distributions of the error statistic values are more condansed in small absolute error regions when compared with the ones in Figures 5.13 and 5.14 which are for the METU-NN model and METU-C model with Polynomial nonlinearity representation, respectively. Thus, the

METU-C model results with Bezier and B-Spline nonlinearity representations are successful.

5.4 Test of Hypothesis for METU-NN and METU-C Models

In the error comparison and analysis, the error values, i.e. the differences of observed and forecast values, are used in t-tests for four of the models. The models are METU-NN, METU-C with Polynomial nonlinearity, METU-C with Bezier nonlinearity, and METU-C with B-Spline nonlinearity. First of all, the population mean is assumed to be zero, i.e. $\mu = 0$. The sample sizes are n = 7942 for four of the model results. The sample means and standard deviations are calculated. Then, using the Equation 5.4, the intervals of hypotheses are calculated.

In the t-test, let the null hypothesis be H_0: $\mu = 0$.

We have assumed that the error distributions were normal. With this assumption, according to the t-tests applied when the result, h is 1 and you can reject the null hypothesis at the significance level α. When h is 0, then you cannot reject the null hypothesis at the α level of significance [MATLAB, 2002].

Table 5.2 gives the t-test results of the models for $\alpha = 10^{-10}$. Similarly, Table 5.3 gives the error statistics when $\alpha = 0.05$. Also, upper and lower bounds of the hypotheses are given.

Table 5.2. Error Statistics Table for $\alpha = 10^{-10}$

	METU-NN Forecast	METU-C with (Polynomial n.l.) Forecast	METU-C with (Bezier C. n.l.) Forecast	METU-C with (B-Spline C. n.l.) Forecast
t-test result (boolean)	h=1	h=0	h=0	h=0
Upper bound of hyp.(TECu)	-0.072	0.092	0.253	0.235
Lower bound of hyp.(TECu)	-0.337	-0.168	-0.002	-0.019

Table 5.3. Error Statistics Table for $\alpha = 0.05$

	METU-NN Forecast	METU-C with (Polynomial n.l.) Forecast	METU-C with (Bezier C. n.l.) Forecast	METU-C with (B-Spline C. n.l.) Forecast
t-test result (boolean)	h=1	h=0	h=1	h=1
Upper bound of hyp.(TECu)	-0.164	0.002	0.164	0.146
Lower bound of hyp.(TECu)	-0.245	-0.077	0.087	0.069

When the t-test results for $\alpha = 0.05$ are computed, it is observed that only the hypothesis for METU-C with polynomial nonlinearity representation model

results can not be rejected. Thus, when the confidence is decreased, i.e. when α is increased, it is observed that the null hypotheses tend to be rejected. It can be due to the fact that the distributions are not exactly normal.

5.5 Upper and Lower Bounds of the Cross Correlation Coefficients

Confidence limits of the cross correlation coefficient can be calculated for normal distributions [Spiegel et al., 2000]. Let n be the sample size, r be the cross correlation coefficient, Z be a statistic, Z_{cr} be the positive critical value of Z for two-tailed tests. With a rough approximation, the Z statistic is normally distributed with mean, μ_z, and standard deviation, σ_z [Spiegel et al., 2000]. The confidence limits for μ_z are as follows [Spiegel et al., 2000],

$$\mu_z = Z \pm Z_{cr}\sigma_z = 1.1513.\log\left(\frac{1+r}{1-r}\right) \pm Z_{cr}.\left(\frac{1}{\sqrt{n-3}}\right) \qquad (5.6)$$

The confidence limits for upper and lower bounds of cross correlation coefficient, ρ, are as follows [Spiegel et al., 2000],

$$\mu_{z1} = 1.1513.\log\left(\frac{1+\rho_1}{1-\rho_1}\right) \qquad (5.7)$$

$$\mu_{z2} = 1.1513.\log\left(\frac{1+\rho_2}{1-\rho_2}\right) \qquad (5.8)$$

Thus, the upper and lower bounds for cross correlation coefficients can be computed. In our case studies, n = 7942. Let Z_{cr} = 1.96 which is the positive critical value of Z for two-tailed tests for 95% confidence. Then, using the cross correlation coefficients, i.e. r values, and Equations 5.6 to 5.8, the upper

and lower bounds of the cross correlation coefficients for four of the case studies are calculated.

Error table for comparison of the METU-NN model operation performance with the METU-C models is given on Table 5.4. The lower and upper bounds of cross correlation coefficients at the 95% confidence limits, i.e. the level of significance is α=0.05 [Spiegel et al., 2000], are also given.

Table 5.4. Error Table

	METU-NN Forecast	METU-C with (Polynomial n.l.) Forecast	METU-C with (Bezier C. n.l.) Forecast	METU-C with (B-Spline C. n.l.) Forecast
Absolute Error (TECu)	1.22	1.17	1.11	1.10
Normalized Error (%)	6.95	6.39	5.51	5.51
RMS Error (TECu)	1.84	1.79	1.75	1.75
Cross Correlation Coeff. $(x10^{-2})$	98.6	98.6	98.7	98.7
upper bound when α=0.05$(x10^{-2})$	98.6	98.7	98.8	98.8
lower bound when α=0.05$(x10^{-2})$	98.5	98.6	98.6	98.6

At the significance level of α=0.05, the cross correlation coefficients are significant. METU-C models with Bezier and B-Spline curve nonlinearity representations have higher performance results with smaller error values [Senalp et al., 2006d]. For example, the absolute error value for the METU-C model with B-Spline nonlinearity representation is 10% smaller than the absolute error value for the METU-NN model performance.

5.6 Performance Comparison of METU-NN and METU-C Models

A performance table is prepared and given in Table 5.5 in order to compare the METU-NN model with METU-C models in qualitative and quantitative manner. The absolute error values and the cross-correlation coefficients between one hour ahead forecast and observed TEC values in April-May 2002 at Hailsham as the quantitative performance values, the improvements of the results of the METU-C models with respect to the METU-NN model results, and the qualitative advantages of the models are given in the table.

Table 5.5. Performance Table

	METU-NN	METU-C					
	METU-NN Forecast	METU-C with (Polynomial n.l.) Forecast	Improvement wrt NN	METU-C with (Bezier C. n.l.) Forecast	Improvement wrt NN	METU-C with (B-Spline C. n.l.) Forecast	Improvement wrt NN
Absolute Error (TECu)	1.22	1.17	4%	1.11	9%	1.10	10%
Normalized Error (%)	6.95	6.39	8%	5.51	21%	5.51	21%
Cross Corr. Coeff. (x10^{-2})	98.6	98.6	.0%	98.7	.1%	98.7	.1%
Need for past input data	YES	NO	+	NO	+	NO	+
Transparency of internal var.	NO	YES	+	YES	+	YES	+
Computation time in operation A < B < C < D	D	A	+	B	+	C	+

When the performance table is examined, after qualitative and quantitative performance comparisons are made it can easily be concluded that METU-C models are superior to the METU-NN model, which is also successful. Among

the models presented the optimum one is the METU-C model with Bezier curve nonlinearity representations. It has advantages. The results of it have small error values and large cross-correlation coefficient. It has simple inputs because it does not need past inputs. It has transparent internal variables, which can be observed and used by the system designers or operators. It is fast in terms of the computation time in operation.

5.7 Comparison of IRI-2001, METU-NN and METU-C Models

International Reference Ionosphere (IRI) is an international project sponsored by the COSPAR and URSI [Bilitza, 2001] [IRI, 2007]. UMLCAR adapted the IRI-2001 model to be used in MS-Windows platform [UMLCAR, 2007]. The results of the METU-C models have been compared with the UMLCAR edition of the IRI-2001 model results for the time period of interest during well-known Space Weather events of April 2002 [Senalp et al., 2007d]. The results have also been compared with the results of the METU-NN model.

The program of the IRI-2001 model gives a single TEC value of a location of interest at a time of interest at a run. The usable locations cover the whole geographic regions of the Earth in 0.1-degree intervals of latititudes and longitudes. The usable time is of 15-minute intervals in terms of Universal Time (UT) or Local Time (LT).

The use of the METU-NN-C technique to forecast the 10 minutes values of the TEC at 5th, 15th, 25th, 35th, 45th and 55th minutes of the hours, one hour ahead, during high solar activity in the solar cycle were examined and the results were presented in Chapters 2, 3, 4, and 5.

In order to use the common location and common time instants within the comparison of the IRI-2001, METU-NN and METU-C model results, the 15th and 45th minutes of hours during 18-19 April 2002 at the location of Hailsham (50.9° N; 0.3° E) GPS receiving station are selected.

The observed TEC data was provided by RAL, UK [COST271 WG 4 STSM, 2002]. One hour in advance forecast TEC values were obtained by using METU-NN model [Tulunay E. et al., 2004a] [Senalp et al., 2006d]. One hour in advance forecast TEC values were also obtained by using METU-C models and the results were presented in Chapters 2, 3, 4 and 5. The TEC values of the time and location of interest are obtained by using the IRI-2001 model as well.

Table 5.6 gives the absolute error values and the cross correlation coefficients between the observed and forecast TEC values at Hailsham in 18-19 April 2002.

Table 5.6. Error Table

	IRI-2001 Output	METU-NN Forecast	METU-C with (Polynomial n.l.) Forecast	METU-C with (Bezier C. n.l.) Forecast	METU-C with (B-Spline C. n.l.) Forecast
Absolute Error (TECu)	15.04	2.09	1.95	1.61	1.62
Cross Corr. Coeff.(x10^{-2})	83.8	98.6	98.8	98.4	98.4

When the absolute error values are compared, it is seen that the results of the METU models have smaller error values than the IRI-2001 model results. Also the cross-correlation coefficients of the observed and forecast TEC values by METU models are higher than the result obtained by IRI-2001 model. The optimum model is the METU-C model with Bezier curve nonlinearity representation.

Figure 5.17 gives the superimposed variations of the observed TEC values at Hailsham in 18-19 April 2002, TEC outputs of the IRI-2001, forecast TEC values by METU-NN and forecast TEC values by METU-C with Bezier curve nonlinearity representation.
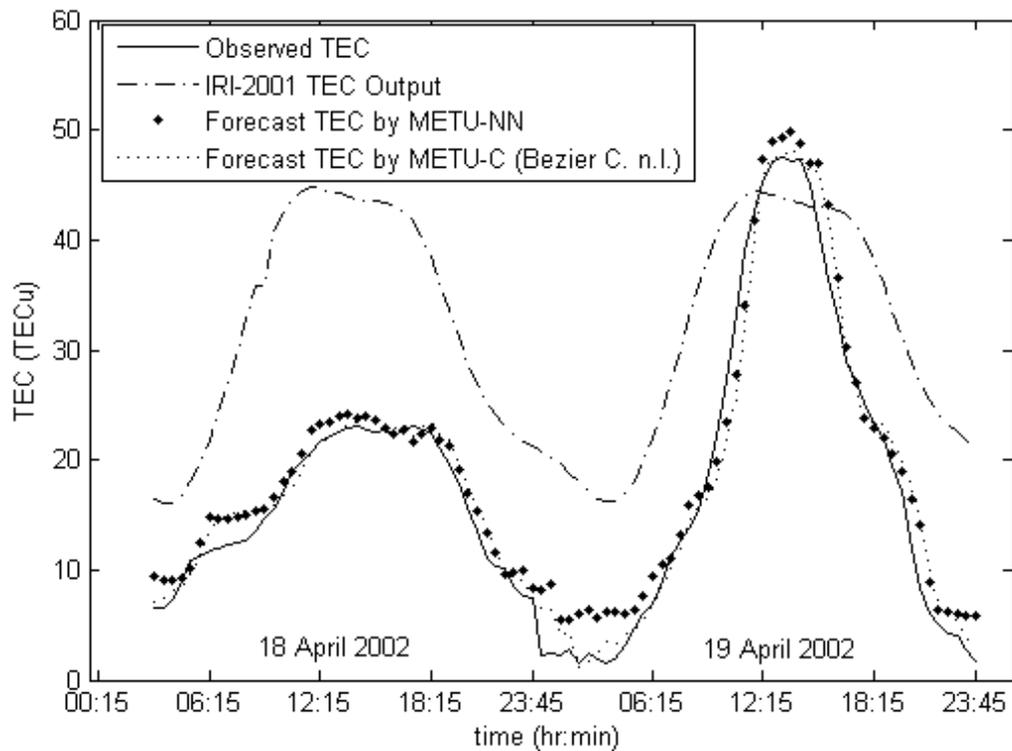
Figure 5.17. Observed GPS TEC values for disturbed solar-terrestrial conditions (solid), IRI-2001 TEC outputs (dash-dotted) 1 hour ahead Forecast TEC values by METU-NN (large dotted) and 1 hour ahead Forecast TEC values by METU-C with Bezier curve nonlinearity representations (small dotted) for the enlarged portion of the time of validation period: 18-19 April 2002 at Hailsham.

When the superimposed TEC variations are compared, it is seen that the variation of one hour in advance forecast TEC values by METU-C with Bezier curve nonlinearity representation follows the observed TEC variation with small error values.

Figure 5.18 gives the scatter diagram for the observed TEC values and IRI-2001 outputs with best-fit line. Figure 5.19 gives the scatter diagram and best-fit line for the observed and forecast TEC values by METU-C with Bezier curve nonlinearity representations.
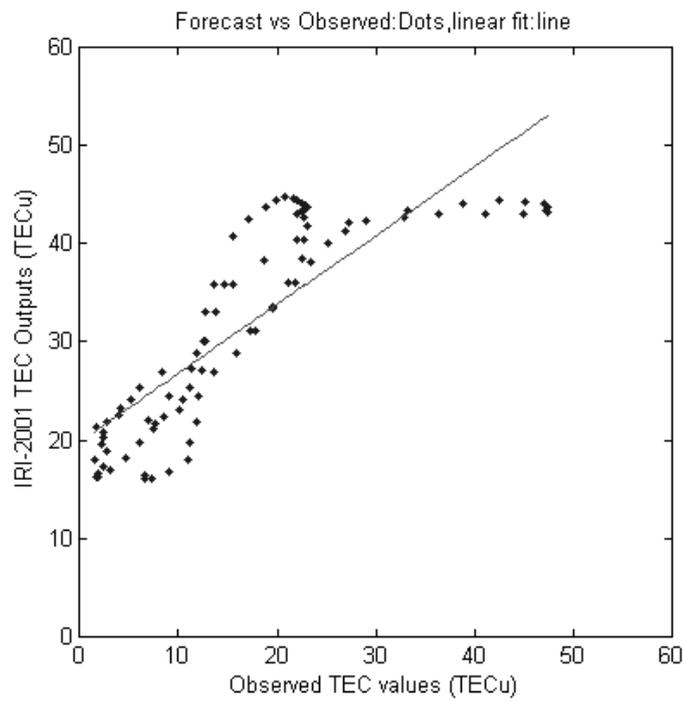
Figure 5.18. Scatter diagram with best-fit line for observed TEC values and IRI-2001 TEC outputs in 18-19 April 2002 at Hailsham.
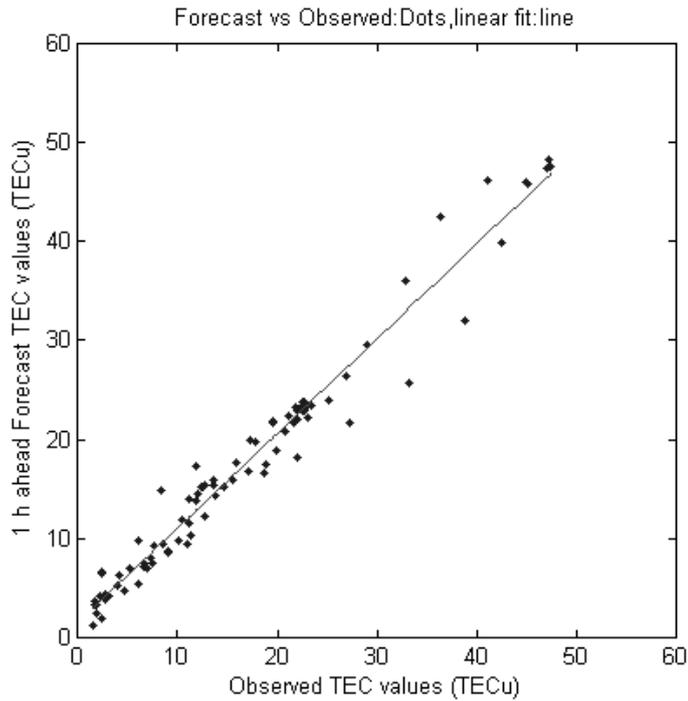
Figure 5.19. Scatter diagram with best-fit line for observed TEC values and one hour ahead forecast TEC values by METU-C with Bezier curve nonlinearity representations in 18-19 April 2002 at Hailsham.

When the scatter diagrams are compared it is seen that the deviations of the scatter points are small for the results of METU-C with Bezier curve nonlinearity. Also, the best-fit line in the scatter diagram for the results of the METU-C has a slope near 45˚ and passes through the origin. Thus, the system reached the correct operating point within the system identification by METU models and the forecasting errors are small. Also the METU-C model learned the shape of the inherent nonlinearities. Thus the deviations from straight line

are small in the scatter diagram, and the correlation coefficients are very close to unity.

To sum up, the METU-C models in the case studies are competitive and they have high performance results when compared with the internationally popular ionospheric model, IRI-2001. The results provide important achievements of the METU-C models. Among the models presented, METU-C with Bezier curve nonlinearity representation is outstanding.

CHAPTER 6

FORECASTING TEC MAPS BY USING METU-NN AND BEZIER SURFACE PATCHES

6.1 Introduction

The model developed is called the Middle East Technical University Neural Network (METU-NN) Model. In order to understand more about the complex response of the magnetosphere and ionosphere to extreme solar events, this time the series of space weather events in November 2003 are chosen. Total Electron Content (TEC) values of the ionosphere are forecast during these space weather events. In order to facilitate an easier interpretation of the forecast TEC values, maps of TEC are produced by using the Bezier surface fitting technique [Tulunay E. et al., 2006a] [Senalp et al., 2006a].

It is most desirable to drive mathematical ionospheric forecasting and mapping models based on physics to incorporate them in ionospheric services and activities. However, this is a very complex and prohibitively difficult task.

In general, mapping of an ionospheric quantity such as ionospheric critical frequency (foF2) or TEC means that a surface fitting is performed based on known values of that quantity on specified points of a surface. Mapping carried out by using a certain method, extrapolates the known discrete values

continuously to the whole surface. There are various widely used ionospheric mapping techniques using both the ionosonde-derived TEC and the GPS-TEC [Samardjiev et al., 1993] [Cander, 2003] [Jakowski et al., 2004] [Stamper et al., 2004] [Zolesi et al., 2004]. Samardjiev et al. (1993) used contouring techniques for ionospheric mapping including Kriging technique, which performs best when compared with inverse distance squared technique and minimum curvature technique. Cander (2003) discussed the findings of the EU Action COST 251 and plans for the COST 271 on TEC forecast and mapping. Jakowski et al. (2004) and Stamper et al. (2004) presented near real time and real time TEC mappings over Europe. Zolesi et al. (2004) presented a method based on a regional model of the standard vertical incidence monthly median ionospheric characteristics, which was updated with real-time ionospheric observations for mapping of ionospheric conditions over Europe. It is suitable to be used in real time for operational applications. These studies did not report mapping based on forecasts.

In this work, a method has been developed to perform TEC forecast mapping by using METU-NN and Bezier surfaces for the first time [Tulunay E. et al., 2006a]. The METU-NN model [Tulunay Y. et al., 2004a] is used to produce TEC forecast maps over Europe using Bezier surfaces which are being used for surface generation in computer graphics [Rogers and Adams, 1990]. Brief information concerning mapping and Bezier surfaces is presented in section 6.4. In this work, one hour in advance forecast of the 10 minute TEC maps over Europe during November 2003 space weather events has been introduced and the results are presented.

Neural Network models are designed and trained with significant inputs. In this approach, the basic inputs for the model are the past TEC values and the

temporal inputs as explained in section 6.3. The forecast results are promising for system operators. This work leads availability of TEC forecast mapping results by METU-NN for making comparisons with the results by METU-NN-C in Chapter 7. The Neural Network architecture of METU-NN is modular. Due to modularity, the model and its input parameters are open to new developments depending on future requirements. The sub blocks in the METU-NN have got one input layer, one hidden layer with the neurons and one output layer. The Neural Network is trained and used to forecast the TEC values for the grids located over Europe. Using these forecast TEC values of the grids, TEC maps as Bezier surfaces are presented.

The main contributions of this work are organization of data for teaching complex processes, Neural Network based modeling of a highly complex nonlinear process such as the TEC forecast mapping, and general demonstration of learning capability and reaching a proper operating point by calculating cross correlations and errors, respectively.

6.2 Preparation of Data for the METU-NN

Ten minute vertical TEC data were evaluated from the GPS measurements that took place between 1st of November and the 11th of December 2003 over Europe centered over Italy based on slant TEC data [Ciraolo, 2004] [Radicella, 2004]. The geographic coverage of the TEC data is between latitudes of (35.5º N; 47.5º N) and longitudes of (5.5º E; 19.5º E). The data belong to the 104 grid locations spaced every 2º longitude by 1º latitude intervals in space. These data consist of the training, test and validation subsets during the development and operation modes of the modeling process.

Table 6.1 illustrates how the data were assigned to be employed by the METU-NN model during the 'training', 'test', and 'validation' modes.

94

Table 6.1. Selection of the time periods for the input data

PHASE	YEAR	DAYS
Train	2003	1–15 Nov.
Test	2003	30 Nov. – 11 Dec.
Validation	2003	16–29 Nov.

In particular, the period of major space weather events were chosen for the 'validation' mode. That is, the solar active region, the sunspot group 484 (or near the sunspot group 501) was the seat of a major coronal mass ejection (CME) on 18th of November 2003. This CME triggered a geomagnetic storm on 20th of November 2003 at around 08:00 UT. This storm was qualified by the three-hour planetary magnetic index of Kp as 8+ [SpaceWeather, 2007] [NGDC, 2007]. However, in principle all the data subsets were chosen from periods of similar Zurich sunspot numbers. The models contain intrinsic information about the solar activity.

6.3 Construction of the Neural Network Based Model

The construction work of the Neural Network based model is carried out in the development mode. It is composed of "training phase or learning phase" and "test phase" [Y. Tulunay et al., 2004a]. Training and test phases are best performed with independent but statistically similar data sets. It is natural that the nonlinear inherent processes are to be learned by the model during the learning phase as fast as possible. The Levenberg-Marquardt Backpropagation algorithm is chosen to be the most convenient one during the training for this work.

The model parameters are optimized and fixed at the end of the construction procedure. In the operation mode the validation data are used for calculating the errors, point by point, to measure the performance of the model.

The value of the TEC at the time instant k is designated by f(k). The output is f(k+60) in 60 minutes in advance forecast. It is the value of the TEC to be observed 1 hour later than the present time for this work. There are 419 inputs fed into the METU-NN model. 3 of the inputs are the temporal inputs; i.e. dnd, Cm, and Sm. The rest of the input parameters are the inputs related to the history of the TEC values for the grids over Europe, i.e. 104 f(k) values, 104 $\Delta_1(k)$ values, 104 $\Delta_2(k)$ values, and 104 RΔ(k) values. Inputs for each METU-NN module are as follows,

1. The present value of the TEC, f(k): see Equation 2.1 in Chapter 2
2. First Difference of the TEC, $\Delta_1(k)$: see Equation 5.1 in Chapter 5
3. Second Difference of the TEC, $\Delta_2(k)$: see Equation 5.2 in Chapter 5
4. Relative Difference of the TEC, RΔ(k): see Equation 5.3 in Chapter 5
5. Serial date number difference, dnd,

dnd = Present date number – The first d.n. of the data of interest (6.1)

6. Cosine component of minute of the day, Cm: see Equation 2.2 in Chapter 2
7. Sine component of the minute of the day, Sm: see Equation 2.3 in Chapter 2

Date numbers start with 1st Jan. of year 0, as date number 1. By calculating the serial date number difference the start value is shifted to the first date of the data of interest. In this study, the first date of the data of interest is 1 Nov. 2003, 00:05 UT.

Figure 1.3 in Chapter 1 shows the architecture of each of the Neural Network module. The modular structure of the METU-NN provides the development and operation modes to be fast and robust. In this work, the METU-NN model has got 104 modules of Neural Networks. The number of modules corresponds to the number of grids for the region of interest. The inputs of the modules are the present TEC values (#:104) and the first differences (#:104) for each grid; first, second and the relative differences (#:3) for the grid of interest; the present date number difference (#:1) and the present trigonometric components (#:2) of minute of the day. Thus, for each module there are 214 inputs. When common inputs of the modules are not counted, the overall number of the inputs for the METU-NN model is 419. During training the parameters, i.e. the weights, of the METU-NN modules are determined for each grid. METU-NN model has 104 outputs corresponding to 104 modules. The output of each module is the forecast value of TEC for the grid of interest. For the modules, among the various Neural Network structures the best configurations are found to be the ones with one hidden layer. 6 neurons are used in the hidden layer of the modules.

6.4 Brief Information Concerning Mapping and Bezier Surfaces

Mapping covers a portion of land. As an example consider a portion of European area which is bounded by the latitudes (35.5º N; 47.5º N) and longitudes (5.5º E; 19.5º E). This area is partitioned by using a grid structure. Grid points or local control points are thus defined.

In practice, the number of control points can be increased by increasing the number of defining polygon vertices. Local control provides the capability of including possible variations around a local control point without interfering other distant localities of the mapping area.

Bezier surfaces, which are used in such mapping for the first time, have some advantages [Rogers and Adams, 1990]. The availability of the GPS data to be used for TEC evaluation provides larger number of polygon vertices for Bezier surfaces. Thus, better surface fit is achieved.

TEC values are forecast by using METU-NN model. Mapping is performed over the area of interest by using Bezier surface. Bezier surface is advantageous since it can provide more control points to increase the quality of fit as compared with other surface patches such as bilinear, ruled, linear Coons, and Coons bicubic surface patches. Coons bicubic surface needs the specification of precise, nonintuitive mathematical information such as position, tangent and twist vectors as in the cubic spline curves [Rogers and Adams, 1990]. Therefore there are difficulties limiting its use in practice. These difficulties are overcome by using Bezier surfaces.

In this work, 104 grid locations corresponding to 104 defining polygon vertices are used to obtain sufficient control in mapping. The TEC forecast value at any location on the Bezier surface can be calculated as,

$$TEC(u,w) = \sum_{i=0}^{n} \sum_{j=0}^{m} B_{i+1,j+1}.J_{n,i}(u).K_{m,j}(w) \qquad (6.2)$$

where

$$J_{n,i}(u) = \binom{n}{i} u^i (1-u)^{n-i} \qquad (6.3)$$

$$K_{m,j}(w) = \binom{m}{j} w^j (1-w)^{m-j} \qquad (6.4)$$

B matrix values correspond to the METU-NN outputs for the grids,

$n+1 = 8$ is the number of longitude grids for each latitude,

$m+1 = 13$ is the number of latitude grids for each longitude,

u is the normalized longitude variable in the region of interest,

w is the normalized latitude variable in the region of interest.

6.5 Results

The TEC trained METU-NN model is used for forecasting TEC values 1 hour in advance during 16-29 November 2003. The time period includes the major November 2003 space weather event. Then, maps of TEC are constructed by using the Bezier surface mapping technique. Observed TEC values are used only for the grid locations. METU-NN is trained with the observed TEC data to give the outputs, the forecast TEC values, for the grid locations. The TEC mapping is not performed during training because the observed TEC values for the whole region are not a priori except the grid locations. After the forecast operation TEC mapping is performed. Figure 6.1a illustrates the variations of both the 1 hour in advance forecast and observed TEC values for the grid location: (13.5° E; 41.5° N), during 16-29 November 2003. Figure 6.1b, covering the period 19-21 November 2003, is a subset of Figure 6.1a. The diurnal minute long variation of the TEC values is shown in the vertical axis and the horizontal axis is the days of the November 2003 in minute intervals. To a first approximation the forecast and observed GPS TEC values are in very good agreement on visual inspection. In 20 November 2003, the three hour planetary magnetic indices of Kp = 6+ during 09:00 – 12:00 UT, Kp = 8- during 12:00 – 15:00 UT, Kp = 9- during 15:00 – 18:00 UT, Kp = 9- during 18:00 – 21:00 UT, and Kp = 8 during 21:00 – 24:00 UT indicate effects of the extreme events [SpaceWeather, 2007] [NGDC, 2007]. Thus, the forecast and observed TEC values are daytime high TEC values during the daytime of 20 November 2003. The forecast TEC values during the afternoon of 20 November 2003 are afternoon-time high TEC values as expected, but the observed TEC values for the period are not afternoon-time high TEC values.

This may be due to lack of actual data in calculation of the observed GPS-TEC values due to communication cut offs during the extreme events.
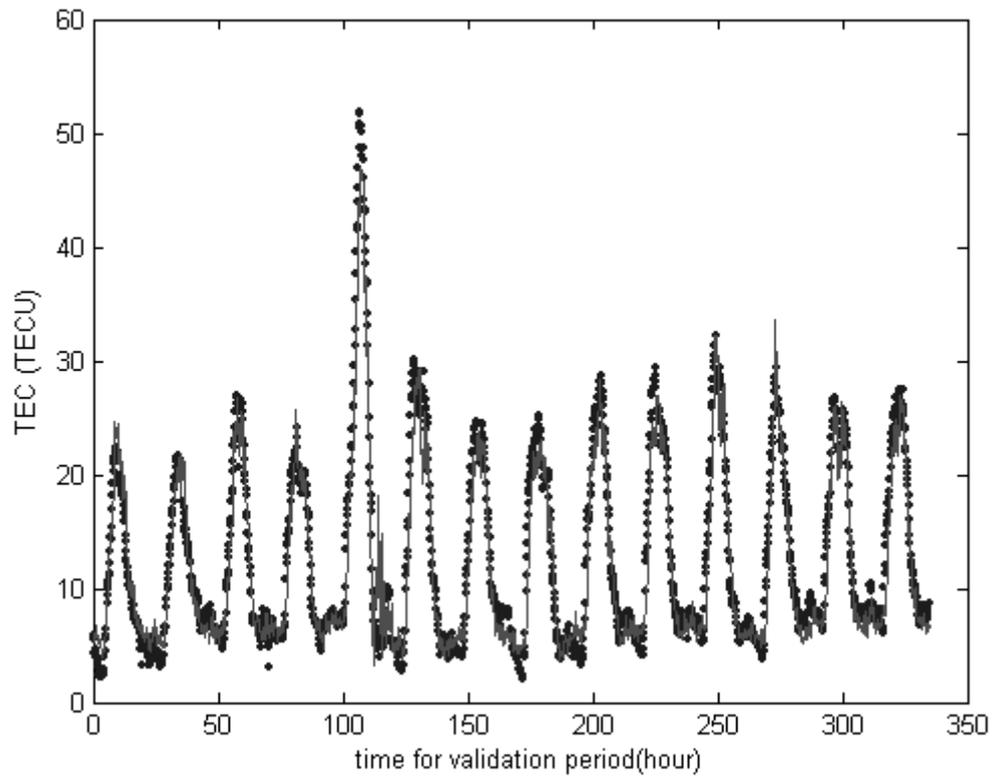
Figure 6.1a. Observed (dotted) and 1 hour ahead forecast (solid) TEC during 16 Nov.2003 01:10UT-29 Nov.2003 24:00UT for the grid point (13.5°E; 41.5°N)
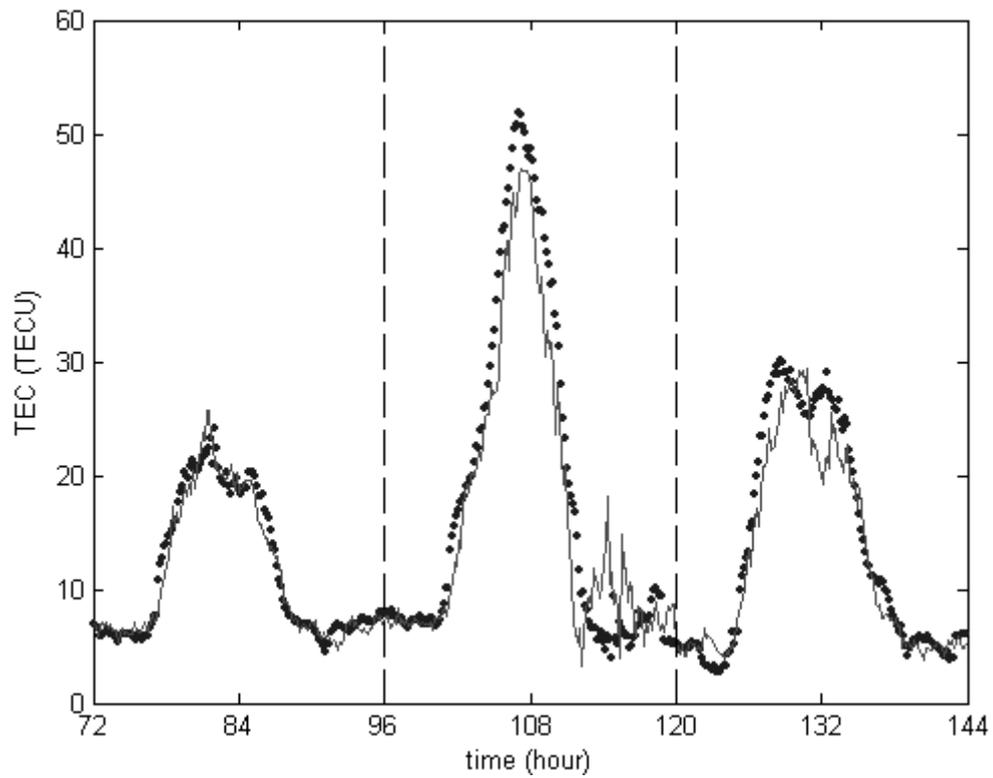
Figure 6.1b. Observed (dotted) and 1 hour ahead forecast (solid) TEC during 19 Nov.2003 00:00UT-21 Nov.2003 24:00UT for the grid point (13.5˚E; 41.5˚N)

Figure 6.2 illustrates the variations of the observed TEC values and 1 hour in advance forecast TEC maps for the big geomagnetic storms of 20th November 2003, at 09:30, 13:40, 15:30, and 17:20 UT, respectively.

101
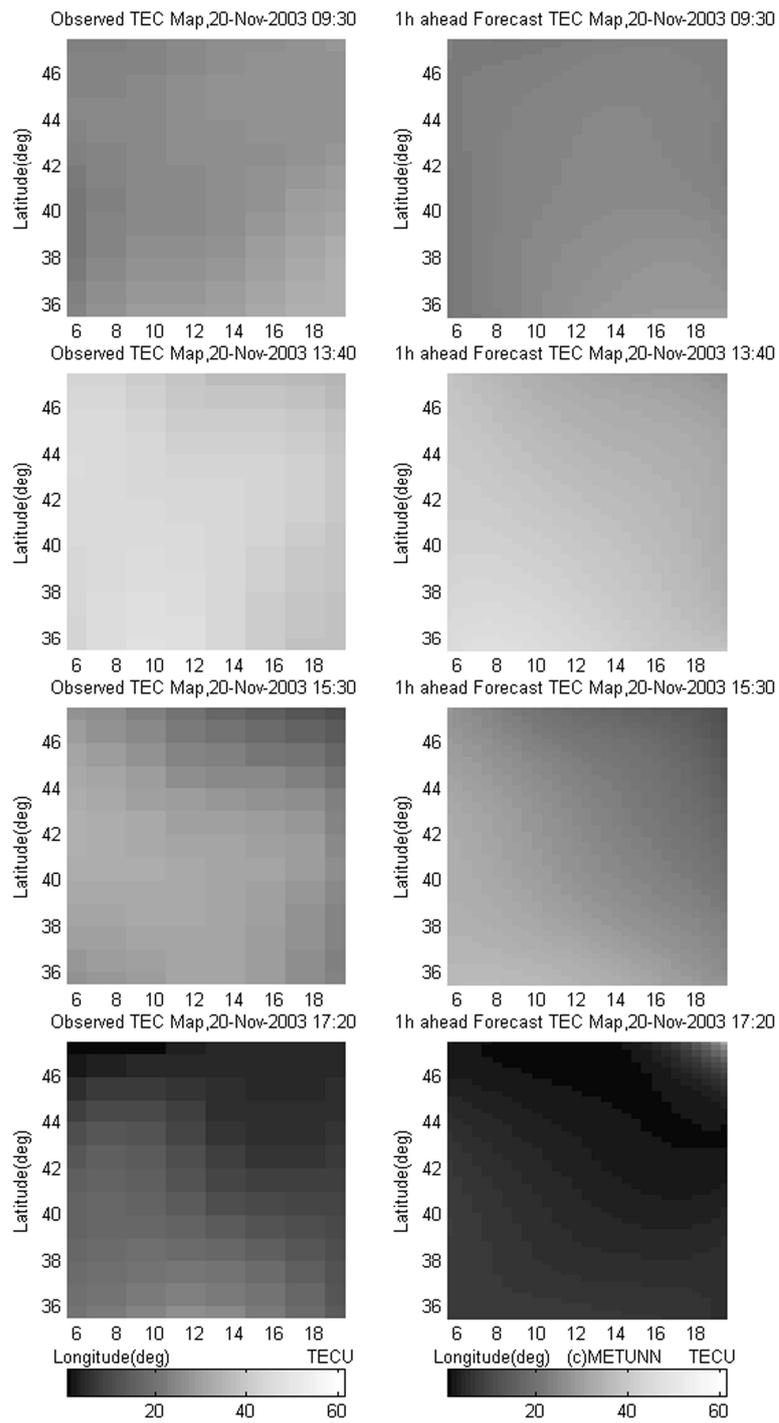
Figure 6.2. Observed TEC values and 1 hour ahead forecast TEC Map examples during 20 Nov. 2003

Figure 6.3a presents the scatter diagram of the 1 hour in advance forecast and observed TEC data for whole of the 104 grid locations during 16-29 November 2003. Figures 6.3b, 6.3c, and 6.3d present the scatter diagrams of the forecast and the observed TEC data at the grid locations: (11.5° E; 38.5° N); (13.5° E; 41.5° N); and (15.5° E; 44.5° N) respectively during 16 November to 29 November 2003.
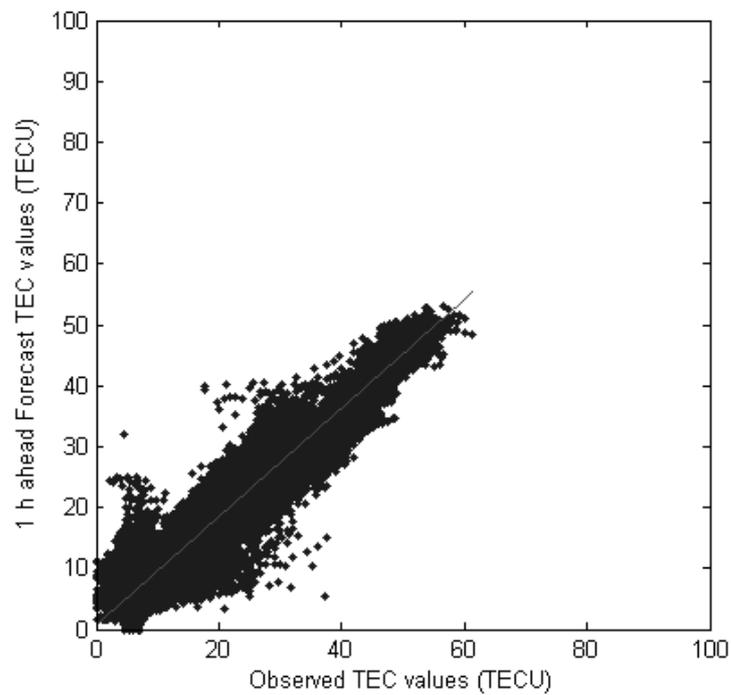
Figure 6.3a. Scatter Diagram (dots) with best-fit line (solid) for the 1 hour ahead Forecast mapping and Observed TEC values for all grid points for the validation time 16-29 November 2003.
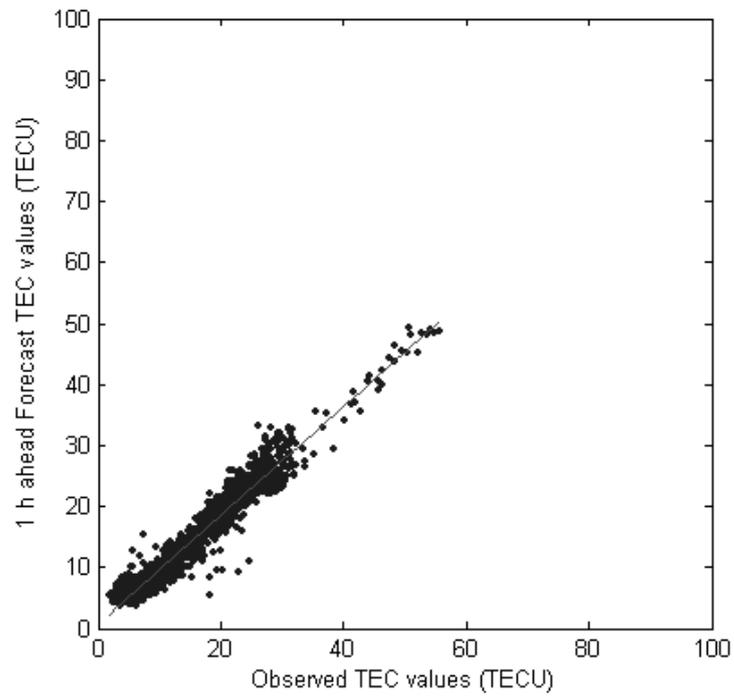
Figure 6.3b. Scatter Diagram (dots) with best-fit line (solid) for the 1 hour ahead Forecast mapping and Observed TEC values for the single grid point (11.5˚ E; 38.5˚ N) for the validation time 16-29 November 2003.
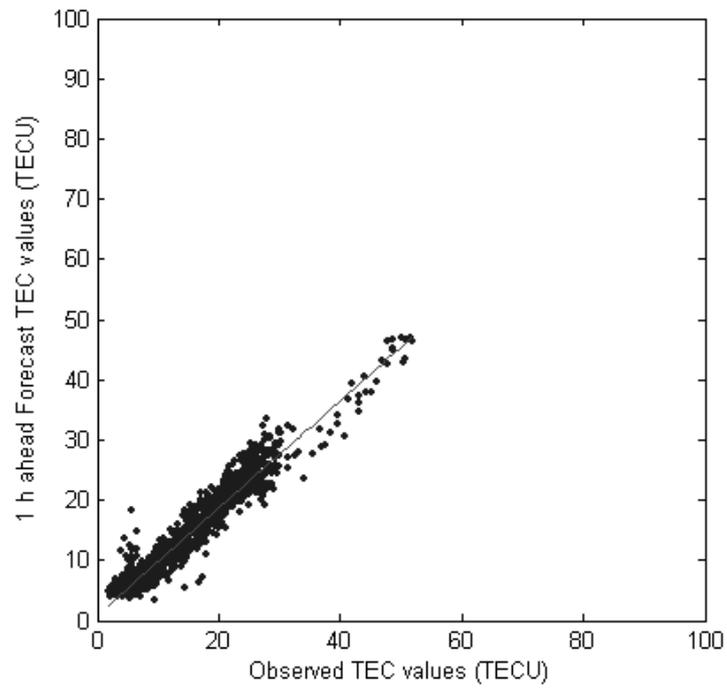
Figure 6.3c. Scatter Diagram (dots) with best-fit line (solid) for the 1 hour ahead Forecast mapping and Observed TEC values for the single grid point (13.5˚ E; 41.5˚ N) for the validation time 16-29 November 2003.
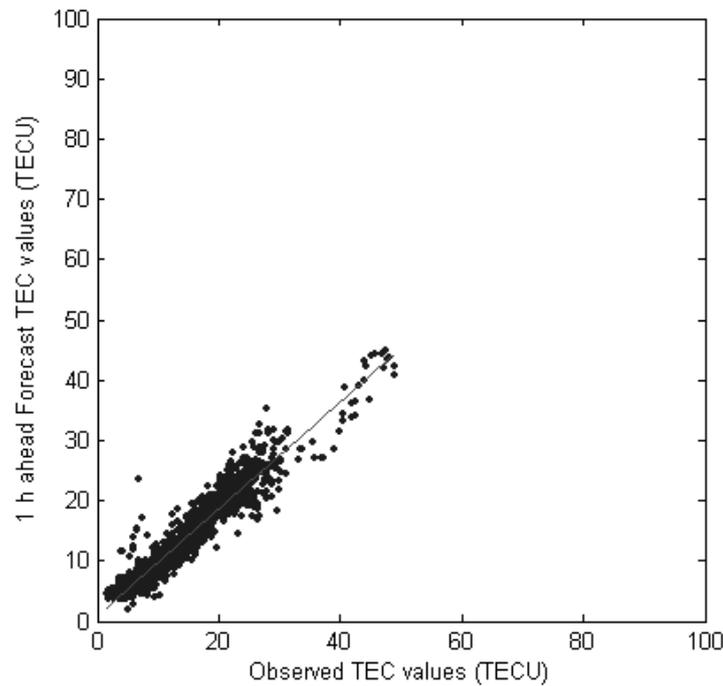
Figure 6.3d. Scatter Diagram (dots) with best-fit line (solid) for the 1 hour ahead Forecast mapping and Observed TEC values for the single grid point (15.5° E; 44.5° N) for the validation time 16-29 November 2003.

Best-fit lines of near to 45° slopes, almost passing through the origins in the Figures 6.3a to 6.3d, indicate small forecasting errors.

In order to examine the performance of the METU-NN during the geomagnetic storm on 20 November 2003, reference can be made to Figures 6.4a and 6.4b. Figure 6.4a illustrates the scatter diagram of the 1 hour in advance forecast and observed TEC data for whole of the 104 grid locations during 20 November 2003. Figure 6.4b presents the scatter diagram of the forecast and the observed TEC data at the grid location: (13.5° E; 41.5° N) during 20 November 2003.
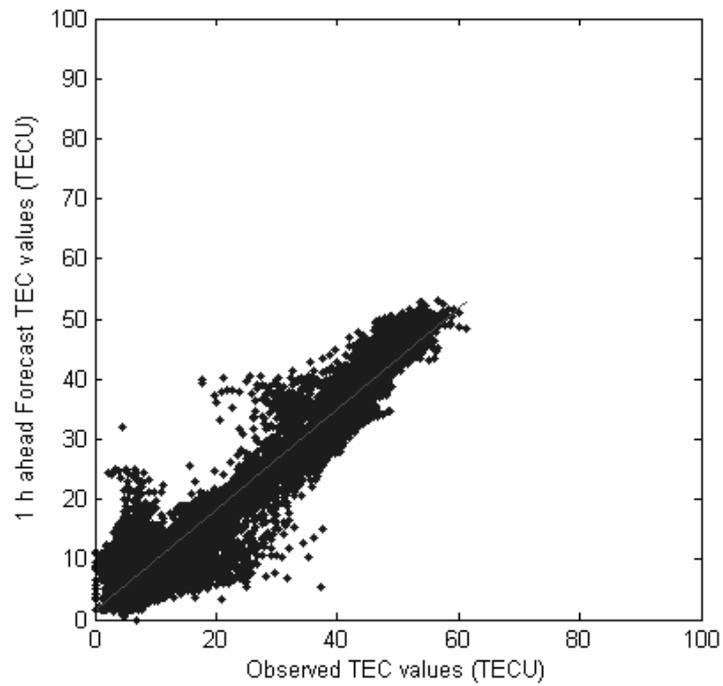
Figure 6.4a. Scatter Diagram (dots) with best-fit line (solid) for the 1 hour ahead Forecast mapping and Observed TEC values for all grid points for the day 20 November 2003.
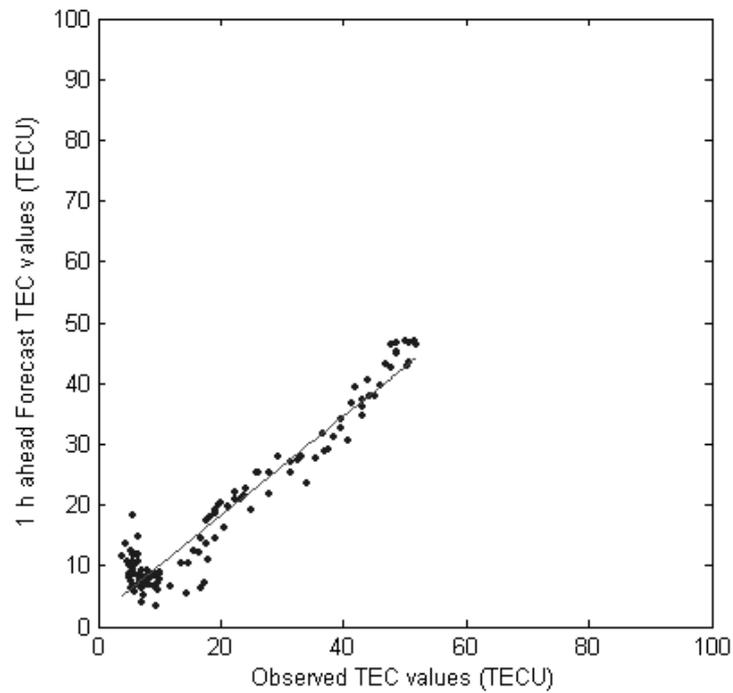
Figure 6.4b. Scatter Diagram (dots) with best-fit line (solid) for the 1 hour ahead Forecast mapping and Observed TEC values for the single grid point (13.5° E; 41.5° N) for the day 20 Nov. 2003.

Summarizing the results, the METU-NN model with Bezier surface TEC mapping learned the shape of the inherent nonlinearities during the severe space weather conditions of the November 2003 period. In other words, the system reached the global error minimum by reaching the correct operating point.

The overall Absolute TEC error map for 1 hour in advance forecasts is plotted in the Figure 6.5. The quantified performance of the model can be studied in terms of the values of errors presented in Tables 6.2 and 6.3.
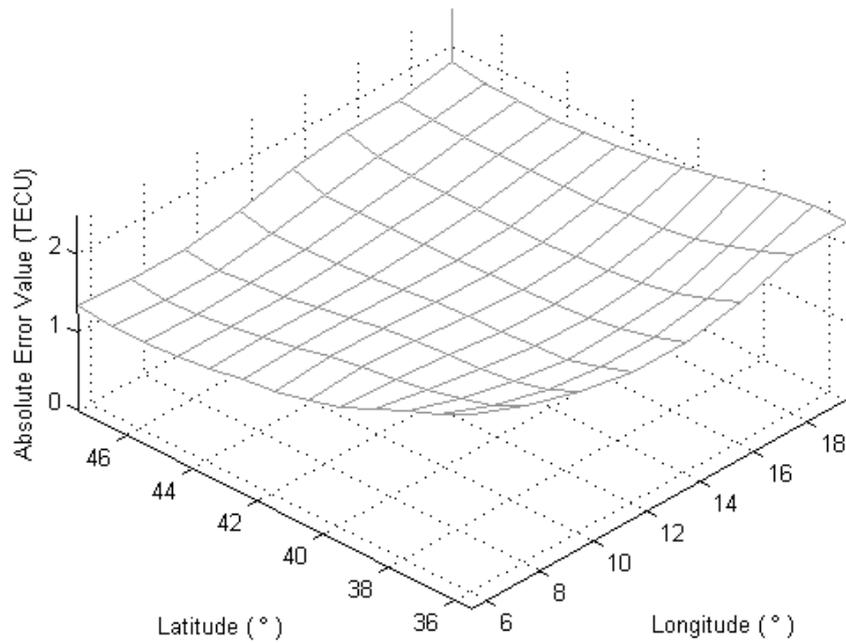
Figure 6.5. Absolute Error Map of observed and 1 hour ahead forecast TEC for 16-29 Nov. 2003.

It is interesting to note that forecasts inside the region of interest exhibit a better match with the observed data leading smaller error values in the inner grids when compared with the corner grids. The reason is that the presence of the neighbor grids increases the learning performance of the model for forecasting. Selecting a wider area in training than the area in operation can be proposed. This may be achieved by discarding the outermost grids of the area of interest during operation and performance analysis. In the current work none of the grids are discarded and the overall performance of the model is presented for discussion.

Table 6.2. Error Table for 1 h in advance forecasts for 16-29 Nov. 2003

Location	11.5°E 38.5°N	13.5°E 41.5°N	15.5°E 44.5°N	Overall TEC Map
Absolute Error (TECu)	1.58	1.49	1.52	1.65
Normalized Error (%)	14.29	15.22	16.30	15.63
Root Mean Square Error (TECu)	2.16	2.05	2.14	2.30
Cross Correlation Coefficient ($x10^{-2}$)	97.75	97.46	96.96	96.99

Table 6.3. Error Table for 1 h in advance forecasts for the day: 20 Nov. 2003

Location	11.5°E 38.5°N	13.5°E 41.5°N	15.5°E 44.5°N	Overall TEC Map
Absolute Error (TECu)	2.90	3.29	3.15	3.26
Normalized Error (%)	19.45	27.32	26.84	29.98
Root Mean Square Error (TECu)	4.07	4.39	4.34	4.50
Cross Correlation Coefficient ($x10^{-2}$)	97.64	96.94	96.45	96.40

Tables 6.2 and 6.3 present the average error values for 1 hour in advance forecasts during 16 to 29 November 2003, and during 20 November 2003, respectively. The first three columns of the tables present the error values for the grid locations: (11.5° E; 38.5° N), (13.5° E; 41.5° N), and (15.5° E; 44.5° N) respectively. For the overall TEC forecast mapping, error values in the fourth columns of Tables 6.2 and 6.3 are presented. They are small. The average absolute error, for example, in Table 6.2 for the 1 hour in advance forecast, is less than 2 TEC units (TECu), which is important for practical applications. The forecast mapping error values are within operational tolerance [Radicella, 2004]. The cross correlation coefficients between the computed and observed TEC values are high as noted in Tables 6.2 and 6.3.

6.6 Conclusions

Characteristics of near-Earth space play vital roles in the ionospheric and trans-ionospheric propagation of radio waves. These parameters are subject to drastic variations depending on the space weather conditions. Thus the reliable operations of radio communication as well as navigation systems and spacecraft control systems largely depend on the reliable information concerning the ionospheric parameters such as TEC. Especially forecast of TEC values are essential in high frequency (HF) and other type of telecommunication system planning.

Space weather conditions also affect Earth bound systems, such as pipelines and electric power networks. By receiving alerts and warnings, pipeline managers can provide efficient systems decreasing the resultant corrosion rate on the pipes, and power companies can minimize resultant power damages.

Mapping is required in telecommunication planning as it involves the whole land, such as Europe in this case.

In this work, a data driven, Neural Network model forecasting the TEC values on the grids is offered, and then Bezier surfaces are used in obtaining the forecast TEC maps over Europe, which is very important for telecommunication and navigation especially during disturbed ionospheric conditions [Tulunay E. et al., 2006a].

Forecasts of an ionospheric process, the TEC variation, using Neural Network based METU-NN model was employed in order to forecast the TEC values 1 hour in advance. The model learned the shape of the inherent nonlinearities and the system reached the correct operating point in the operation time period of 16-29 November 2003. Forecasting errors are small. This fact is the indication of the system reaching the correct operating point within training. In other terminology, the system is prevented to reach local minima and it is succeeded to reach the global minimum of the error cost function. The correlation coefficients are very close to unity, which means that the METU-NN model learned the shape of the inherent nonlinearities. Therefore, the deviations from straight line are small in the scatter diagrams. In other words, it is shown that METU-NN modules, trained and tested with properly organized data are promising in modeling the complex nonlinear processes, such as the unpredictable variability of the ionospheric TEC values.

Briefly, it is the first time that METU-NN modules and Bezier surfaces are used to forecast and map TEC values over Europe [Tulunay E. et al., 2006a].

CHAPTER 7

FORECASTING TEC MAPS BY USING METU-NN-C AND BEZIER SURFACE PATCHES

7.1 Introduction

Middle East Technical University Neural Network and Cascade Modeling (METU-NN-C) technique by using polynomial, Bezier curve and B-Spline curve nonlinearity representations to forecast Total Electron Content (TEC) values for single station were presented in Chapters 2, 3 and 4. In Chapter 6, forecasting TEC maps by METU-NN model was presented. In this chapter, the use of METU-NN-C technique based on Hammerstein system modeling with Bezier curve nonlinearity representation in system identification to forecast complex nonlinear processes, TEC grid values; and the use of the Bezier surface in mapping of the METU-NN-C outputs, i.e. mapping of the forecast grid data values, are presented [Senalp et al., 2006b]. In order to compare the METU-NN-C results with the METU-NN results presented in Chapter 6, the series of space weather events in November 2003 are chosen again. 1 hour ahead forecast mapping of the TEC values during disturbances is performed.

This chapter also outlines preparation of data, gives the results with error tables, cross correlation coefficients and scatter diagrams. It discusses the generalized and fast learning and operation of the METU-NN-C models with

Bezier curve nonlinearities, and mapping by using Bezier surfaces [Rogers and Adams, 1990].

In our approach, the basic inputs for the model are the Bezier curve representation of the present TEC values on the grids and the temporal inputs. The state-like internal variables are estimated by METU-NN. The static nonlinearity of METU-C represented by Bezier curves, and the dynamic linearity of METU-C are estimated by using the cascade modeling technique. The outputs are 1 hour in advance forecast TEC grid values. Then, those values are used to obtain TEC forecast maps by employing Bezier surfaces.

7.2 Preparation of Data for the METU-NN

As in Chapter 6, ten-minute vertical TEC data, which were evaluated from the GPS measurements of the time interval, 1 November - 11 December 2003, over a portion of the European area centered over Italy, based on slant TEC data were used herewith [Ciraolo, 2004] [Radicella, 2004]. Again the data belong to the 104 grid locations spaced every 2º longitude by 1º latitude intervals in space between latitudes of (35.5ºN; 47.5ºN) and longitudes of (5.5ºE; 19.5ºE).

Table 6.1 in Chapter 6 illustrates how the data were assigned to be employed by the METU-NN and METU-NN-C models during the training, test and validation within development and within operation.

In this chapter, the period of major space weather events in November 2003 were chosen for the 'validation' mode again. In principle all the data subsets were chosen from periods of similar Zurich sunspot numbers. Thus, the models contain intrinsic information about the solar activity.

7.3 Construction of the METU-NN

The METU-NN-C model has 104 METU-C modules. Each module has its state-like variable estimator module, the METU-NN module. For the process of interest, Feedforward Neural Network architecture with four neurons in one hidden layer is used in each of the METU-NN module. The description continues by considering any one of the 104 METU-NN modules. Hyperbolic tangent sigmoids in the hidden layer and a linear function in the output layer are the activation functions. The hidden layer outputs of each of the METU-NN module can represent the static part of the state-like internal variables in cascade modeling. During training Levenberg-Marquardt Backpropagation algorithm is used [Hagan and Menhaj, 1994] [Haykin, 1999]. Each METU-NN module is used to estimate the internal variables of its corresponding METU-C module with Bezier curve nonlinearity. The 107 inputs used for each METU-NN module are as follows,

1 - 104. The present grid values of the TEC, f(k): see Equation 2.1 in Chapter 2

105. Cosine component of minute, m, of the day: see Equation 2.2 in Chapter 2

106. Sine component of the minute of the day: see Equation 2.3 in Chapter 2

107. Serial date number difference, dnd: see Equation 6.1 in Chapter 6

While the output layer of each METU-NN hosts the TEC value being observed 60 minutes later than the present time in a grid location, the outputs of the hidden layer in each METU-NN are four of the internal variables for each METU-C.

7.4 Construction of the METU- C

The METU-NN-C model has 104 METU-C modules. In the development mode, the construction work of each METU-C module is carried out in

"training phase" and "test phase" as in the Neural Network approach [Tulunay Y. et al., 2004a]. The parameters of the cascaded static nonlinear block and dynamic linear block in each METU-C module are optimized in the training phase. The description continues by considering any one of the 104 METU-C modules. In each METU-C, the inputs, $u_p(k)$, are normalized in order to use them in Bezier curve representation of the nonlinearity. The outputs of the nonlinear element in each METU-C, i.e. the internal variables $x_q(k)$, can be expressed as Bezier curves as in Equation 1.22 in Chapter 1. In the equation, R = 107 is the number of inputs, m+1 = 3+1 = 4 is the number of defining polygon points. Thus, the product R(m+1) = 428 gives the number of static block coefficients, B_{pi}, to be determined. The defining polygon points are the local control points [Rogers and Adams, 1990].

The output $y_1(k)$ is represented as in Equation 1.24 in Chapter 1 by using a dynamic linearity relationship for the internal variables $x_q(k)$ and their past values $x_q(k-j)$. For the equation, the product S.(n+1) gives the number of dynamic internal variables. The coefficients of the linearity, i.e. $h_q(j)$, are also determined.

The outputs of the first stage, i.e. 4 outputs of the static nonlinear block, $x_q(k)$, and their one hour and two hours past values are stored as internal variables so that S=4 and n=2 in Equation 1.24 in Chapter 1. These internal variables are the inputs to the second stage of the cascade model, i.e. 12 inputs for the dynamic linear block of the METU-C model.

For fast learning of the process with large sized input data the "Levenberg-Marquardt" optimization algorithm has been used within training again. Memorization is prevented by using independent validation data and by

terminating training when the gradient of the validation within development error becomes near zero. In the operation mode another data set is used for calculating the errors, point by point, to measure the performance of the model.

The output of each METU-C module is the value of the TEC to be observed 60 minutes later than the present time in one of the 104 grid locations. Then with the 104 outputs of the METU-NN-C model, 1 hour ahead TEC forecast maps over Europe are obtained by using Bezier surfaces [Rogers and Adams, 1990].

TEC forecast value at any location on the map can be computed by using Bezier surfaces as in Equation 6.2 in Chapter 6. In the equation, B matrix values correspond to the METU-NN-C outputs for the grids.

7.5 Results

Operation has been performed on validation data set by producing the forecast TEC maps over Europe for 16-29 November 2003. The cross correlation coefficients between the observed TEC and forecast TEC at 104 grid locations have been calculated. The root mean square, normalized and absolute error values have also been calculated. Tables 7.1 and 7.2 are the error tables displaying the results for three grid locations and for the overall TEC map. The time period includes the major November 2003 space weather (SW) event, which caused disturbance on TEC variation on 20 November 2003 [SpaceWeather, 2007].

Table 7.1. Error Table for 1 h in advance TEC forecasts on 16-29 Nov. 2003

Location	11.5°E 38.5°N	13.5°E 41.5°N	15.5°E 44.5°N	Overall TEC Map
Absolute Error (TECu)	1.42	1.32	1.38	1.50
Normalized Error (%)	13.09	13.88	15.27	14.75
Root Mean Square Error (TECu)	2.03	1.89	1.95	2.14
Cross Correlation Coefficient (x10^{-2})	97.74	97.56	97.27	97.08

Table 7.2. Error Table for 1 h in advance TEC forecasts on 19-21 Nov. 2003

Location	11.5°E 38.5°N	13.5°E 41.5°N	15.5°E 44.5°N	Overall TEC Map
Absolute Error (TECu)	1.89	1.98	1.99	2.12
Normalized Error (%)	15.72	18.25	18.67	20.29
Root Mean Square Error (TECu)	2.90	2.91	2.94	3.16
Cross Correlation Coefficient (x10^{-2})	97.56	97.20	97.03	96.71

Figure 7.1 shows the observed and forecast TEC variation at the location: 13.5˚E, 41.5˚N for 16-29 Nov. 2003. Figure 7.2 shows the scatter diagram for the same location and for 16-29 Nov. 2003. Figure 7.3 gives the variations of the observed TEC values and 1 hour in advance forecast TEC maps for the SW event of 20th Nov. 2003, at 13:00, 15:30 and 17:20 UT, respectively.

In the scatter diagram in Figure 7.2, the fitted line has a slope close to one and the forecasting errors are small for system operators. Thus, the system reached the correct operating point or the global minimum of the error cost function in system identification. Deviations from straight line are small in the scatter diagram and the correlation coefficients are very close to unity. Thus, the METU-NN-C model learned the shape of the inherent nonlinearities. The model gives accurate TEC forecast values and maps before, during and after the disturbed conditions as in Figures 7.1 and 7.3.
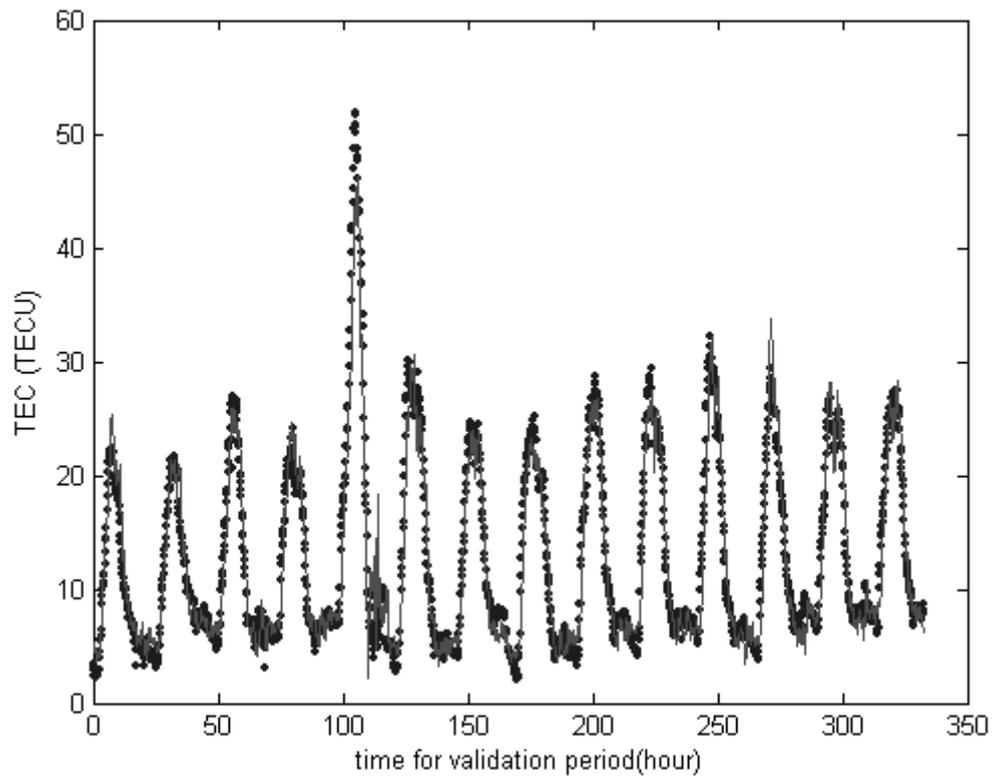
Figure 7.1. Location: 13.5˚E, 41.5˚N: Observed (dotted) and 1 hour in advance forecast (solid) TEC variation for 16-29 Nov. 2003.
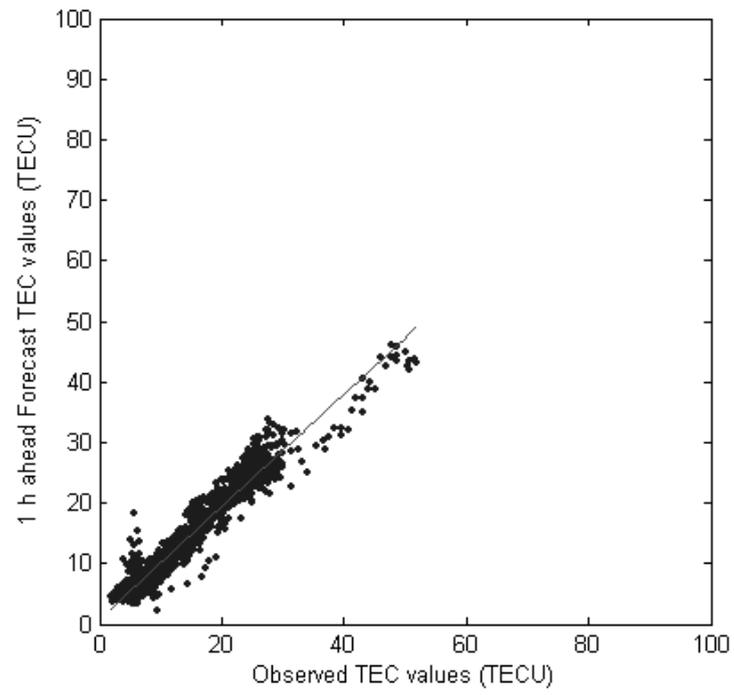
Figure 7.2. Location: 13.5°E, 41.5°N: Scatter diagram for 16-29 Nov. 2003
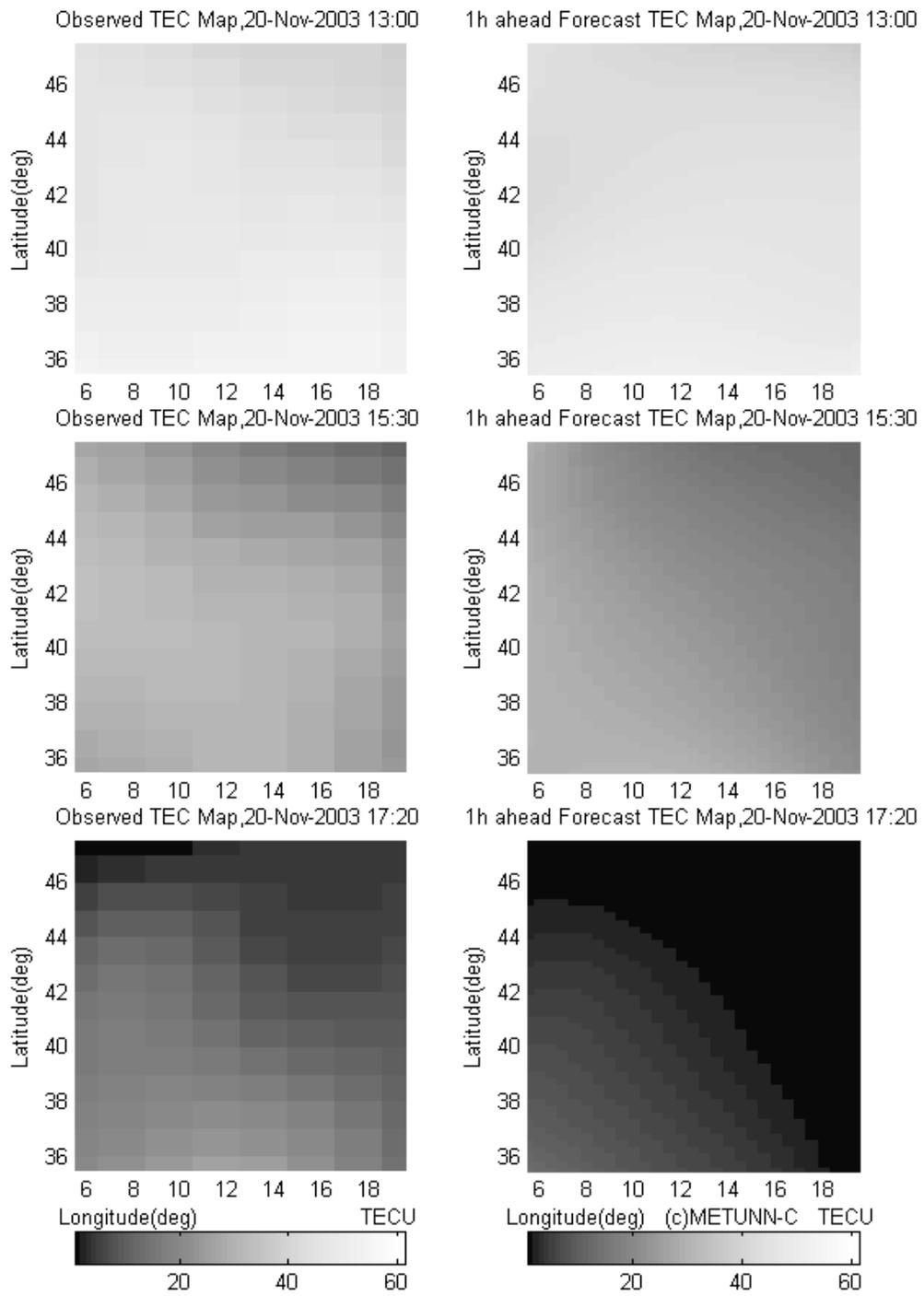
Figure 7.3. Observed TEC values and 1 hour ahead forecast TEC Map examples for 20 Nov. 2003.

The overall Absolute TEC error map is plotted in the Figure 7.4. The occurrence of the neighbor grids increases the learning performance of the model for forecasting.
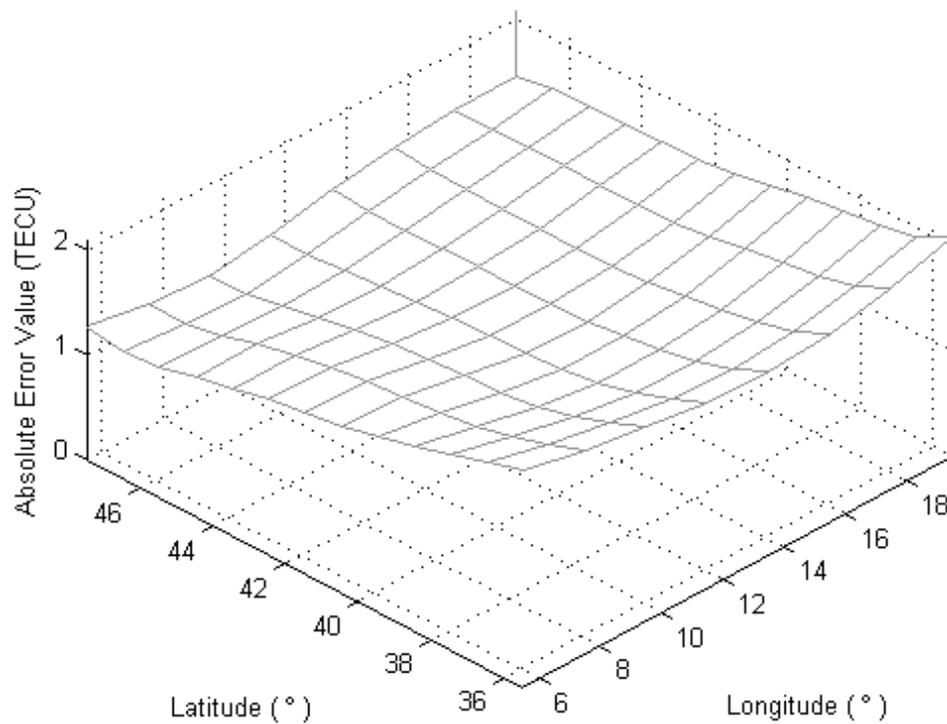
Figure 7.4. Absolute error map for observed and 1 h. ahead forecast TEC during 16-29 Nov. 2003

7.6 Conclusions

Since the reliable operations of radio communication as well as navigation systems and spacecraft control systems largely depend on the reliable

information concerning the ionospheric parameters such as TEC, developing new techniques to identify those processes with higher accuracy is the basic requirement, and forecast mapping of TEC values are essential in high frequency (HF) telecommunication system planning as it involves the whole land, such as Europe in this and previous cases.

In this work, Hammerstein system modeling based METU-NN-C to forecast the TEC values on the grids is offered, and then Bezier surfaces are used in obtaining the forecast TEC maps over Europe. This is very important for telecommunication and navigation especially during disturbed ionospheric conditions.

In this work, the developed METU-NN-C model has 104 METU-NN and 104 METU-C modules for the process of interest. The METU-NN modules estimated the state-like variables of the METU-C modules. The METU-NN-C learned the shape of the inherent nonlinearities and reached the correct operating points even in the disturbed Space Weather conditions. It can be concluded that the identification of the complex nonlinear processes, such as the TEC forecast mapping, can be achieved by Hammerstein forms in which a static nonlinear block and a linear dynamic block are cascaded. The inner locations on the forecast maps gave higher performance results because those have more neighbor grids increasing the learning performance.

The METU-NN-C model results are compared with the METU-NN model results being presented in Chapter 6.

Considering the error tables and scatter diagrams in Chapter 6 and 7, it is concluded that METU-NN-C models are successful in process identification.

Error values in Table 7.1 are smaller than the ones in Table 6.2, and cross correlation coefficients in Table 7.1 are higher. For the overall TEC forecast mapping, error values in the fourth columns of Tables 7.1 and 7.2 are small. The forecast mapping error values are within operational tolerance [Radicella, 2004].

Briefly, it is the first time that METU-NN-C modules and Bezier surfaces are used to forecast and map TEC values over Europe.

CHAPTER 8

THE USE OF METU-NN-C FOR KNOWN NONLINEAR DYNAMIC PROCESSES

8.1 Introduction

Middle East Technical University Neural Network and Cascade Modeling (METU-NN-C) technique with Bezier curve nonlinearity is used to identify a simple forced pendulum; a spring loaded inverted double pendulum with a forced table; two speakers; and a Van der Pol oscillator in order to further show generalized usage of METU-NN-C [Senalp et al., 2006e] [Senalp et al., 2007b] [Senalp, 2007a] [Senalp, 2007c].

8.2 Simple Forced Pendulum

The simple forced pendulum in Figure 8.1 is a well-known nonlinear problem, whose state equations are known as follows [Franklin et al., 1990],

$$\dot{\omega} = -b\omega - \Omega^2 \sin\vartheta + \frac{1}{ml^2}T_{in} \qquad (8.1)$$

$$\dot{\vartheta} = \omega \qquad (8.2)$$

where T_{in} is the input torque generated by a buffeting wind, θ is the output angular position, b is the coefficient of drag, and $\Omega = \sqrt{g/l}$ is the oscillation frequency for small initial conditions, small angles [Franklin et al., 1990].
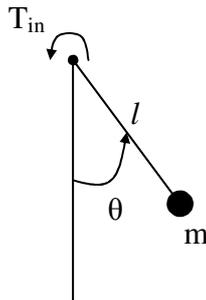
Figure 8.1. Schematic of a simple pendulum [Franklin et al., 1990]

8.2.1 Data for METU-NN-C

The response of the simple forced pendulum angle to a complex input torque generated by a buffeting wind was obtained [Franklin et al, 1990]. Figure 8.2 shows the input representing random wind force acting on the pendulum, whereas Figure 8.3 shows the response of the pendulum angle [Franklin et al, 1990].
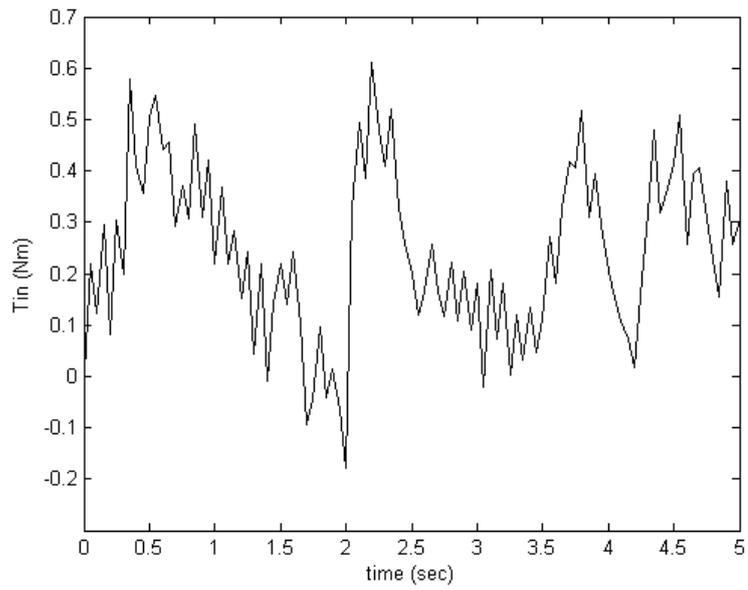
Figure 8.2. Torque generated by a buffeting wind [Franklin et al., 1990]
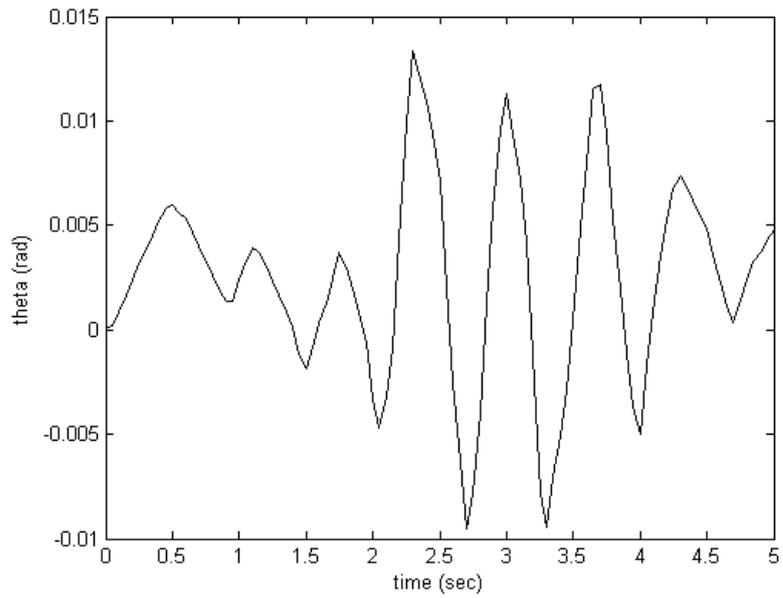
Figure 8.3. Response of the pendulum angle to the torque given in Figure 8.2.

Those input and response data are used to identify the process by METU-NN-C model. The sampling time is selected as 0.05 sec. By giving the initial conditions, the 0.05 sec in advance values of the response of the pendulum are to be obtained by using the METU-NN-C model [Senalp et al., 2007b].

8.2.2 Construction of the METU-NN

The METU-NN-C model has one METU-C module. The module has its state-like variable estimator module, the METU-NN module. The 2 inputs used for the METU-NN module are the initial angle and the present torque. For the process of interest, Feedforward Neural Network architecture with two neurons in one hidden layer is used in the METU-NN module. Hyperbolic tangent sigmoids in the hidden layer and a linear function in the output layer are the activation functions. The hidden layer outputs of the METU-NN module can represent the static part of the state-like internal variables in cascade modeling. During training Levenberg-Marquardt Backpropagation algorithm has been used [Hagan and Menhaj, 1994] [Haykin, 1999].

The METU-NN module is used to estimate the internal variables of the METU-C module with Bezier curve nonlinearity. While the output layer of the METU-NN hosts the response of the pendulum angle value being observed 0.05 sec later than the initial time, the outputs of the hidden layer in the METU-NN are two of the internal variables for the METU-C.

8.2.3 Construction of the METU-C

The METU-NN-C model has one METU-C module. The parameters of the cascaded static nonlinear block and dynamic linear block in the METU-C module are optimized in the training phase. The inputs are normalized in order to use them in Bezier curve representation of the static nonlinearity. The outputs of the nonlinear element in each METU-C, i.e. the internal variables

129

$x_q(k)$, can be expressed as Bezier curves as in Equation 1.22 in Chapter 1. In the equation, R = 2 is the number of inputs, m+1 = 3+1 = 4 is the number of defining polygon points. Thus, the product R(m+1) = 8 gives the number of static block coefficients, B_{pi}, to be determined.

The output y(k) is represented as in Equation 1.24 in Chapter 1. The coefficients of the linearity, i.e. $h_q(j)$, are also determined.

The outputs of the first stage, i.e. 2 outputs of the static nonlinear block, $x_q(k)$, and their one step and two step past values are stored as internal variables so that S=2 and n=2 in Equation 1.24 in Chapter 1. These internal variables are the inputs to the second stage of the cascade model, i.e. S.(n+1) = 6 inputs for the dynamic linear block of the METU-C model.

The "Levenberg-Marquardt" optimization algorithm has been used within training again.

The output of the METU-C module is the value of the response of the pendulum angle to be observed 0.05 sec later than the initial time. In the operation mode the data set is used for calculating the errors, point by point, to measure the performance of the model.

8.2.4 Results

The root mean square, normalized and absolute error values; the cross correlation coefficients between the observed angles and estimated angles have been calculated [Senalp et al., 2007b]. Table 8.1 is the error table displaying the results. Figure 8.4 shows the observed and estimated angle variation. Figure 8.5 shows the scatter diagram.

130

Table 8.1. Error Table for estimating the response of the pendulum angle

Absolute Error (rad)	0.0007
Normalized Error (%)	9.45
Root Mean Square Error (rad)	0.0009
Cross Corr. Coeff. $(\times 10^{-2})$	98.12
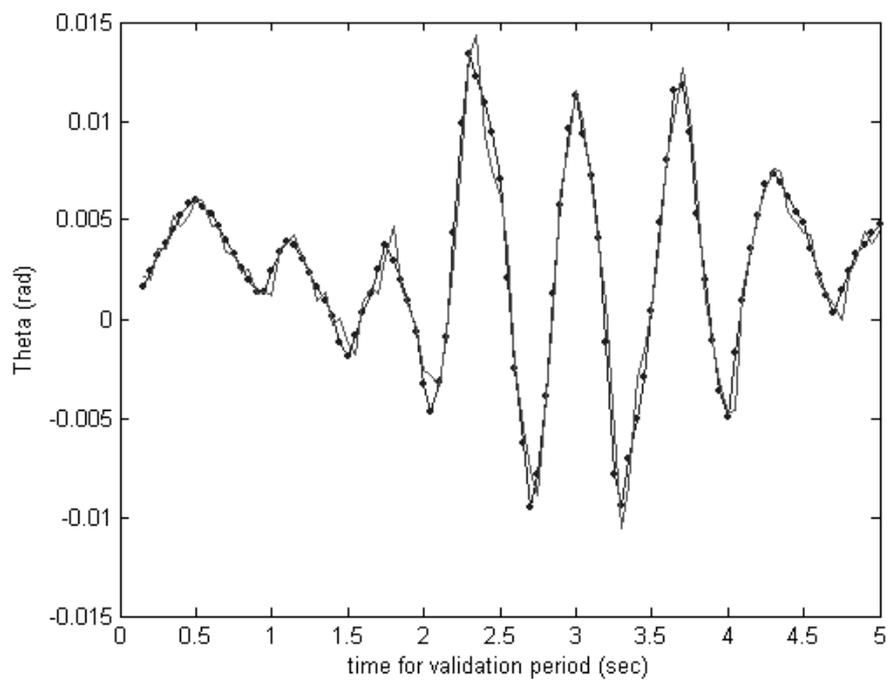
Figure 8.4. Estimated (solid), and observed angle variation (dotted).
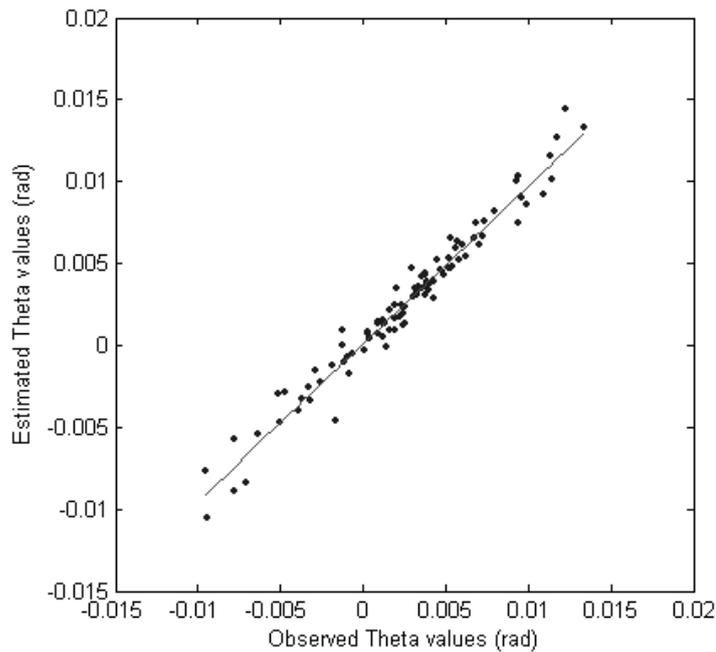
Figure 8.5. Scatter diagram for the estimated and observed angle values

In the scatter diagram the fitted line has a slope close to one and the forecasting errors are small. Thus, the system reached the correct operating point. METU-NN-C model learned the shape of the inherent nonlinearities because deviations from straight line are small in the scatter diagram and the correlation coefficients are very close to unity.

8.3 Spring Loaded Inverted Double Pendulum with a Forced Table

The inverted double pendulum is an important example for model developers [Aristoff et al., 2003]. In this section, the joint angles of a spring loaded inverted double pendulum with a forced table are estimated by using METU-NN-C with Bezier nonlinearity representations [Senalp et al., 2006e] [Senalp et

al., 2007b]. In Figure 8.6, spring loaded inverted double pendulum with a forced table is shown schematically.
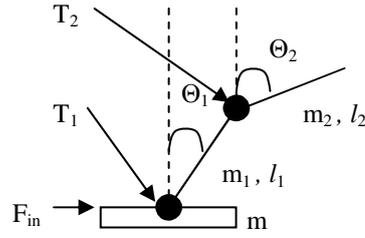
Figure 8.6. Inverted double pendulum

The positions of gravity centers of the pendulum rods, s_1 and s_2, in terms of the base table position, s_m, and pendulum joint angles, Θ_1 and Θ_2, are as follows,

$$s_1(k) = \begin{bmatrix} s_m(k) + l_1 . \sin\Theta_1(k) \\ l_1 . \cos\Theta_1(k) \end{bmatrix} \tag{8.3}$$

$$s_2(k) = \begin{bmatrix} s_m(k) + l_1 . \sin\Theta_1(k) + l_2 . \sin\Theta_2(k) \\ l_1 . \cos\Theta_1(k) + l_2 . \cos\Theta_2(k) \end{bmatrix} \tag{8.4}$$

The torques, T_1 and T_2, generated by the springs in the system are as follows,

$$T_i(k) = K . \Theta_i(k) \tag{8.5}$$

where K is the spring constant.

133

8.3.1 Data for METU-NN-C

By using MATLAB SimMechanics simulations of inverted double pendulums are performed [MATLAB, 2002]. Performing those simulations creates input data and observed data for inverted pendulum systems to be used in development and operation of the METU-NN-C model.

As a first input data set, pendulum joint angle values, Θ_1 and Θ_2; generated torques of the springs at the pendulum joints, T_1 and T_2; and the external force values applied to the base table in the system, F_{in}, are observed after 10-second simulations with 0.02 seconds sampling time. For the time interval of 0.1 and 0.15 seconds, F_{in} is adjusted to 160N in x direction; for the time interval of 5 and 5.05 seconds, F_{in} is adjusted to 320N in the –x direction.

To obtain a second input data set, the same simulation procedure is performed after changing the external force values to be applied on the base table of the system. For the time interval of 0.1 and 0.15 seconds, F_{in} is adjusted to 80N in x direction; for the time interval of 5 and 5.05 seconds, F_{in} is adjusted to 160N in the –x direction.

In the simulations, two of the thin pendulum rod (B_1, B_2) masses, m_1 and m_2, are chosen to be 1 kg.; two of the thin pendulum rod lengths, l_1 and l_2, are chosen to be 1 m.; and the base table (B_0) mass, m, is chosen to be 5 kg. The spring constants, K, of the springs at the pendulum joints are chosen to be –0.9. The damper constants at the pendulum joints are chosen to be zero. The simulation blocks are given in Figure 8.7 [MATLAB, 2002].
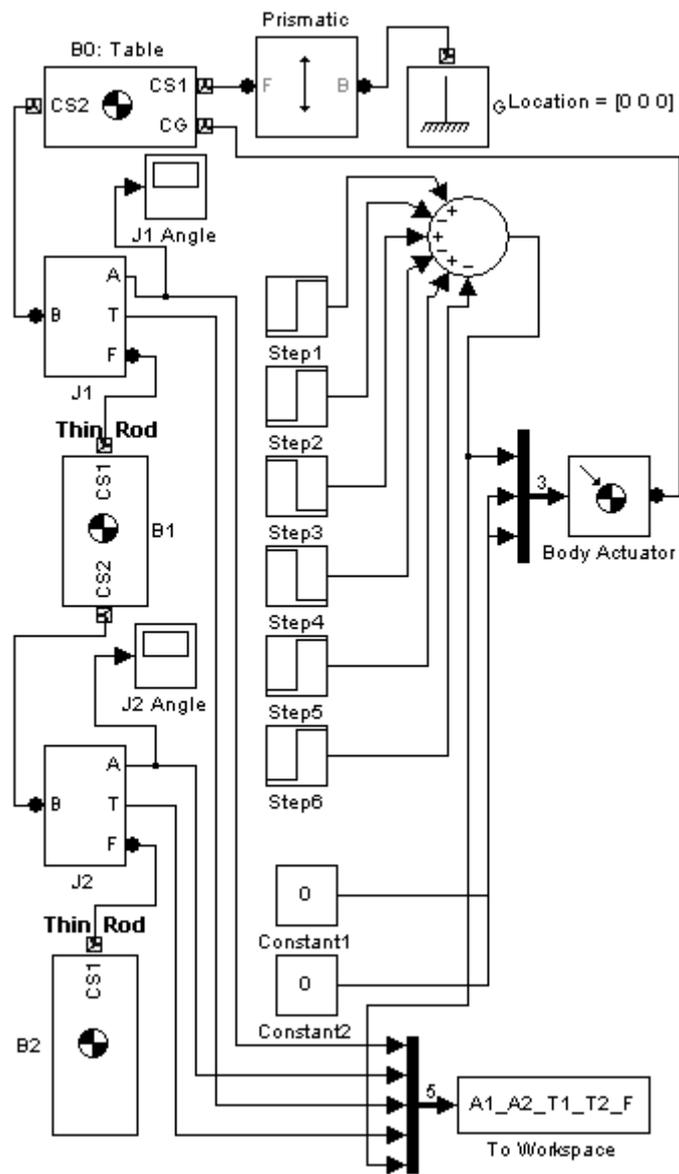
Figure 8.7. Construction of the spring loaded inverted double pendulum with a forced table by using "Matlab, SimMechanics" simulation tool.

8.3.2 Construction of the METU-NN

The METU-NN-C model has one METU-C module. The module has its state-like variable estimator module, the METU-NN module. The 5 inputs used for the METU-NN module are 2 initial angle values, Θ_1 and Θ_2, for two joints, 2 present torque values, T_1 and T_2, for the joints, and 1 external force value, F_{in}, applied on the base table. For the process of interest, Feedforward Neural Network architecture with six neurons in one hidden layer is used in the METU-NN module. Hyperbolic tangent sigmoids in the hidden layer and a linear function in the output layer are the activation functions. The hidden layer outputs of the METU-NN module can represent the static part of the state-like internal variables in cascade modeling. During training Levenberg-Marquardt Backpropagation algorithm has been used [Hagan and Menhaj, 1994] [Haykin, 1999].

The METU-NN module is used to estimate the internal variables of the METU-C module with Bezier curve nonlinearity. While the output layer of the METU-NN hosts the response of the pendulum angle values being observed 0.02 sec later than the initial time, the outputs of the hidden layer in the METU-NN are six of the internal variables for the METU-C.

8.3.3 Construction of the METU-C

The METU-NN-C model has one METU-C module. The parameters of the cascaded static nonlinear block and dynamic linear block in the METU-C module are optimized in the training phase. The inputs are normalized in order to use them in Bezier curve representation of the static nonlinearity. The outputs of the nonlinear element in each METU-C, i.e. the internal variables $x_q(k)$, can be expressed as Bezier curves as in Equation 1.22 in Chapter 1. In the equation, R = 5 is the number of inputs, m+1 = 3+1 = 4 is the number of

defining polygon points. Thus, the product R(m+1) = 20 gives the number of static block coefficients, B_{pi}, to be determined.

The output y(k) is represented as in Equation 1.24 in Chapter 1. The coefficients of the linearity, i.e. $h_q(j)$, are also determined.

The outputs of the first stage, i.e. 6 outputs of the static nonlinear block, $x_q(k)$, and their one step and two step past values are stored as internal variables so that S=6 and n=2 in Equation 1.24 in Chapter 1. These internal variables are the inputs to the second stage of the cascade model, i.e. S.(n+1) = 18 inputs for the dynamic linear block of the METU-C model.

The "Levenberg-Marquardt" optimization algorithm has been used within training again.

In the operation mode the data set is used for calculating the errors, point by point, to measure the performance of the model. The output of the METU-C module is the value of the response of the pendulum angle to be observed 0.02 sec later than the initial time.

8.3.4 Results
For the performance analysis, the METU-C model is operated with the second data set. Also another METU-NN model with additional inputs, i.e. first and second differences of the present inputs, is developed and operated for performance analysis. The cross correlation coefficients between the observed angles and estimated angles have been calculated. The root mean square, normalized and absolute error values have also been calculated [Senalp et al., 2006e]. Tables 8.2 and 8.3 are the error tables displaying the results for joints 1

and 2, respectively. Figures 8.8 and 8.9 show the observed and estimated angle variations by METU-NN for the two joints. Figures 8.10 and 8.11 show the observed and estimated angle variations by METU-NN-C for the two joints. Scatter diagrams for the same cases are given in Figures 8.12, 8.13, 8.14, and 8.15.

Table 8.2. Error Table for estimating the response of the pendulum angle, Θ_1

	METU-NN	METU-C (Bezier)
Absolute Error (°)	0.296	0.038
Root Mean Square Error (°)	0.493	0.103
Cross Corr. Coeff. $(x10^{-2})$	99.7	99.9

Table 8.3. Error Table for estimating the response of the pendulum angle, Θ_2

	METU-NN	METU-C (Bezier)
Absolute Error (°)	0.327	0.103
Root Mean Square Error (°)	0.534	0.226
Cross Corr. Coeff. $(x10^{-2})$	99.2	99.8
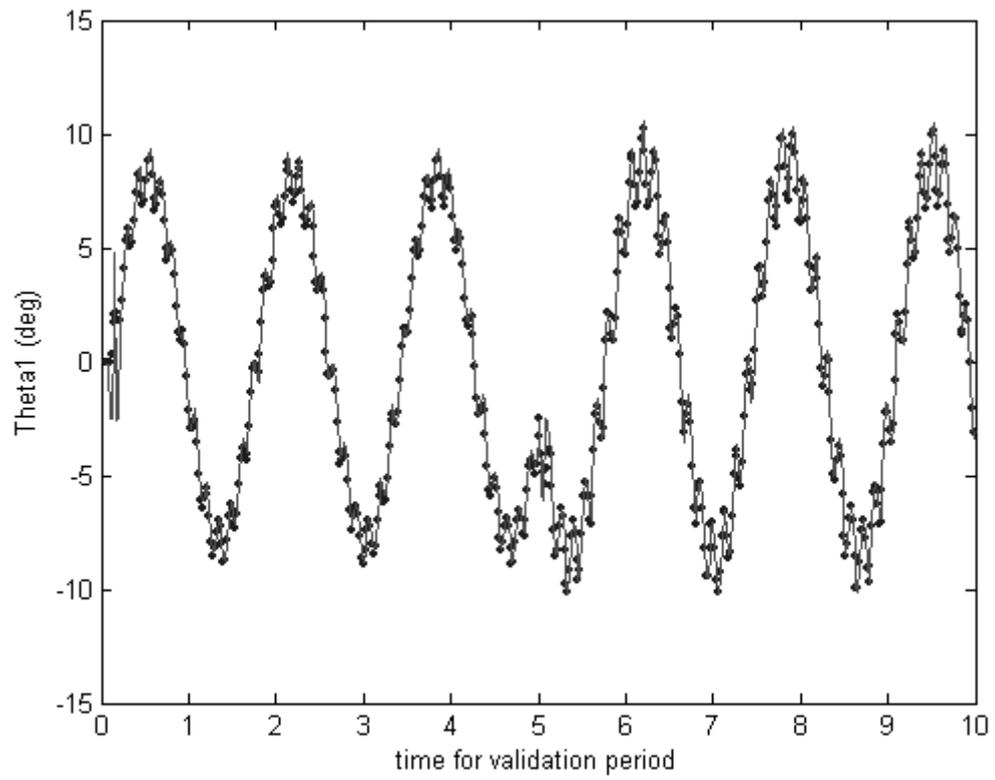
Figure 8.8. For Θ_1, observed (dotted) and estimated angle variations (solid) by METU-NN
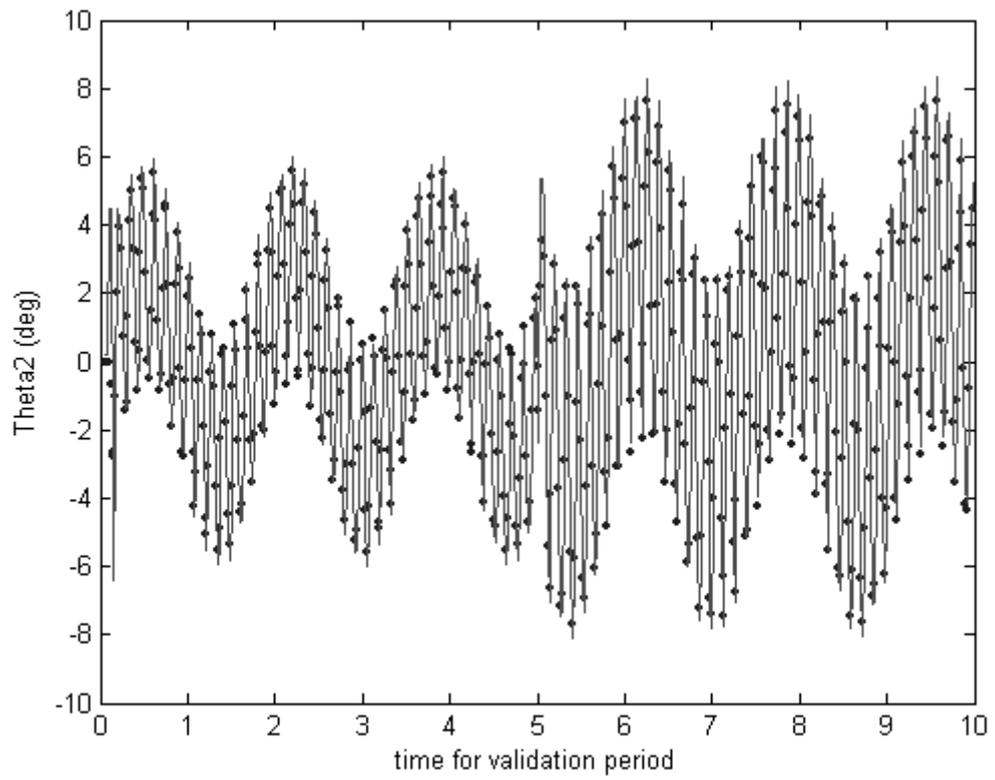
Figure 8.9. For Θ_2, observed (dotted) and estimated angle variations (solid) by METU-NN
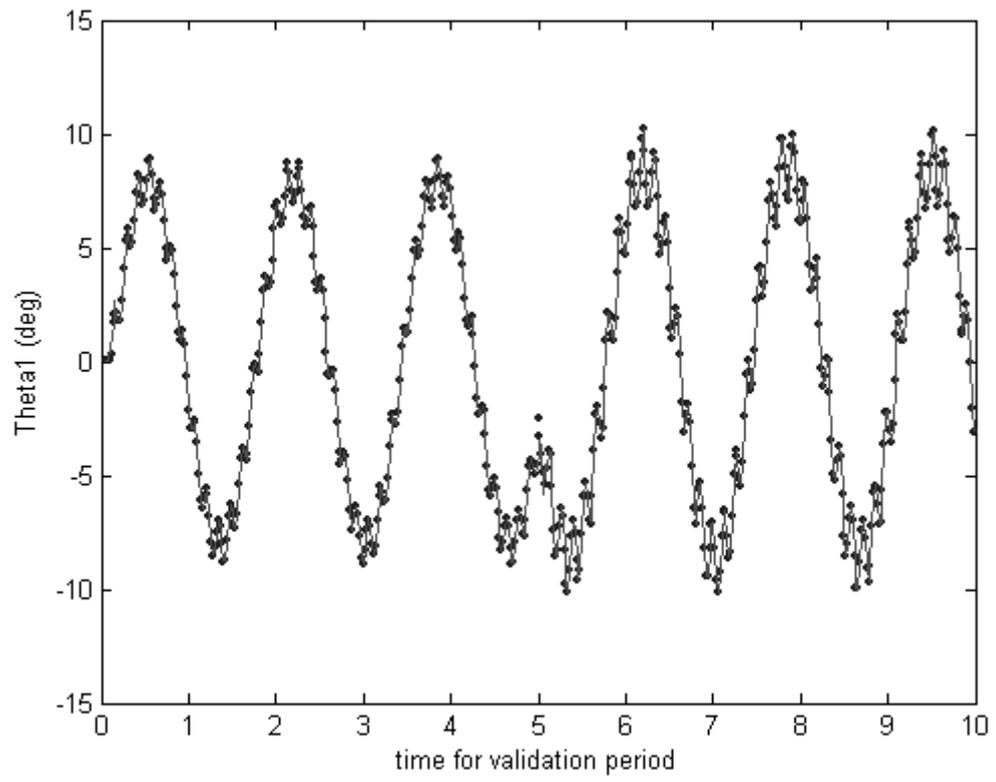
Figure 8.10. For Θ_1, observed (dotted) and estimated angle variations (solid) by METU-C.
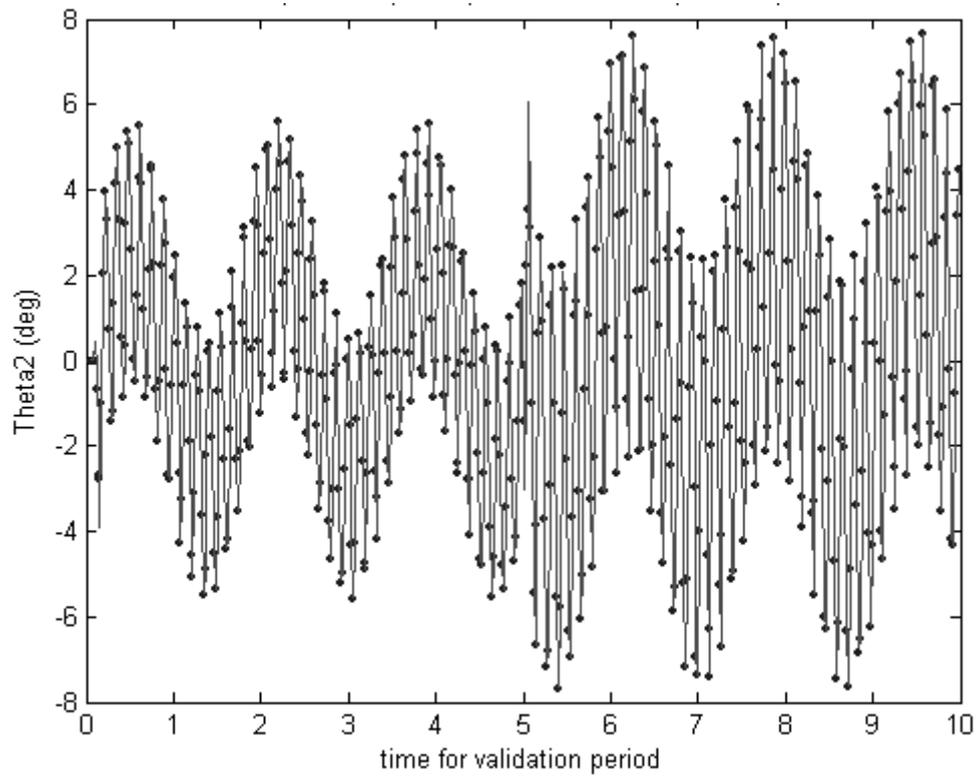
Figure 8.11. For Θ_2, observed (dotted) and estimated angle variations (solid) by METU-C.
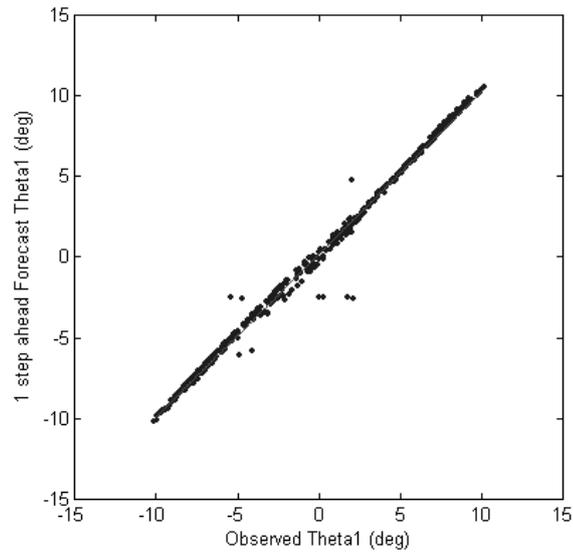
Figure 8.12. For Θ_1, Scatter diagram with best fit line for the estimated and observed angle values by METU-NN
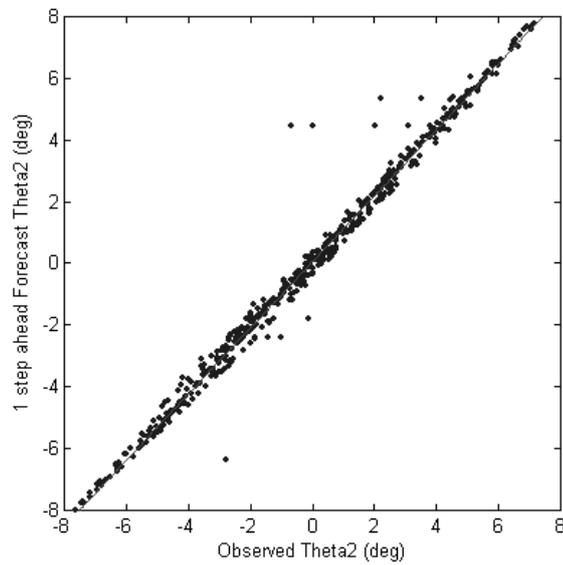
Figure 8.13. For Θ_2, Scatter diagram with best fit line for the estimated and observed angle values by METU-NN
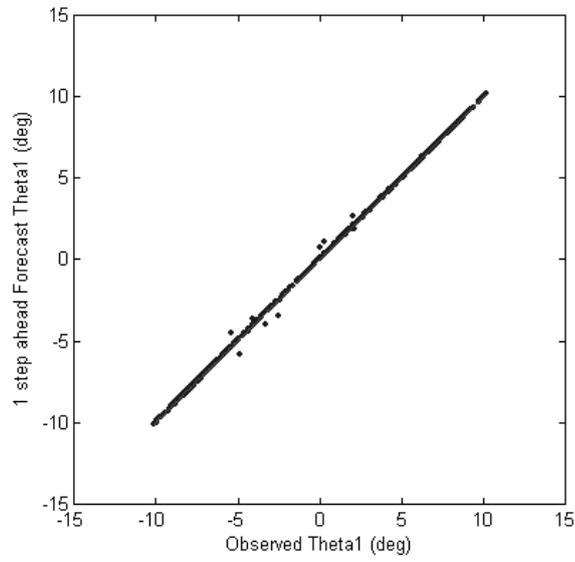
Figure 8.14. For Θ_1, Scatter diagram with best fit line for the estimated and observed angle values by METU-NN-C
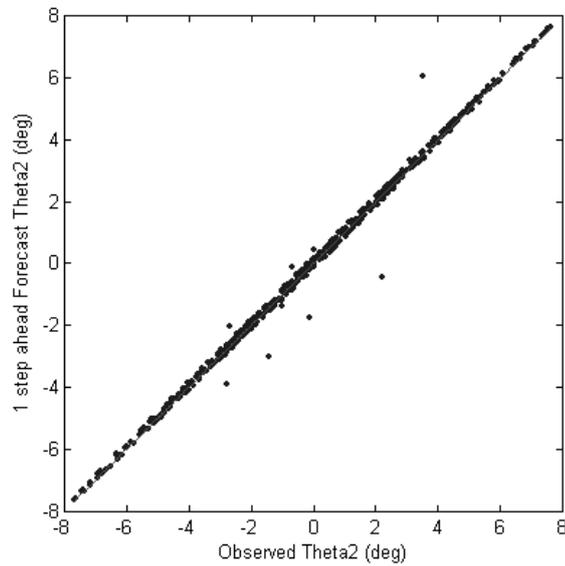
Figure 8.15. For Θ_2, Scatter diagram with best fit line for the estimated and observed angle values by METU-NN-C.

In the scatter diagrams the fitted lines have slope close to one and the forecasting errors are small. Thus, the systems reached the correct operating points. Deviations from straight line are small in the scatter diagrams and the correlation coefficients are very close to unity. Thus, the models learned the shape of the inherent nonlinearities. When the performance results of METU-NN and METU-NN-C models are compared it is observed that the error values for the METU-NN-C model are smaller, thus the scatter diagrams for the METU-NN-C model have slopes closer to one. Also, the cross-correlation coefficients for the METU-NN-C performance results are higher and the deviations of the scatter points for the METU-NN-C performance results are smaller when they are compared with the METU-NN performance results.

8.4 Identification of Speakers by METU-NN-C

The objective of this section is to give the results of the first attempt on identification of speakers by using cascade modeling technique. In this work the METU-NN-C model is used to identify speakers by using some features related to speech of the speakers [Senalp, 2007a]. The speech features used are normalized Mel Frequency Cepstrum Coefficients (MFCC) and (Moving Picture Expert Group) MPEG frames of the speakers.

8.4.1. Inputs and Outputs for METU-NN-C

The raw input data have been organized by Dr. C. Ergun under supervision of Assoc. Prof. Dr. T. Ciloglu [Ciloglu and Ergun, 2007]. It consists of MFCC and MPEG frames of speakes. Each MFCC frame is of size 16 and each MPEG frame is of size 24. The harmonic components of one MPEG frame are of size 8. The raw data consist of normalized MFCC frames of size 16 and normalized harmonic components of the MPEG frames of size 8. Thus, one total frame consists of 16+8=24 components [Ciloglu and Ergun, 2007].

By using the raw input data, the inputs and outputs for the METU-NN-C are organized by E.T. Senalp. Training data set of two speakers with 793 feature vectors, validation in training data set of two speakers with 428 feature vectors, and validation in operation data set of two speakers with 8555 feature vectors are prepared.

The outputs of the METU-NN-C model are the identification codes for the speakers. The identification code targets for the Speakers A and B are 0 and 1, respectively.

8.4.2. METU-NN-C Model for Speaker Identification

A small group at the METU in Ankara has works on data driven generic modeling of near-Earth space processes since 1990's. The Neural Network based model is the METU-NN model [Tulunay, 1991] [Altinay et al., 1997] [Tulunay Y. et al., 2004a] [Tulunay Y. et al., 2004b] [Tulunay E. et al., 2006a]. Cascade modeling of several natural, nonlinear, dynamic processes have been performed and presented in this Thesis and in national and international journal and conferences cited in the Thesis. The Hammerstein system modeling based cascade model, METU-NN-C, has been developed and employed [Senalp et al., 2006c]. METU-NN has been used as one of the important modules of the METU-NN-C to estimate the state-like interior variables of METU-C. The nonlinearities have been represented by using several representations including the Bezier curves [Senalp et al., 2006b] [Senalp et al., 2006d] [Senalp et al., 2006e] [Senalp et al., 2007b].

In this work, METU-NN-C with Bezier curve nonlinearity representations are used to identify speakers. The model has 24 inputs, 12 interior variables and one output. First, the interior variables are estimated by using METU-NN.

METU-NN is a feed-forward NN having 24 inputs, 12 hidden neurons in one hidden layer and one output. Hyperbolic tangent sigmoid activation functions are used in the first layer and linear transfer function is used in the second layer. Levenberg-Marquardt Backpropagation algorithm is used within training of the METU-NN.

Using the estimates of the interior variables of the METU-C, and using the Bezier curve nonlinearity representations of the inputs, the parameters of the nonlinear static block METU-C are identified by Levenberg-Marquardt optimization. The internal variables $x_q(k)$, are expressed by using the Bezier curve representations as in Equation 1.22 in Chapter 1. The number of defining polygon points is chosen to be 4 in the Bezier curves.

Using the interior variables and training set outputs; the parameters of the linear block of the METU-C are identified by Levenberg-Marquardt optimization as well. Then, the METU-C is ready to be operated by using the validation in operation data set.

8.4.3. Results

The performance of the model is visualized by obtaining the observed and estimated outputs of the METU-C using the validation in operation data set [Senalp, 2007a]. The observed identification codes for the Speakers A and B are 0 and 1, respectively.

Figure 8.16 gives the observed (targets, dashed) and estimated (METU-C outputs, solid) identification values for the frames of the speakers. Figure 8.17 gives the observed (targets, dashed) and limited average values of the estimated (METU-C outputs, solid) identification values for the frames of the speakers.
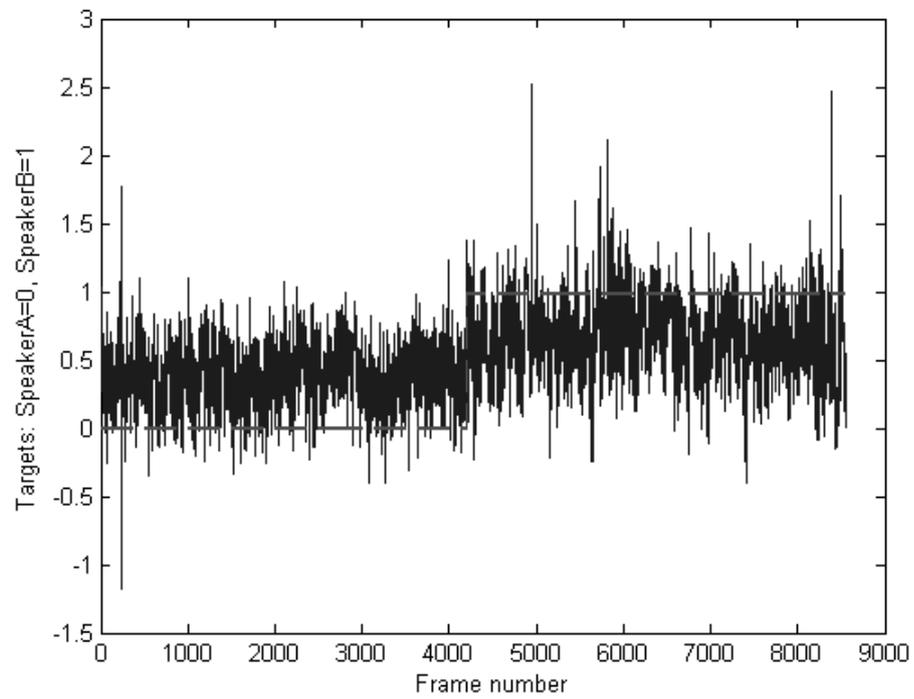
Figure 8.16. Observed (targets, dashed) and estimated (METU-C outputs, solid) identification values for the frames of the speakers
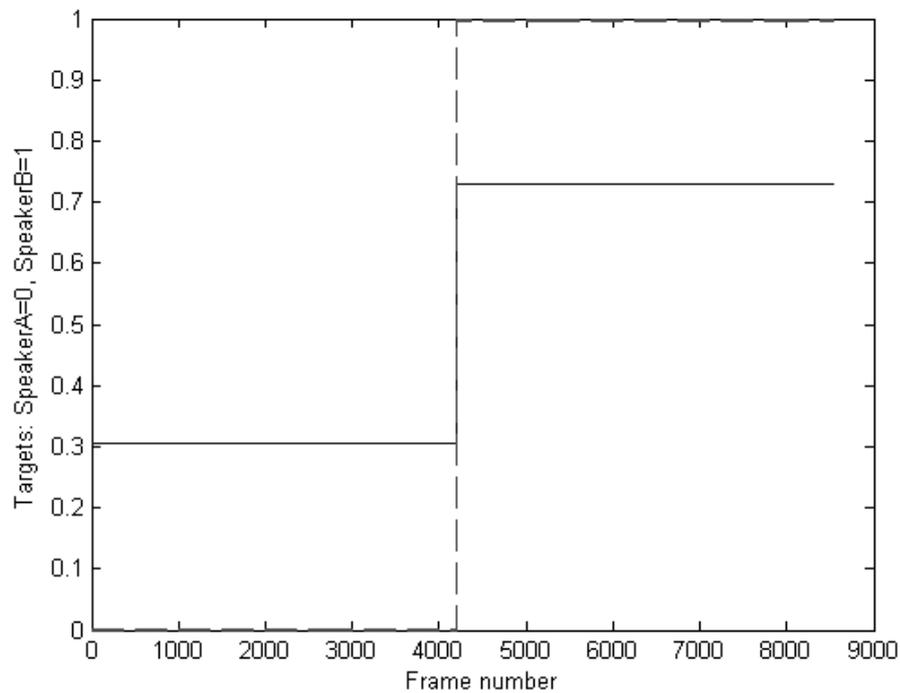
Figure 8.17. Observed (targets (0, 1), dashed) and limited average values of the estimated (METU-C outputs, solid) identification values for the frames of the speakers

The speakers are identified successfully. As a first attempt, the performance of the METU-NN-C model to identify the speakers is shown to be promising.

8.5 Van der Pol Oscillator

Van der Pol oscillator is an important basic example for unforced nonlinear second order systems having limit cycles in their solution space [MATLAB, 2002] [Uraz, 2007]. In this section, the solution values of a Van der Pol oscillator are estimated by using METU-NN-C with Bezier nonlinearity representations [Senalp, 2007c].

149

The equation of a Van der Pol oscillator is as follows,

$$\ddot{y} - \mu.(1 - y^2)\dot{y} + y = 0 \qquad (8.6)$$

where $\mu > 0$ is a scalar parameter. The Van der Pol oscillator equation when $\mu = 1$ is given as follows,

$$\ddot{y}_1 - (1 - y_1^2)\dot{y}_1 + y_1 = 0 \qquad (8.7)$$

The system as first order differential equations is given as follows,

$$\dot{y}_1 = y_2 \qquad (8.8)$$

$$\dot{y}_2 = -y_1 + (1 - y_1^2)y_2 \qquad (8.9)$$

8.5.1 Data for METU-NN-C

By using MATLAB, simulations of Van der Pol oscillators with different initial conditions are performed [MATLAB, 2002]. Performing those simulations creates input data and observed data for Van der Pol oscillator systems to be used in development and operation of the METU-NN-C model.

As a first input data set, solutions of the Van der Pol oscillators with initial conditions, $y_{a1,2}$ (t = 0) = {-1, 1}; $y_{b1,2}$ (t = 0) = {0, 1}; $y_{c1,2}$ (t = 0) = {1, 1}; $y_{d1,2}$ (t = 0) = {-1, -1}; $y_{e1,2}$ (t = 0) = {0, -1}; and $y_{f1,2}$ (t = 0) = {1, -1}, are simulated. Those data are used in 'training' phase. Then, as another input data set, solutions of the Van der Pol oscillators with initial condition, $y_{g1,2}$ (t = 0) = {-0.5, 0}; and $y_{h1,2}$ (t = 0) = {0.5, 0}, are simulated. Those data are used in 'validation within training' and 'validation within operation' phases.

Solutions are observed after 20-second simulations with 0.1 seconds sampling time [MATLAB, 2002].

8.5.2 Construction of the METU-NN

The METU-NN-C model has one METU-C module. The module has its state-like variable estimator module, the METU-NN module. The 2 inputs used for the METU-NN module are 2 solution values, y_1 and y_2. For the process of interest, Feedforward Neural Network architecture with two neurons in one hidden layer is used in the METU-NN module. Hyperbolic tangent sigmoids in the hidden layer and a linear function in the output layer are the activation functions. The hidden layer outputs of the METU-NN module can represent the static part of the state-like internal variables in cascade modeling. During training Levenberg-Marquardt Backpropagation algorithm has been used [Hagan and Menhaj, 1994] [Haykin, 1999].

The METU-NN module is used to estimate the internal variables of the METU-C module with Bezier curve nonlinearity. While the output layer of the METU-NN hosts the solutions of the Van der Pol oscillator, which are observed 0.1 sec later than the initial time, the outputs of the hidden layer in the METU-NN are two of the internal variables for the METU-C.

8.5.3 Construction of the METU-C

The METU-NN-C model has one METU-C module. The parameters of the cascaded static nonlinear block and dynamic linear block in the METU-C module are optimized in the training phase. The inputs are normalized in order to use them in Bezier curve representation of the static nonlinearity. The outputs of the nonlinear element in each METU-C, i.e. the internal variables $x_q(k)$, can be expressed as Bezier curves as in Equation 1.22 in Chapter 1. In the equation, R = 2 is the number of inputs, m+1 = 2+1 = 3 is the number of defining polygon points. Thus, the product R(m+1) = 6 gives the number of static block coefficients, B_{pi}, to be determined.

The output $y(k)$ is represented as in Equation 1.24 in Chapter 1. The coefficients of the linearity, i.e. $h_q(j)$, are also determined.

The outputs of the first stage, i.e. 2 outputs of the static nonlinear block, $x_q(k)$, and their one step past values are stored as internal variables so that $S=2$ and $n=1$ in Equation 1.24 in Chapter 1. These internal variables are the inputs to the second stage of the cascade model, i.e. $S.(n+1) = 6$ inputs for the dynamic linear block of the METU-C model.

The "Levenberg-Marquardt" optimization algorithm has been used within training again.

The output of the METU-C module is the value of the response of the pendulum angle to be observed 0.1 sec later than the initial time. In the operation mode the data set is used for calculating the errors, point by point, to measure the performance of the model.

8.5.4 Results

For the performance analysis, the METU-C model is operated with the data set for operation. The cross correlation coefficients between the observed solutions and estimated solutions have been calculated. The absolute error values have also been calculated [Senalp, 2007c]. Table 8.4 is the error table displaying the results for the solutions y_1 and y_2.

Table 8.4. Error Table for estimating the solutions of the Van der Pol oscillator

	y_1	y_2
Absolute Error (unit)	0.006	0.044
Cross Corr. Coeff. (x10^{-2})	100.0	99.9

Figures 8.18 and 8.19 show the observed and estimated solution variations by METU-C for the two solutions.
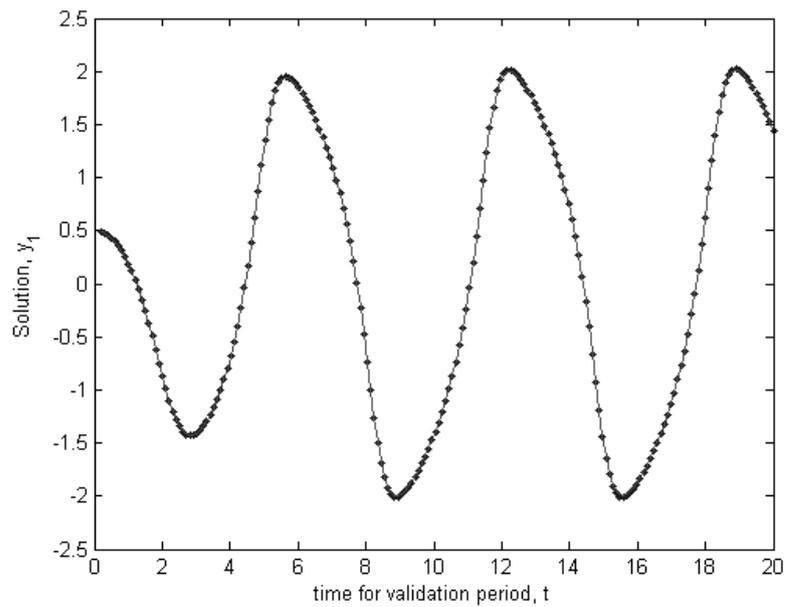
Figure 8.18. For y_1, observed (dotted) and estimated solution variations (solid) by METU-C.
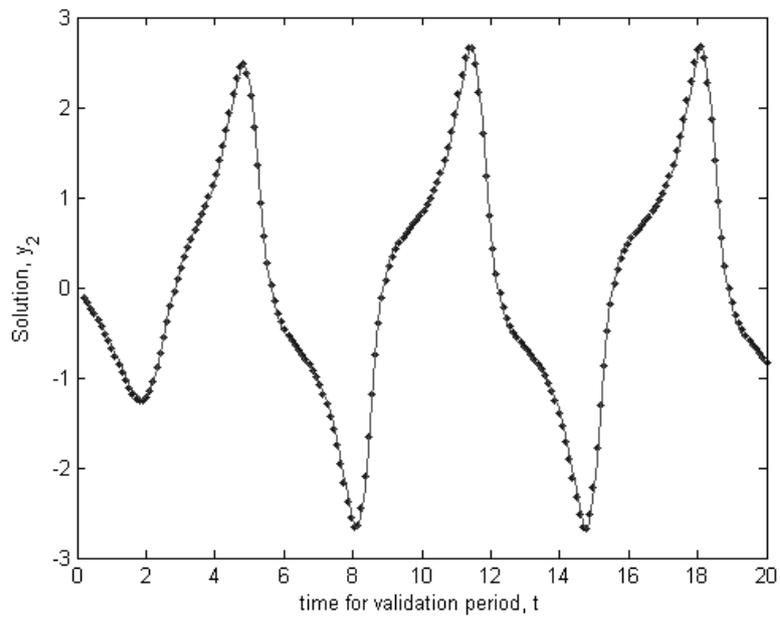
Figure 8.19. For y_2, observed (dotted) and estimated solution variations (solid) by METU-C.

Scatter diagrams with best-fit lines for the same cases are given in Figures 8.20 and 8.21. Figure 8.22 shows the trajectories of the observed solutions and estimated solutions by METU-C.
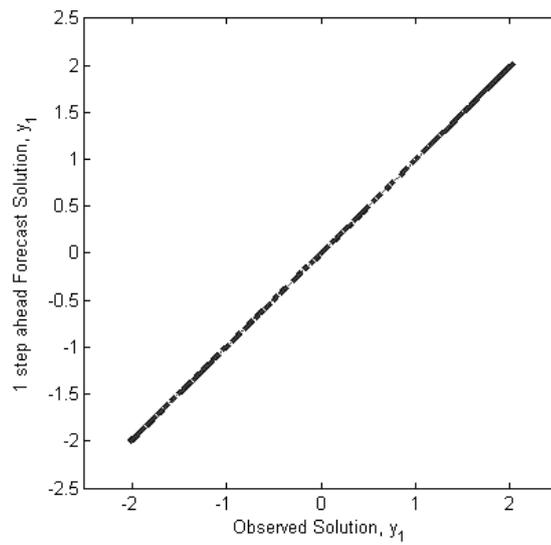
Figure 8.20. For y_1, Scatter diagram with best fit line for the estimated and observed solution values by METU-C.
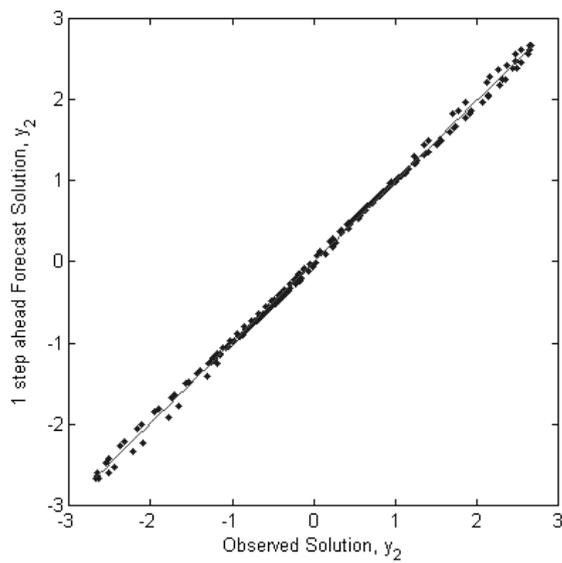
Figure 8.21. For y_2, Scatter diagram with best fit line for the estimated and observed solution values by METU-C.
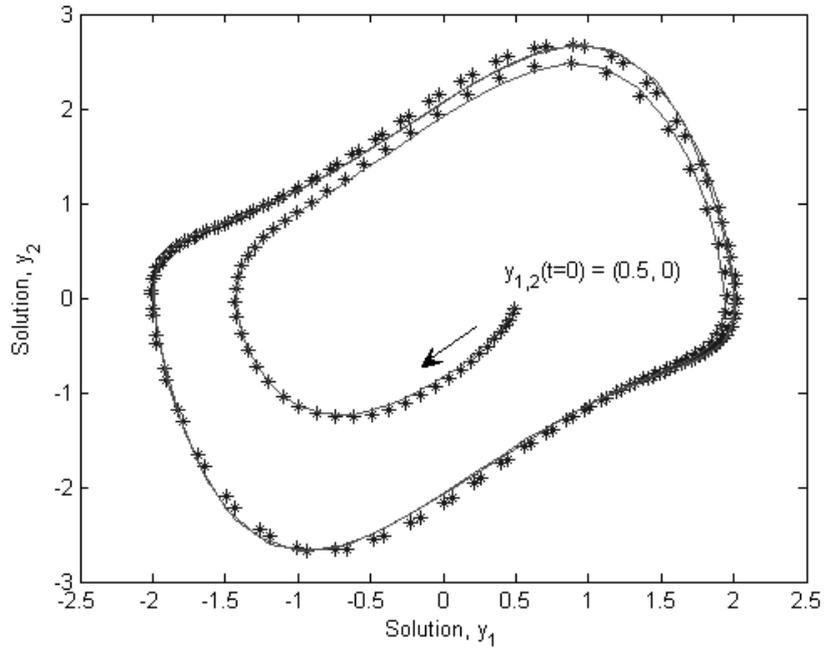
Figure 8.22. For y_1 and y_2, trajectories of the observed (dotted) and one step ahead forecast (solid) solution values by METU-C.

In the scatter diagrams the fitted lines have slope close to one and the forecasting errors are small. Thus, the systems reached the correct operating points. Deviations from straight line are small in the scatter diagrams and the correlation coefficients are very close to unity. Thus, the models learned the shape of the inherent nonlinearities. It is to be noted that the trajectories of the observed solutions and the estimated solutions by METU-C are coherent.

8.6 Conclusions

In this work, Hammerstein system modeling based METU-NN-C to estimate the response of the angle values of the simple forced pendulum and spring

loaded inverted double pendulum with forced table, and to identify speakers and a Van der Pol oscillator are presented.

The state equations of the simple forced pendulum process were known. So the observed angle values correspond to the computed ones through mathematical simulation [Franklin et al., 1990]. The estimated angle values correspond to the METU-C output values.

For the inverted double pendulum, input data and target data are obtained by performing simulation on computer.

For the identification of speakers, normalized MFCC and MPEG data as the speech features of speakers are used in raw inputs.

The state equations of the Van der Pol oscillator process were known. The observed state values correspond to the computed ones through simulation [MATLAB, 2002]. The estimated state values correspond to the METU-C output values.

The METU-NN modules estimated the state-like variables of the METU-C modules. The METU-NN-C learned the shape of the inherent nonlinearities. It can be concluded that the generalized usage of METU-NN-C has further been demonstrated. As a conclusion, identification of nonlinear dynamical processes can be achieved by using Hammerstein forms in which a static nonlinear block and a linear dynamic block are cascaded. It is also concluded that METU-NN-C models are successful in mechanical process identification and speaker identification. Error values in Tables 8.1, 8.2, 8.3, and 8.4 are small, and cross correlation coefficients are high.

CHAPTER 9

CONCLUSIONS

Modeling of nonlinear systems has been studied with particular emphasis on Hammerstein system modeling. In Hammerstein system modelling, the inputs of the process of interest are connected to a static nonlinearity block. The static nonlinearity block outputs, which are the state-like interior variables, and their past values are connected to a dynamic linearity block to identify the nonlinear dynamic process. The ouput of the cascade form is the forecast or estimated process parameter of interest.

In order to build and develop the Middle East Technical University (METU) Cascade Model (METU-C) for operation mode, the METU Neural Networks and Cascade Model (METU-NN-C) for development mode has been constructed.

In Chapter 1, the objective of the thesis, the background, previous works and the models have been presented in details. As stated in the objective, some special forms of nonlinearities for cascade models based on Hammerstein system modeling have been developed and then the parameters of the static nonlinear block and dynamic linear block in cascade modeling have been calculated by using smart techniques so that high accuracy and high sensitivity have been attained in process identification.

In this study, in addition to polynomial representation, two new techniques for Hammerstein system modeling are using Bezier curves and using B-Spline curves in defining the static nonlinearity. As a result, local control in nonlinear system modeling is achieved. Thus, unexpected variations of the output can be modeled more closely.

Several case studies have been given in the thesis. The case studies and the models developed have been presented in international scientific journals, national and international conference proceedings, workshops and meetings including EU COST 296 and EU COST 724 Actions cited in the thesis. The processes in case studies have been exposed to disturbances. The quantitative results have been given in terms of error values, cross correlation coefficients, scatter diagrams and observed and forecast or estimated variations of the process variables of interest.

Forecasts of ionospheric parameters, i.e. Total Electron Content (TEC) values, are important for navigation, telecommunication and many other technical applications.

METU-NN was developed and operated to forecast TEC values one hour in advance [Tulunay E. et al., 2004-a].

In Chapter 2, a case study on forecasting of TEC values one hour in advance by using METU-NN-C with polynomial nonlinearity representations has been presented. METU-NN-C was applied to a near-Earth space process for the first time and the results of the METU-C were promising for further research and development on the cascade models.

In Chapter 3, the case study on forecasting of TEC values one hour in advance by using METU-NN-C with Bezier curve nonlinearity representations has been presented. The performance of the METU-NN-C is superior; the results of the METU-C are outstanding. The forecast error values are within operational tolerance [Radicella, 2004].

In Chapter 4, the case study on forecasting of TEC values one hour in advance by using METU-NN-C with B-Spline curve nonlinearity representations has been presented. The results of the METU-C are outstanding again. As a numerical example, in forecasting the TEC one hour in advance by using the METU-C having B-Spline curves in nonlinearity representation for Hailsham in April and May 2002, the average absolute error is 1.10 TECu. In the case studies, it has been noted that METU-C with Bezier curve nonlinearity is faster than METU-C with B-Spline curve nonlinearity in terms of the computation time in operation because formulation of the B-Spline curve representations requires higher number of calculations.

In Chapter 5, the METU-NN and METU-C models forecasting TEC values one hour in advance have been compared in terms of 'performance' criteria in details. It is known that it is useful to make assumptions about the populations involved in order to reach statistical decisions on error values [Spiegel et al., 2000]. First of all, definitions on the statistical analysis and test of hypothesis were given [MATLAB, 2002] [Spiegel et al., 2000]. Then, error histograms, distributions, normal probability plots and test of hypothesis results, cross correlation coefficients and error values of the observed and forecast TEC values for METU-NN and METU-C models have been presented.

When the empirical Cumulative Distribution Function (CDF) plots are examined, it is observed that the error distributions for the model results do not

exactly fit to corresponding normal distributions, but a rough assumption that they fit to the normal distributions can be made.

When the normal probability plots are examined, it is observed that the error distributions for the model results have curvatures and do not exactly fit to the superimposed lines. Thus, they do not exactly fit to corresponding normal distributions, but a rough assumption that they fit to the normal distributions can again be made, as it has been made in observing the empirical CDF plots. For the METU-C models with Bezier and B-Spline nonlinearity representations, the distributions of the error statistic values are more condansed in small absolute error regions when compared with the ones that are for the METU-NN model and METU-C model with Polynomial nonlinearity representation. After the statistical quantitative analysis it can be concluded that the METU-C models with Bezier and B-Spline nonlinearity representations have been very successful.

The performance comparisons of the models have been presented in quantititative and qualitative manner. Then, it can easily be concluded that METU-C models have been superior to the METU-NN model, which has also been successful. Among the models presented the optimum one has been the METU-C model with Bezier curve nonlinearity representations. It has advantages as the METU-C model with B-Spline curve nonlinearity representations have. The results of it have small error values and large cross-correlation coefficient. As a numerical example, in forecasting the TEC one hour in advance by using the METU-C having Bezier curves in nonlinearity representation for Hailsham in April and May 2002, the average absolute error is 1.11 TECu. It has simple inputs because it does not need past inputs. It has transparent internal variables, which can be observed and used by the system

161

designers or operators. It is also fast in terms of the computation time in operation when compared with the METU-NN and the METU-C with B-Spline curve nonlinearity representations.

A detailed performance comparison of the International Reference Ionosphere model (IRI-2001), METU-NN model and METU-C models has also been presented. The METU-C models in the case studies are competitive and they have high performance when compared with the internationally popular ionospheric model, IRI-2001. The results provide important achievements of the METU-C models. Among the models presented, METU-C with Bezier curve nonlinearity representation is outstanding.

In Chapter 6, a case study on forecasting TEC maps one hour in advance by using the METU-NN and Bezier surface patches has been presented. Brief information on mapping and Bezier surfaces has been given. TEC forecast maps over Europe have been obtained. Then, absolute error maps have been plotted. The results show that the model is very promising.

In Chapter 7, the case study on forecasting TEC values one hour in advance by using the METU-NN-C with Bezier curve nonlinearity representations and mapping the forecast TEC values by using the Bezier surface patches has been presented. TEC forecast maps over Europe and the absolute error maps have been obtained. The results of the model are outstanding.

The METU-C model results presented in Chapter 7 can be compared with the METU-NN model results presented in Chapter 6. Considering the error tables and scatter diagrams in Chapter 6 and 7, it can be concluded that METU-C model is very successful in process identification. Error values for METU-C results are smaller than the ones for METU-NN, and cross correlation

coefficients for METU-C results are higher. For the overall TEC forecast mapping, error values are small. The forecast mapping error values are within operational tolerance [Radicella, 2004]. Briefly, it is the first time that METU-NN-C modules and Bezier surfaces are used to forecast and map TEC values over Europe.

In Chapter 8, the use of METU-NN-C for known nonlinear dynamic processes has been discussed. METU-NN-C models with Bezier curve nonlinearity representations have been employed to estimate the response of the joint angle values of a simple forced pendulum and a spring loaded inverted double pendulum with a forced table. METU-NN-C models with Bezier curve nonlinearity representations have also been developed and implemented to identify two speakers, and to estimate the states of a Van der Pol oscillator. Thus, the generalized usage of METU-NN-C has further been shown. The state equations of the simple forced pendulum process were known. So the observed angle values correspond to the computed ones through mathematical simulation [Franklin et al., 1990]. The estimated angle values correspond to the METU-C output values. For the inverted double pendulum, input data and target data have been obtained by performing simulation on computer. The joint angles of the pendulums have been estimated accurately. For the identification of speakers, speech features of speakers have been used in raw inputs. The model developed identified the speakers successfully. The state equations of the Van der Pol oscillator process were known. So the observed state values correspond to the computed ones through mathematical simulation [MATLAB, 2002]. It has been shown that the process with limit cycles can also be modelled precisely. It is concluded that METU-NN-C models are successful in mechanical process identification and speaker identification.

METU-NN modules of the METU-NN-C estimated the state-like interior variables of the METU-C. METU-NN-C learned the shape of the inherent nonlinearities.

When the overall performance results of the models are examined, it can be concluded that the METU-C models have small error values. The best-fit line in the scatter diagram for the results of the METU-C has a slope near 45° and passes through the origin. Thus, the system reached the correct operating point within the system identification by METU-C models. Also the cross-correlation coefficients of the observed and forecast or estimated values by METU-C models are high. It is seen that the deviations of the scatter points from the best-fit line are small for the results of METU-C. Thus, the model learned the shape of the inherent nonlinearities. Among the models presented, the optimum model in quantitative and qualitatitive manner is the METU-C model with Bezier curve nonlinearity representation.

The generalized usage of METU-NN-C has been demonstrated. Thus, it is concluded that identification of nonlinear dynamical processes can be achieved by cascade models based on Hammerstein system modelling in which a static nonlinear block and a linear dynamic block are cascaded. The static nonlinear block of the METU-NN-C can be modeled by employing the special nonlinearity representations, i.e. Polynomial, Bezier Curve, and B-Spline Curve representations, presented.

As a future work, the use of the METU-NN-C models in controllers of nonlinear dynamic processes can be discussed.

REFERENCES

Alonge F., D'Ippolito F., Raimondi F.M., Tumminaro S., Identification of Nonlinear Systems Described by Hammerstein Models, *Proceedings of the 42nd IEEE Conf. on Decision and Control*, pp. 3990-3995, Hawaii, USA, December 2003.

Altinay O., Nonlinear Black-Box Modeling of Ionospheric Critical Frequency Process Using Neural Networks, *MSc. Thesis*, Middle East Technical University, Department of Electrical and Electronics Engineering, Ankara, Turkey, June 1996.

Altinay O., Tulunay E., Tulunay Y., Forecasting of ionospheric critical frequency using neural networks, *Geophysical Research Letter*, Vol. 24, No. 12, pp. 1467-1470, 1997.

Altuntas E., Tulunay Y., Tulunay E., Şenalp E.T., Bahadırlar Y., Yer İyonosfer Kovuk Değişimi'nin Schumann Rezonanslarına Dayalı İncelenmesi, *1. Ulusal Havacılık ve Uzay Konferansı*, 21-23 September 2006, ODTÜ / METU, Ankara, Turkey.

Altuntas E., Yapıcı T., Tulunay Y., Tulunay E., Kocabas Z., Senalp E.T., A Hybrid Approach In Fof2 Forecast Mapping Including Disturbed Conditons, *The 5th IFAC DECOM-TT 2007*, pp. 51-56, 17-20 May 2007, Cesme, Izmir, Turkey.

Aristoff D.G., "Inverted Double Planar Pendulum on a Cart: Feedback Stabilization Using the Method of Controlled Lagrangians", Department of Mathematics, University of Michigan, 2003.

Bai E.W., Fu M., A Blind Approach to Hammerstein Model Identification, *IEEE Transactions on Signal Processing*, Vol. 50, No. 7, pp. 1610-1619, July 2002.

Bézier, P., *Numerical Control – Mathematics and Applications*, Translated by Forrest A.R. and Pankhurst A.F., pp. 115-136, John Wiley & Sons Ltd., England, 1972.

Bilitza, D., International Reference Ionosphere 2000, *Radio Science*, Vol. 36, No. 2, pp. 261-275, 2001.

Cander Lj.R., Towards forecasting and mapping ionospheric space weather under COST actions, *Adv. Space Res.*, Vol. 31, No. 4, pp. 957-964, 2003.

Chilbolton Weather Web, Space Weather – Total Electron Content of the Ionosphere, Rutherford Appleton Laboratory, UK, Last date accessed: 6 Aug. 2007, http://www.chilbolton.rl.ac.uk/weather/tec.htm, 2004.

Ciloglu T., Ergun C., private communication, 2007.

COST 238: PRIME (Prediction and Retrospective Ionospheric Modelling over Europe), EU Action, 1992-1995, *Management Committee, Final Report*, Ed. P.A. Bradley, Commission of the European Communities, February 1999.

COST 251: Improved Quality of Service in Ionospheric Telecommunication Systems Planning and Operation, EU Action, 1995-1999, *Management Committee, Final Report*, Ed. R. Hanbaba, April 1999.

COST 271: Effects of the Upper Atmosphere on Terrestrial and Earth-Space Communications, EU Action, 2000-2004, *Annals of Geophysics*, Supplement to Vol. 47, No. 2/3, 2004.

COST271 WG 4 STSM, *"Effects of the Upper Atmosphere on Terrestrial and Earth-Space Communications"*, Short term scientific mission work on the TEC data available at RAL to organize the input data for the METU NN model by E.T. Senalp under the supervision of Dr. Lj. Cander, Terms of Reference, COST 271 Action, WG 4, 30 June 2002 – 7 July 2002, RAL, Chilton, Didcot, U.K.

COST 296: MIERS (Mitigation of Ionospheric Effects on Radio Systems), EU Action, 2005-2009, 2007.

COST 724: Developing the scientific basis for monitoring, modeling and predicting Space Weather, EU Action, 2005-2008, 2007.

Ciraolo, G., Private communication, 2004.

Dempsey, E.J.; Westwick, D.T., Identification of Hammerstein models with cubic spline nonlinearities, *IEEE Transactions on Biomedical Engineering*, Vol. 51, No. 2, pp. 237-245, February 2004.

Duwaish H.Al., Karim M.N., Chandrasekar V., Hammerstein model identification by multilayer feedforward neural networks, *International Journal of Systems Science*, Vol. 28, No. 1, pp. 49-54, 1997.

Ertac, E., Tulunay.Y., Ionospheric Total Electron Content Measurements from Turkey During the Solar Eclipse of 29 April 1976, Advanced Study Institute on Dynamical And Neutral and Ionized Atmospheres, Nord Torpa, Norway, 1979.

Eskinat E., Johnson S.H., Luyben W.L., Use of Hammerstein Models in Identification of Nonlinear Systems, *AICHE Journal*, Vol. 37, No. 2, pp. 255-268, February 1991.

Franklin F.F., Powell J.D., Workman M.L., *Digital Control of Dynamic Systems*, 2nd ed., pp. 518-520, Addison-Wesley Publishing Company Inc., USA, 1990.

Fruzzetti, K.P., Palazoğlu A., McDonald K.A., Nonlinear model predictive control using Hammerstein models, *J. Proc. Cont.*, Vol. 7, No. 1, pp.31-41, 1997.

Guarnieri, S., Piazza, F., Uncini, A., Multilayer feedforward networks with adaptive spline activation function, *IEEE Transactions on Neural Networks*, Vol. 10, No. 3, pp. 672-683, May 1999.

Hagan M.T., Menhaj M.B., Training Feedforward Networks with the Marquard Algorithm, *IEEE Transactions on Neural Networks*, Vol. 5, No. 6, pp. 989-993, 1994.

Haykin S., *Neural Networks: A Comprehensive Foundation*, 2nd ed., pp. 2, 10, 21-22, 83-84, 169, 215, Prentice-Hall, Inc., New Jersey, USA, 1999.

Ikonen E., Najim K., Learning control and modelling of complex industrial processes, Overview report of the activities within the European Science Foundation's programme on Control of Complex Systems (COSY) Theme 3: Learning control, February 1999.

IRI, International Reference Ionosphere project, web page, COSPAR, URSI, NASA, Last date accessed: 6 Aug. 2007, http://modelweb.gsfc.nasa.gov/ ionos/iri/iri_members.html, 2007.

Jakowski N., Leitinger R., Ciraolo L., Behaviour of large scale structures of the electron content as a key parameter for range errors in GNSS applications, *Annals of Geophysics*, Vol. 47, No. 2/3, pp. 1031-1047, 2004.

Kapoor, N., McAvoy T.J., Marlin T.E., Effect of Recycle Structure on Distillation Tower Time Constants, *AICHE Journal*, Vol. 32, No. 3, pp. 411-418, March 1986.

Kumluca A., Neural Network Modeling of an Ionospheric Process: Temporal and Spatial Forecasting of the Critical Frequencies, *MSc. Thesis*, Middle East Technical University, Department of Electrical and Electronics Engineering, Ankara, Turkey, June 1997.

Marchi, P.A., Coelho L.S., Coelho A.R., Comparative Study of Parametric and Structural Methodologies in Identification of an Experimental Nonlinear Process, *Proceedings of the 1999 IEEE International Conference on Control Applications*, Hawaii, USA, pp. 1062-1067, 22-27 August 1999.

MATLAB v6.5 R13, Documentation, The MathWorks, Inc. 2002.

Narendra K.S., Gallman P.G., An Iterative Method for the Identification of Nonlinear Systems Using a Hammerstein Model, *IEEE Transactions on Automatic Control*, pp. 546-550, 1966.

NGDC, Kp-Ap Indices, National Geophysical Data Center, Last date accessed: 6 Aug. 2007, ftp://ftp.ngdc.noaa.gov/STP/GEOMAGNETIC_DATA/ INDICES/KP_AP/, 2007.

Ozkaptan C., Modeling of Ionospheric Propagation In The HF Band Using Neural Networks: HF Propagation Modeling, *MSc. Thesis*, Middle East Technical University, Department of Electrical and Electronics Engineering, Ankara, Turkey, December 1999.

Radicella S.M., private communication, 2004.

Rogers D.F., Adams J.A., *Mathematical Elements for Computer Graphics*, 2nd ed., pp. 289-308, 379-477, McGraw-Hill, Inc., New York, USA., 1990.

Samardjiev T., Bradley P.A., Cander Lj.R., Dick M.I., Ionospheric mapping by computer contouring techniques, *Electronics Letters*, Vol. 29, No. 20, pp. 1794-1795, 1993.

Schoenberg I.J., Contributions to the Problem of Approximation of Equidistant Data by Analytic Functions, *Q. Appl. Math.*, Vol. 4, pp. 45-99; pp. 112-141, 1946.

Schultheiss J., Re L., Neural Networks Identification of Muscular Response Using Extended Hammerstein Models, *Proceedings of the 20th Annual International Conference of the IEEE Engineering in Medicine and Biology Society*, Vol. 20, No. 5, pp. 2566-2569, 1998.

Senalp E.T., Neural Network Based Forecasting For Telecommunications Via Ionosphere, *MSc. Thesis*, Middle East Technical University, Department of Electrical and Electronics Engineering, Ankara, Turkey, August 2001.

Senalp E.T., Tulunay E., Tulunay Y., Neural Network Based Approach to Forecast the Total Electron Content Values, *EGS 2002 Conference, 27th General Assembly of the European Geophysical Society*, CD of Abstracts, EGS02-A-00867, 21-26 April 2002, Nice, France, 2002-a.

Senalp E.T., Tulunay E., Tulunay Y., Toplam Elektron Yoğunluğu Değerlerini Sinirsel Ağlar Kullanarak Öngörüde Bulunma, *URSI-TÜRKİYE'2002 Bilimsel Kongresi*, pp.407-410, 18-20 September 2002, İTÜ - İstanbul, Turkey, 2002-b.

Senalp E.T., Sibeck D.G., Tulunay Y., Tulunay E., Forecasting Magnetopause Crossing Locations by Using Neural Networks, *34th COSPAR Scientific Assembly - The Second World Space Congress*, Poster, 10 - 19 October 2002, Houston, Texas, USA, 2002-c.

Senalp E.T., Tulunay E., Tulunay Y., Neural Network Based Forecasting with Adaptation Capability, *13th Turkish Symposium on Artificial Intelligence and Neural Networks, TAINN 2004*, pp.585-592, 10-11 June 2004, Foca, Izmir, Turkey.

Senalp E.T., Tulunay E., Tulunay Y., Neural Networks and Cascade Modeling Technique in System Identification, *14th Turkish Symposium on Artificial Intelligence and Neural Networks, TAINN 2005*, pp.286-293, 16-17 June 2005, Cesme, Izmir, Turkey.

Senalp E.T., Tulunay E., Radicella S.M., Tulunay Y., Forecasting Total Electron Content (TEC) for Constructing Maps Especially During High Solar Activity Periods, *International Advanced School on Space Weather*, CD-ROM, 2-19 May 2006, ICTP, Trieste, Italy, 2006-a.

Senalp E.T., Tulunay E., Tulunay Y., System Identification by using Cascade Modeling Technique with Bezier Curve Nonlinearity Representations, *15th Turkish Symposium on Artificial Intelligence and Neural Networks, TAINN 2006*, pp.75-82, 21-23 June 2006, Akyaka, Mugla, Turkey, 2006-b.

Senalp E.T., Tulunay E., Tulunay Y., Neural Networks and Cascade Modeling Technique in System Identification, Revised selected papers from TAINN2005, *Lecture Notes in Artificial Intelligence*, Vol. 3949 / 2006, Savaci, F. Acar (Ed.), pp.84-91, 2006-c.

Senalp E.T., Tulunay E., Tulunay Y., Toplam Elektron Niceliği Öngörümünde Ardışık Benzekleme Tekniği, *3. URSI-TÜRKİYE'2006 Bilimsel Kongresi*, pp. 360-362, Hacettepe Üniversitesi, 4-8 September 2006, Ankara, Turkey, 2006-d.

Senalp E.T., Tulunay E., Tulunay Y., Ardışık Benzekleme Tekniğinin Kullanımı: Ters Çift Sarkaç, *TOK'06 Otomatik Kontrol Ulusal Toplantısı*, pp. 533-537, TOBB Ekonomi ve Teknoloji Üniversitesi, 6-8 November 2006, Ankara, Turkey, 2006-e.

Senalp E.T., Identification of Speakers by Using Cascade Modeling Technique, Report submitted to E. Tulunay and T. Ciloglu, 1, 4 May 2007, METU, Ankara, Turkey, 2007-a.

Senalp E.T., Tulunay E., Tulunay Y., Identification of Processes by Cascade Modeling Technique, *The 5th IFAC DECOM-TT 2007*, pp. 117-122, 17-20 May 2007, Cesme, Izmir, Turkey, 2007-b.

Senalp E.T., Identification of a Van der Pol Oscillator by Using Cascade Modeling Technique, Report submitted to E. Tulunay, 1, 14 July 2007, METU, Ankara, Turkey, 2007-c.

Senalp E.T., Tulunay Y., Tulunay E., Total Electron Content (TEC) Forecasting by Cascade Modeling: A Possible Alternative to the IRI-2001, *Radio Science*, (submitted), 2007-d.

SpaceWeather, News and information about the Sun-Earth Environment, Last date accessed: 6 Aug. 2007, http://www.spaceweather.com, 2007.

Spiegel M.R., Schiller J., Srinivasan R.A., *Schaum's Outline of Theory and Problems of Probability and Statistics*, 2nd ed., pp.206-209, 224-229, 287-288, 313-314, McGraw-Hill, New York, USA, 2000.

Stamper R., Belehaki A., Buresova D., Cander Lj.R., Kutiev I., Pietrella M., Stanislawska I., Stankov S., Tsagouri I., Tulunay Y.K., Zolesi B., Nowcasting, forecasting and warning for ionospheric propagation: tools and methods, *Annals of Geophysics*, Vol. 47, No. 2/3, pp. 957-983, 2004.

Stapleton J.C., Bass S.C., Adaptive noise cancellation for a class of nonlinear, dynamic reference channels, *IEEE Transactions on Circuits and Systems*, Vol. 32, No. 2, pp. 143-150, February 1985.

Tulunay E., Introduction to Neural Networks and their Application to Process Control, in *Neural Networks Advances and Applications*, edited by E. Gelenbe, pp. 241-273, Elsevier Science Publishers B.V., North-Holland, 1991.

Tulunay E., Tulunay Y., Senalp E.T., Neural Network Based Approach to Forecast Ionospheric Parameters, *SPECIAL Workshop*, 8-11 November 2000, Lindau, Germany.

Tulunay E., Senalp E.T., Tulunay Y., Forecasting the Total Electron Content By Neural Networks, *COST 271 Workshop, Ionospheric Modeling and Variability Studies for Telecommunications Applications*, Book of Abstracts, p.47, 25-27 September 2001, Sopron, Hungary.

Tulunay E., Tulunay Y., Ozkaptan C., Senalp E.T., Aydogdu M., Ozcan O., Guzel E., Yesil A., Unal I., Canyilmaz M., Ipekcioglu E., Two Solar Eclipses Observations in Turkey, *IL NUOVO CIMENTO, Nuovo Cimento Della Societa Italiana Di Fisica C-Geophysics and Space Physics*, Vol. 25 C, No.2, pp. 251-258, March – April 2002, 2002-a.

Tulunay E., Senalp T., Tulunay Y., Aslan Z., Development of Neural Network Based Models for Non-Linear Agro-Environment Systems, *Third International Symposium on Sustainable Agro-Environmental Systems: New Technologies & Applications*, p.139, 26-29 October 2002, Cairo, Egypt, 2002-b.

Tulunay E., Senalp E.T., Spalla P., Tulunay Y., Franceschi G.D., Forecasting the Total Electron Content Values by Using Neural Networks and MAC Index, *COST 271 Workshop: Significant results in COST271 Action: a review*, Poster, 23-27 September 2003, Spetses, Greece, 2003.

Tulunay E., Senalp E.T., Cander Lj. R., Tulunay Y., Bilge A.H., Mizrahi E., Kouris S.S., Jakowski N., Development of algorithms and software for

forecasting, nowcasting and variability of TEC, *Annals of Geophysics*, Supplement to Vol. 47, No. 2/3, pp. 1201-1214, 2004-a.

Tulunay E., Tulunay Y., Senalp E.T., Cander Lj.R., Forecasting GPS TEC Using the Neural Network Technique "A Further Demonstration", *Bulgarian Geophysical Journal*, Vol. 30, No. 1-4, pp.53-61, 2004-b.

Tulunay E., Tulunay Y., Senalp E.T., Cander L., Forecasting GPS TEC upto 24 Hours in Advance by Neural Network Technique, *EGU General Assembly 2004*, ST14, Poster: EGU04-A-02260, 25 - 30 April 2004, Nice, France, Geophysical Research Abstracts, Vol. 6, 02260, 2004-c.

Tulunay E., Senalp E.T., Radicella S.M., Tulunay Y., Forecasting Total Electron Content Maps by Neural Network Technique, *Radio Science*, Vol. 41, No. 4, RS4016, 2006-a.

Tulunay E., Heynderickx D., Senalp E.T., Ozdemirci M., Ozkok Y.I., Tulunay Y., Integration of METU-IFS Server to COST 724 Server (BIRA), *COST 724 MCM and Scientific Workshop*, Proceedings CD, 27-30 March 2006, Antalya, Turkey, 2006-b.

Tulunay E., Warrington E.M., Tulunay Y., Bahadırlar Y., Türk A.S., Yapıcı T. , Şenalp E.T., Altuntaş E., Sarı M.Ö., Büyükpabuşçu O., COST296 WG2.2 Activity Report: Radio Propagation Measurements During the 29 March 2006 Total Eclipse Week, *4th COST 296 MCM and WG meetings*, 27-29 April 2006, Neustrelitz, Germany, 2006-c.

Tulunay E., Warrington E.M., Tulunay Y., Bahadırlar Y., Türk A.S., Çaputçu R., Yapıcı T. , Şenalp E.T., Propagation Related Measurements during Three Solar Eclipses in Turkey, *IET 10th International Conference on Ionospheric Radio Systems&Techniques, IRST2006*, 18-21 July 2006, London, UK, 2006-d.

Tulunay E., Tulunay Y., Warrington E.M., Bahadirlar Y., Yapici T. , Senalp E.T., Turk A.S., Recent COST 296 Propagation Related Measurements During the 29th March 2006 Solar Total Eclipse in Antalya, Turkey, *Second COST 296 Workshop and 5th MC Meeting, Radio Systems and Ionospheric Effects*, 3-7 October 2006, Univ. of Rennes 1, Rennes, France, 2006-e.

Tulunay E., Tulunay Y., Altuntas E., Senalp E.T., Bahadirlar Y., Neural Network Forecasting of Schumann Resonances in the Near Earth Space, *Third European Space Weather Week (ESWW3)*, 13-17 November 2006, Royal Library of Belgium, Brussels, Belgium, 2006-f.

Tulunay Y., Tulunay E., Senalp E.T., Ozkaptan C., Neural Network Modeling of the Effect of the IMF Turning on the Variability of HF Propagation Medium, *AP 2000, Millennium Conference on Antennas & Propagation,* ICAP&JINA, p.132, 9-14 April 2000, Davos, Switzerland.

Tulunay Y., Tulunay E., Senalp E.T., An Attempt to Model the Influence of the Trough on HF Communication by Using Neural Network, *Radio Science,* Vol. 36, No. 5, pp. 1027-1041, September - October 2001, 2001-a.

Tulunay Y., Tulunay E., Senalp E.T., The Trough Based Neural Network Model of the foF2 Values, *COST 271 Workshop, Ionospheric Modeling and Variability Studies for Telecommunications Applications*, Book of Abstracts, p.8, 25-27 September 2001, Sopron, Hungary, 2001-b.

Tulunay Y., Tulunay E., Kutay A.T., Senalp E.T., Doğrusal Olmayan Bazı Süreçler İçin Sinirsel Ağ Tabanlı Yaklaşımlar, *URSI-TÜRKİYE'2002 Bilimsel Kongresi*, pp. 403-406, 18-20 September 2002, İTÜ - İstanbul, Turkey, 2002-a.

Tulunay Y., Tulunay E., Senalp E.T., Neural Network Based Approach to Model Near Earth Space Processes, *34th COSPAR Scientific Assembly - The Second World Space Congress*, C4.3-0018-02, 10 - 19 October 2002, Houston, Texas, USA, 2002-b.

Tulunay Y., Mentes S., Tulunay E., Senalp E.T., Akcan E., Forecasting Regional Cloudness and Cloud Top Temperature By Neural Networks, *ESF Scientific Network on Space Weather and the Earth's Weather and Climate*, 20-23 February 2003, Frankfurt am Main, Germany; *EGS-AGU-EUG Joint Assembly 2003*, Poster: P0976, 06-11 April 2003, Nice, France; *Geophysical Research Abstracts*, Vol.5, 13915, 2003, EGS, Lindau, Germany, 2003-a.

Tulunay Y., Karpacev A., Tulunay E., Senalp E.T., Spatial Prediction of foF2 In Modeling The Influence Of Trough on HF Communication By Using Neural Networks, *COST 271 Workshop: Significant results in COST271 Action: a review*, Poster, 23-27 September 2003, Spetses, Greece, 2003-b.

Tulunay Y., Tulunay E., Senalp E.T., The Neural Network Technique-1: A General Exposition, *Adv. Space Res.*, Vol. 33, No. 6, pp. 983-987, 2004-a.

Tulunay Y., Tulunay E., Senalp E.T., The Neural Network Technique-2: An Ionospheric Example Illustrating its Application, *Adv. Space Res.*, Vol. 33, No. 6, pp. 988-992, 2004-b.

Tulunay Y., Tulunay E., Senalp E.T., Karl Rawer's Interest and Encouragement Regarding New Approaches to Ionospheric Modeling, *Advances in Radio Science*, Vol. 2, pp. 281-282, 2004-c.

Tulunay Y., Tulunay E., Senalp E.T., Aslan Z., Neural Network Application on Agro-Environment Problems, *Proceedings: Measuring and Computing Technologies on Agricultural Issue, AGROENVIRON 2004 Role of Multi-purpose Agriculture in Sustaining Global Environment*, pp. 27-36, 20-24 October 2004, Udine, Italy, 2004-d.

Tulunay Y., Sibeck D.G., Senalp E.T., Tulunay E., Forecasting magnetopause crossing locations by using Neural Networks, *Adv. Space Res.*, Vol 36, No.12, pp. 2378-2383, 2005-a.

Tulunay Y., Messerotti M., Senalp E.T., Tulunay E., Molinaro M., Ozkok Y.I., Yapici T., Altuntas E., Cavus N., Neural Network Modeling in Forecasting the Near Earth Space Parameters: Forecasting of the Solar Radio Fluxes, *COST 724 Scientific Workshop*, Proceedings CD, 10-14 October 2005, Athens, Greece, 2005-b.

Tulunay Y., Tulunay E., Kocabas Z., Altuntas E., Yapici T., Senalp E.T., International Heliophysical Year 2007 (IHY), Turkish National Activities, *Official IHY Opening Ceremony, IHY Kick-off Event*, Poster, 17-21 February 2007, Vien, Austria, 2007-a.

Tulunay Y., Altuntas E., Price C., Ciloglu T., Tulunay E., Bahadirlar Y., Senalp E.T., A Case Study on the ELF Characterization of the Earth-Ionosphere Cavity: Forecasting the Schumann Resonances, *Journal of Atmos. and Solar-Terrestrial Physics (ISROSES-2006)*, (accepted), 2007-b.

Tulunay Y., Senalp E.T., Oz S., Dorman L.I., Tulunay E., Mentes S.S., Akcan M.E., Forecasting Total Cloud Amount Maps and Cloud Top Temperature Maps by using Fuzzy Neural Networks and Bezier Surfaces, *The 9th WMO Scientific Conference on Weather Modification*, 22-24 October 2007, Antalya, Turkey, (accepted), 2007-c.

UMLCAR web page, Center for Atmospheric Research, University of Massachusetts Lowell, USA, Last date accessed: 6 Aug. 2007, http://umlcar.uml.edu, 2007.

Uraz A., private communication, 2007.

Westwick, D.T., Kearney, R.E., Identification of a Hammerstein model of the stretch reflex EMG using separable least squares, *Engineering in Medicine*

and Biology Society, 2000. *Proceedings of the 22nd Annual International Conference of the IEEE*, Vol. 3, pp.1901-1904, 23-28 July 2000.

Zhu Y., Estimation of an N–L–N Hammerstein–Wiener model, *Automatica*, Vol. 38, No. 9, pp. 1607-1614, September 2002.

Zolesi B., Belehaki A., Tsagouri I., Cander Lj.R., Real-time updating of the Simplified Ionospheric Regional Model for operational applications, *Radio Science,* Vol. 39, No. 2, RS2011, April 2004.

CURRICULUM VITAE OF THE AUTHOR

PERSONAL INFORMATION:

Surname, Name:	Şenalp, Erdem Türker
Nationality:	Turkish (TC)
Date and Place of Birth:	24 July 1977, Bursa
Marital Status:	Single
Email:	etsenalp@gmail.com
Foreign Languages:	English (fluent), German (fair).

EDUCATION:

Ph D:	METU, Electrical and Electronics Eng., Ankara,	2007
MS:	METU, Electrical and Electronics Eng., Ankara,	2001
BS:	METU, Electrical and Electronics Eng., Ankara,	1999
High School:	Ulubatlı Hasan Anadolu Lisesi, Bursa,	1995

TRAINING PROGRAMS:

Internship: Intern Engineering Student, Bosch, Bursa, Turkey
(23 Jun. – 18 Jul. 1997)

Internship: Intern Engineering Student, Renault, Bursa, Turkey
(29 Jun. – 24 Jul. 1998)

Course: "The Abdus Salam International Centre for Theoretical Physics – School on Physics of the Equatorial Atmosphere", Trieste, Italy (24 Sep. – 5 Oct. 2001).

Course: Turkish Acreditation Organisation, Training on TS EN ISO/IEC 17025 Standard, Ankara, Turkey (9 – 10 Mar. 2002).

Course: International School of Geophysics, 24th Course: Ionospheric Physics and Applications: Present and Future, Erice, Italy (24-29 Sep. 2004).

Course: "The Abdus Salam International Centre for Theoretical Physics – International Advanced School on Space Weather", Trieste, Italy (2–19 May 2006).

Workshop: "High Performance Computing Workshop", Sun Microsystems & TOBB University of Economics & Technology, Ankara, Turkey (24–25 Apr. 2007).

PROFESSIONAL CAREER AS RESEARCH PERSONNEL IN:

METU Dept. of Electrical and Electronics Eng., Ankara, Turkey, 1999–2006, *Research Assistant*, Instructing Process Control Laboratory experiments on courses EE 407 "Process Control" and EE 408 "Process Instrumentation and Control" and departmental work.

Turkish State Planning Organisation (DPT) Project: *"Neuro Fuzzy Systems Based HF Channel Characterisation and Selection"*, **METU, EEE**, Ankara, Turkey, 1999–2004, *Researcher,* Modeling and research activities, Project Head: Prof. Dr. Ersin Tulunay.

177

EU COST 271 Project: *"Effects of the Upper Atmosphere on Terrestrial and Earth-Space Communications"*, **METU, Dept. of Aerospace Eng. and Dept. of Electrical and Electronics Eng.**, Ankara, Turkey, 1999–2004, *Researcher,* Modeling and research activities, National Representatives: Prof. Dr. Yurdanur Tulunay and Prof. Dr. Ersin Tulunay.

EU COST 296 Project: *"Mitigation of Ionospheric Effects on Radio Systems"*, **TUBITAK, METU, Dept. of Aerospace Eng. and Dept. of Electrical and Electronics Eng.**, Ankara, Turkey, 2004–2007, *Researcher and Assistant Personel,* Modeling and research activities, National Representatives: Prof. Dr. Yurdanur Tulunay and Prof. Dr. Ersin Tulunay.

EU COST 724 Project: *"Developing the Scientific Basis for Monitoring, Modelling and Predicting Space Weather"*, **TUBITAK, METU, Dept. of Aerospace Eng. and Dept. of Electrical and Electronics Eng.**, Ankara, Turkey, 2004–2007, *Researcher,* Modeling and research activities, National Representatives: Prof. Dr. Yurdanur Tulunay and Prof. Dr. Ersin Tulunay.

PROFESSIONAL EXPERIENCES:

Programming:	MATLAB, Simulink, C++, Visual C++, Visual Java, Pascal,
Computer applications:	WEB design and programming, EWB, MSOffice, Project, EA,

AI Studies:	Neural Network based modeling of the Near-Earth Space processes, ionospheric modeling and variability studies for telecommunication applications. Neural Network based character recognition on WEB. Intelligent control, Industrial Automation Process Control,
Cascade Modeling:	Cascade Modeling of Nonlinear Systems.

SCIENTIFIC MEMBERSHIPS AND JOINT WORKS:

Joint Work and Presentation: Forecasting Magnetopause Crossing Locations by Using Neural Networks, Applied Physics Laboratory, Johns Hopkins University, Laurel, USA; Center for Space Research, Massachusetts Institute of Technology, Boston, USA, 2-9 Dec. 2000.

COST 271 Short-Term Scientific Mission: Working on the TEC data available at RAL and organizing the input data for the METU NN model under the supervision of Dr. Lj. Cander, Didcot, UK, 30 Jun. – 7 Jul. 2002.

TUBITAK-COST296 Short-Term Scientific Mission: Working on High Frequency (HF) Receiver System in the TUBITAK-MRC-ITI, Gebze, Kocaeli, Turkey, 10-13 Mar. 2006.

TUBITAK-COST 296 Experiment: HF Channel Occupancy and Atmospheric Noise Measurements over the HF Band during the Solar Eclipse, Antalya, Turkey, 25-31 Mar. 2006.

AREAS OF INTEREST:

Sports:	Basketball, swimming,
Books:	Reading novels and scientific publications,
Dance:	Group dances.
Music:	Classical.

SCIENTIFIC PUBLICATIONS:

Thesis:

1. 2001 Neural Network Based Forecasting For Telecommunications Via Ionosphere, MSc. Thesis, (Supervisor: E. Tulunay, Co-supervisor: Y. Tulunay), Middle East Technical University, Dept. of Electrical and Electronics Eng., Ankara, Turkey, August 2001.
E.T. Şenalp

2. 2007 Cascade Modeling of Nonlinear Systems, Ph-D Thesis, (Supervisor: E. Tulunay), Middle East Technical University, Dept. of Electrical and Electronics Eng., Ankara, Turkey, August 2007.
E.T. Şenalp

Papers in Journals:

1. 2001 An Attempt to Model the Influence of the Trough on HF Communication by Using Neural Networks, *Radio Science*, Vol. 36, No. 5, pp. 1027-1041, Publisher: American Geophysical Union, Washington, Sep. – Oct. 2001.
Y.Tulunay, E.Tulunay, E.T.Senalp

2. 2002 Two Solar Eclipses Observations in Turkey, *IL NUOVO CIMENTO, Nuovo Cimento Della Societa Italiana Di Fisica C-Geophysics and Space Physics*, 25 C, N.2, pp. 251-258, Publisher: Editrice Compositori Bologna, Siena, Mar. – Apr. 2002.
E. Tulunay, Y. Tulunay, C. Özkaptan, E.T. Senalp, M. Aydogdu, O. Ozcan, E. Guzel, A. Yesil, I. Unal, M. Canyilmaz, E. Ipekcioglu.

3. 2004 The Neural Network Technique-1: A General Exposition, *Advances in Space Research*, Publisher: Elsevier, Vol 33/6 pp. 983-987.
Y. Tulunay, E. Tulunay, E.T. Senalp.

4. 2004 The Neural Network Technique-2: An Ionospheric Example Illustrating Its Application, *Advances in Space Research*, Publisher: Elsevier, Vol 33/6 pp. 988-992.
Y. Tulunay, E. Tulunay, E.T. Senalp.

5. 2004 Karl Rawer's Interest and Encouragement Regarding New Approaches to Ionospheric Modeling, *Advances in Radio Science*, Publisher: Copernicus G mbH, URSI, Vol. 2, pp. 281-282.
Y. Tulunay, E. Tulunay, E.T. Senalp.

6. 2004 Development of algorithms and software for forecasting, nowcasting and variability of TEC, *Annals of Geophysics*, Vol. 47, N. 2/3, pp. 1201-1214.
E.Tulunay, E.T. Senalp, Lj. R. Cander, Y. Tulunay, A.H. Bilge, E. Mizrahi, S.S. Kouris, N.Jakowski.

7. 2004 Forecasting GPS TEC Using the Neural Network Technique "A Further Demonstration", *Bulgarian Geophysical Journal*, Geophys. Institute, Bulgarian Academy of Sci., Vol. 30, 1-4, pp.53-61.
E. Tulunay, Y. Tulunay, E.T. Senalp, Lj.R. Cander.

8. 2005 Forecasting magnetopause crossing locations by using Neural Networks, *Advances in Space Research*, Publisher: Elsevier, Vol 36/12 pp. 2378-2383.
Y. Tulunay, D.G. Sibeck, E.T. Senalp, E. Tulunay

9. 2006 Neural Networks and Cascade Modeling Technique in System Identification, Artificial Intelligence and Neural Networks, 14th Turkish Symposium, TAINN 2005, Izmir, Turkey, 16-17 Jun. 2005, Revised Selected Papers, Series: *LNCS*, Subseries: *Lecture Notes in Artificial Intelligence* , Vol. 3949 / 2006, Savaci, F. Acar (Ed.), Publisher: Springer Berlin / Heidelberg, pp.84-91.
E.T. Senalp, E. Tulunay, Y. Tulunay

10. 2006 Forecasting Total Electron Content Maps by Neural Network Technique, *Radio Science*, Vol. 41, No. 4, RS4016, Publisher:

American Geophysical Union, Washington,
http://dx.doi.org/10.1029/2005RS003285.
E.Tulunay, E.T.Senalp, S.M.Radicella, Y.Tulunay

11. 2007 A Case Study on the ELF Characterization of the Earth-
Ionosphere Cavity: Forecasting the Schumann Resonances,
Journal of Atmos. and Solar-Terrestrial Physics (ISROSES-2006)
(accepted).
Y. Tulunay, E. Altuntas, C. Price, T. Ciloglu, E. Tulunay, Y.
Bahadirlar, E.T. Senalp

12. 2007 Total Electron Content (TEC) Forecasting by Cascade Modeling:
A Possible Alternative to the IRI-2001, *Radio Science*,
(submitted).
E.T. Senalp, Y. Tulunay, E. Tulunay

Papers in International Workshops and Conference Proceedings

1. 2000 Neural Network Modeling of the Effect of the IMF Turning on the
Variability of HF Propagation Medium, *AP 2000*; *Millennium
Conference on Antennas and Propagation*, *ICAP and JINA*, p.132,
9-14 Apr. 2000, Davos, Switzerland.
Y. Tulunay, E. Tulunay, E.T. Senalp, C. Özkaptan

2. 2000 An Attempt for the Modeling of Trough by Using Neural
Networks, *COSPAR,* CD-ROM; 16-23 Jul., 2000, Warsaw,
Poland
Y.Tulunay, E. Tulunay, E.T. Senalp

3. 2000 An Attempt For the Modeling of the Mid-Latitude Electron
Density Trough on the Ionospheric Critical Frequencies by Using
Neural Network, *Intercomparative Magnetosheath Studies*, 4-8
Sep. 2000, Antalya, Turkey.
Y.Tulunay, E. Tulunay, E.T. Senalp

4. 2000 Neural Network Based Approach to Forecast Ionospheric
Parameters, *SPECIAL Workshop*, abstract in
www.sgo.fi/SPECIAL/Contributions/abstracts2000.html, 8-11
Nov. 2000, Lindau, Germany
E. Tulunay, Y.Tulunay, E. T. Senalp

5. 2001 Development of Neural Net Based Models for Some Non-Linear

Processes, *The 4th Pacific Int. Conf. on Aerospace Science and Technology*, *PICAST 4*, 21-23 May 2001, Kaohsiung, Taiwan.
Y.Tulunay, E.Tulunay, A.T. Kutay, E.T.Senalp

6. 2001 Forecasting the Total Electron Content by Neural Networks, *COST 271 Workshop*, *Ionospheric Modeling and Variability Studies for Telecommunications Applications*, Book of Abstracts, p.47, CD of Proceedings, WG4_P006, 25-27 Sep. 2001, Sopron, Hungary.
E. Tulunay, E.T. Senalp, Y. Tulunay

7. 2001 The Trough Based Neural Network Model of the foF2 Values, *COST 271 Workshop*, *Ionospheric Modeling and Variability Studies for Telecommunications Applications*, Book of Abstracts, p.8, CD proceedings of the 1st COST 271 Workshop, 25-27 Sep. 2001, Sopron, Hungary.
Y. Tulunay, E. Tulunay, E.T. Senalp

8. 2002 The Trough Based Neural Network Model of the foF2 Values, *SPECIAL II Workshop*, 3-6 Jan. 2002, Cambridge, U.K.
Y. Tulunay, E. Tulunay, E.T. Senalp

9. 2002 Neural Network Based Approach to Forecast the Total Electron Content Values, *EGS 2002 Conference, 27th General Assembly of the European Geophysical Society*, CD of Abstracts, EGS02-A-00867, 21-26 Apr. 2002, Nice, France.
E.T. Senalp, E. Tulunay, Y. Tulunay.

10. 2002 Forecasting GPS TEC During High Solar Activity by Neural Network Technique, *COST Workshop*, *Products for ITU-R and other Radiocommunication Applications*, 2nd COST271 Workshop Proceedings CD, 1-5 Oct. 2002, Univ. do Algarve, Faro, Portugal.
E. Tulunay, E.T. Senalp, Lj. R. Cander, Y. Tulunay, L.Ciraolo

11. 2002 Neural Network Based Magnetopause Crossings Forecast, *COST 271Workshop*, *Products for ITU-R and other Radiocommunication Applications*, Poster, 1-5 Oct. 2002, Universidade do Algarve, Faro, Portugal.
E.T. Senalp, D.G. Sibeck, Y. Tulunay, E.Tulunay

12. 2002 Neural Network Based Approach to Model Near Earth Space Processes, *34th COSPAR Scientific Assembly - The 2nd World*

Space Congress, C4.3-0018-02, 10 - 19 Oct. 2002, Houston,
Texas, USA.
Y. Tulunay, E. Tulunay, E.T. Senalp

13.   2002   Forecasting Magnetopause Crossing Locations by Using Neural
Networks, *34th COSPAR Scientific Assembly – The 2nd World
Space Congress*, Poster, PSW1-C0.2-D0.1-E2.4-F0.1-PSRB2-
0113-02, 10 - 19 Oct. 2002, Houston, USA.
E.T. Senalp, D.G. Sibeck, Y. Tulunay, E. Tulunay

14.   2002   Development of Neural Network Based Models for Non-Linear
Agro-Environment Systems, *3rd International Symposium on
Sustainable Agro-Environmental Systems: New Technologies &
Applications*, 139, 26-29 Oct. 2002, Cairo, Egypt.
E. Tulunay, T. Senalp, Y. Tulunay, Z. Aslan

15.   2003   Forecasting Regional Cloudness and Cloud Top Temperature By
Neural Networks, *European Science Foundation Meeting: ESF
Scientific Network on Space Weather and the Earth's Weather
and Climate,* 20-23 February 2003, Frankfurt am Main, Germany,
EGS-AGU-EUG Joint Assembly 2003, Poster: P0976, 06-11 Apr.
2003, Nice, France, EAE03-A-13915, Geophysical Research
Abstracts, Vol.5, 13915, 2003, EGS, Lindau, Germany.
Y. Tulunay, S. Mentes, E. Tulunay, E.T. Senalp, E. Akcan

16.   2003   Spatial Prediction of foF2 In Modeling The Influence Of Trough
on HF Communication By Using Neural Networks, *COST 271
Workshop: Significant results in COST271 Action: a review,*
Poster, 23-27 Sep. 2003, Spetses, Greece.
Y. Tulunay, A. Karpacev, E. Tulunay, E.T. Senalp

17.   2003   Forecasting the Total Electron Content Values by Using Neural
Networks and MAC Index, *COST 271 Workshop: Significant
results in COST271 Action: a review,* Poster, 23-27 Sep. 2003,
Spetses, Greece.
E. Tulunay, E.T. Senalp, P. Spalla, Y. Tulunay, G.D. Franceschi

18.   2004   Forecasting GPS TEC upto 24 Hours in Advance by Neural
Network Technique, *EGU General Assembly 2004*, ST14, Poster:
EGU04-A-02260, 25 - 30 Apr. 2004, Nice, France, Geophysical
Research Abstracts, Vol. 6, 02260, 2004.
E. Tulunay, Y. Tulunay, E.T. Senalp, L. Cander.

19. 2004 Neural Network Based Forecasting with Adaptation Capability, *13ᵗʰ Turkish Symposium on Artificial Intelligence and Neural Networks, TAINN 2004*, pp. 585-592, 10-11 Jun. 2004, Foca, Izmir, Turkey.
E.T. Senalp, E. Tulunay, Y. Tulunay.

20. 2004 Neural Network Application on Agro-Environment Problems, *Proceedings of the Workshop "Measuring and Computing Technologies on Agricultural Issue", AGROENVIRON 2004 Role of Multi-purpose Agriculture in Sustaining Global Environment*, pp. 27-36, Udine, Italy, 20-24 Oct. 2004.
Y. Tulunay, E. Tulunay, E.T. Senalp, Z. Aslan

21. 2005 Neural Networks and Cascade Modeling Technique in System Identification, *14ᵗʰ Turkish Symposium on Artificial Intelligence and Neural Networks, TAINN 2005*, pp.286-293, 16-17 Jun. 2005, Cesme, Izmir, Turkey.
E.T. Senalp, E. Tulunay, Y. Tulunay

22. 2005 Neural Network Modeling in Forecasting the Near Earth Space Parameters: Forecasting of the Solar Radio Fluxes, *COST 724 Scientific Workshop*, Proceedings CD, 10-14 Oct. 2005, Athens, Greece.
Y. Tulunay, M. Messerotti, E.T. Senalp, E. Tulunay, M. Molinaro, Y.I. Ozkok, T. Yapici, E. Altuntas, N. Cavus

23. 2006 Integration of METU-IFS Server to COST 724 Server (BIRA), *COST 724 MCM and Scientific Workshop*, Proceedings CD, 27-30 Mar. 2006, Antalya, Turkey.
E. Tulunay, D. Heynderickx, E.T. Senalp, M. Ozdemirci, Y.I. Ozkok, Y.Tulunay

24. 2006 COST296 WG2.2 Activity Report : Radio Propagation Measurements During the 29 March 2006 Total Eclipse Week, *4ᵗʰ COST 296 MCM and WGM* 27-29 Apr.2006, Neustrelitz, Germany
E. Tulunay, E.M. Warrington, Y. Tulunay, Y. Bahadırlar, A.S. Türk, T. Yapıcı, E.T. Şenalp, E. Altuntaş, M.Ö. Sarı, O. Büyükpapuşcu

25. 2006 Forecasting Total Electron Content (TEC) for Constructing Maps Especially During High Solar Activity Periods*, Int. Adv. School*

on Space Weather, CD, 2-19 May 2006, ICTP, Trieste, Italy.
E.T. Senalp, E. Tulunay, S.M. Radicella, Y. Tulunay

26. 2006 System Identification by using Cascade Modeling Technique with Bezier Curve Nonlinearity Representations, *15th Turkish Symposium on Artificial Intelligence and Neural Networks*, *TAINN 2006*, pp.75-82, 21-23 Jun. 2006, Akyaka, Muğla, Turkey.
E.T. Senalp, E. Tulunay, Y. Tulunay

27. 2006 Propagation Related Measurements during Three Solar Eclipses in Turkey*, IET 10th International Conference on Ionospheric Radio Systems & Techniques, IRST 2006*, 18-21 Jul. 2006, London, UK.
E. Tulunay, E. M. Warrington, Y. Tulunay, Y. Bahadırlar, A.S. Türk, R. Çaputçu, T. Yapıcı , E.T. Şenalp.

28. 2006 The ELF Characterization of the Earth–Ionosphere Cavity: Forecasting the Schumann Resonances, Poster, *International Symposium on Recent Observations and Simulations of the Sun-Earth System (ISROSES) 2006*, 17-22 Sep. 2006, Varna, Bulgaria.
E. Altuntas, Y. Tulunay, Y. Bahadirlar, E. Tulunay, E.T. Senalp

29. 2006 Recent COST 296 Propagation Related Measurements During the 29th March 2006 Solar Total Eclipse in Antalya, Turkey, *2nd COST 296 Workshop and 5th MCM, Radio Systems and Ionospheric Effects*, Univ. Of Rennes 1, 3-7 Oct. 2006, Rennes, France.
E. Tulunay, Y. Tulunay, E.M. Warrington, Y. Bahadirlar, T. Yapici, E.T. Senalp, A.S. Turk

30. 2006 Neural Network Forecasting Of Schumann Resonances In The Near Earth Space, *Third European Space Weather Week (ESWW3)*, 13-17 Nov. 2006, Royal Library of Belgium, Brussels, Belgium.
E. Tulunay, Y. Tulunay, E. Altuntas, E.T Senalp, Y. Bahadirlar

31. 2007 International Heliophysical Year 2007 (IHY), Turkish National Activities, Poster, *Official IHY Opening Ceremony, IHY Kick-off Event*, 17-21 Feb. 2007, Vien, Austria
Y. Tulunay, E. Tulunay, Z. Kocabas, E. Altuntas, T. Yapici, E.T. Senalp

32. 2007 Identification of Processes by Cascade Modeling Technique, *The 5th IFAC DECOM-TT 2007*, pp. 117-122, 17-20 May 2007, Cesme, Izmir, Turkey
E.T. Senalp, E. Tulunay, Y. Tulunay

33. 2007 A Hybrid Approach In Fof2 Forecast Mapping Including Disturbed Conditons, *The 5th IFAC DECOM-TT 2007*, pp. 51-56, 17-20 May 2007, Cesme, Izmir, Turkey
E. Altuntas, T. Yapıcı,Y. Tulunay, E. Tulunay, Z. Kocabas, E.T. Senalp

34. 2007 Forecasting Total Cloud Amount Maps and Cloud Top Temperature Maps by using Fuzzy Neural Networks and Bezier Surfaces, *The 9th World Meteorological Organization Scientific Conference on Weather Modification*, 22-24 Oct. 2007, Antalya, Turkey (accepted)
Y. Tulunay, E.T. Senalp, S. Oz, L.I. Dorman, E. Tulunay, S.S. Mentes, M.E. Akcan

Papers in National Workshops and Conference Proceedings:

1. 2002 Toplam Elektron Yoğunluğu Değerlerini Sinirsel Ağlar Kullanarak Öngörüde Bulunma, *URSI-TÜRKİYE'2002 Bilimsel Kongresi*, pp.407-410, ITÜ - İstanbul, 18-20 Sep. 2002.
E.T. Senalp, E. Tulunay, Y. Tulunay

2. 2002 Doğrusal Olmayan Bazı Süreçler İçin Sinirsel Ağ Tabanlı Yaklaşımlar, *URSI-TÜRKİYE'2002 Bilimsel Kongresi*, pp. 403-406, ITÜ - İstanbul, 18-20 Sep. 2002.
Y. Tulunay, E. Tulunay, A.T. Kutay, E.T. Senalp

3. 2006 Toplam Elektron Niceliği Öngörümünde Ardışık Benzekleme Tekniği, *3. URSI-TÜRKİYE'2006 Bilimsel Kongresi*, pp. 360-362, Hacettepe Üniversitesi, Ankara, 4-8 Sep. 2006.
E.T. Şenalp, E. Tulunay, Y. Tulunay

4. 2006 Yer İyonosfer Kovuk Değişimi'nin Schumann Rezonanslarına Dayalı İncelenmesi, *1. Ulusal Havacılık ve Uzay Konferansı*, ODTÜ, Ankara, 21-23 Sep. 2006.
E. Altuntaş, Y. Tulunay, E. Tulunay, E.T. Şenalp, Y. Bahadırlar

5. 2006 Ardışık Benzekleme Tekniğinin Kullanımı: Ters Çift Sarkaç, *TOK'06 Otomatik Kontrol Ulusal Toplantısı*, pp. 533-537, TOBB Ekonomi ve Teknoloji Üniversitesi, Ankara, 6-8 Nov. 2006.
E.T. Şenalp, E. Tulunay, Y. Tulunay